POLITECNICO DI TORINO
Repository ISTITUZIONALE

Friction damping for turbomachinery: A comprehensive review of modelling, design strategies, and testing capabilities

(Article begins on next page)
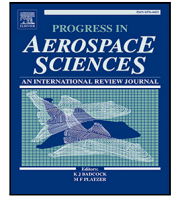
01 September 2025

Friction damping for turbomachinery: A comprehensive review of modelling, design strategies, and testing capabilities

Jie Yuan [a],[*], Chiara Gastaldi [b], Enora Denimal Goy [c], Benjamin Chouvion [d]

[a] *Department of Aeronautics and Astronautics Engineering, University of Southampton, Southampton, SO17 1BJ, UK*
[b] *Department of Mechanical & Aerospace Engineering, Politecnico Di Torino, Corso Duca degli Abruzzi 24, Turin 10129, Italy*
[c] *Inria, CMAP, Ecole Polytechnique, IPP, Palaiseau, France*
[d] *Centre de Recherche de l'Ecole de l'Air (CREA), Ecole de l'air et de l'espace, 13661 Salon-de-Provence, France*

ARTICLE INFO

ABSTRACT

This paper presents a comprehensive review of recent advancements in modelling approaches, design strategies, and testing techniques applied to friction damping in turbomachinery. It critically evaluates experimental testing, design processes, and optimisation studies, along with the latest developments in numerical modelling techniques. The review begins with an overview of vibration mitigation methods and the historical development of friction dampers for bladed disk systems. Subsequent sections explore research efforts aimed at enhancing numerical and simulation modelling capabilities, encompassing contact friction models, reduced-order modelling methods, and numerical solvers suitable for real-world applications and industrial high-fidelity models. The paper also delves into available testing rigs for experimental validation and characterisation of various friction damper types, as well as the literature on uncertainty quantification in friction damping. It concludes by highlighting recent trends in novel concepts, modelling techniques, and testing technologies shaping the design of next-generation friction dampers.

1. Introduction

1.1. Vibration problems in turbomachinery

Bladed disks in turbomachinery represent about 30% of the overall weight and are critical components for the structural and aerodynamic efficiency of the whole system. They work under severe operational environments and loadings making them undergo extreme static and dynamic stresses. The former is predominantly attributed to thermal loads, static fluid pressures, and rotation-induced centrifugal loads, whereas the latter arises from mechanical vibrations caused by two fundamental mechanisms:

- Synchronous vibrations: they originate from blade rotation within a pressure field that is non-uniform circumferentially, induced by interactions between blade rows and non-uniform inflow conditions (non-uniformity in the intake, obstruction to the flow, etc.). From the rotating bladed disk point of view, the pressure field takes the shape of a wave moving at the rotor speed. Consequently, the structure experiences dynamic loading at frequencies that are multiples of the rotational frequency, leading to synchronous excitation. When the excitation frequency of the

pressure field coincides with a natural frequency of the structure, leading to resonance, the forced vibration response can become significantly amplified. Further explanation about synchronous vibrations can be found in [1,2]. The synchronous vibration becomes more complex when mistuning due to manufacturing tolerance and defects is present. It will lead to mode localisation phenomena and to the modal energy being confined to a certain set of blades. The vibration can be triggered by multiple harmonics of the rotating frequency possibly, resulting in much larger vibration amplitudes compared to the tuned counterpart. Readers are invited to refer to [3,4] for a more detailed review of this topic. In addition, out of balance of the rotor is also a common source for dynamic loading that alternates at a frequency equal to the speed of the rotation [1].

- Non-synchronous vibrations: they appear at frequencies that are not proportional to the rotational speed, but that still correspond to one of the structure's modes of vibration. In this context, non-synchronous vibrations group unsteady flow-driven vibration (vortex shedding, buffering, rotating stall, etc.) [5], flutter [6] and acoustic resonance [7,8].

* Corresponding author.
E-mail addresses: j.yuan@soton.ac.uk (J. Yuan), chiara.gastaldi@polito.it (C. Gastaldi), enora.denimal-goy@inria.fr (E. Denimal Goy),
benjamin.chouvion@ecole-air.fr (B. Chouvion).

The persistence of high dynamic stresses, contingent on the extent of static stress, can result in high cycle fatigue (HCF), which is one of the most common causes of failure in gas [9,10] and steam [11] turbines.

1.2. Vibration mitigation methods

The most effective way to reduce vibrations is to prevent any potential excitations of forced resonances, aeroelastic instabilities, and mechanical interactions. During the design stage, adjusting design parameters to change the natural frequencies can help to some extent. However, mitigating the onset of resonance regimes caused by synchronous forced responses is challenging, given the extensive modal density in bladed disks and the broad spectrum of aerodynamic excitation forces. Moreover, the incidence of flutter is on the rise as a result of the growing trend towards slender blades with increased aspect ratios, aimed at curbing fuel consumption and reducing weight. Still, to preserve structural integrity, it is essential to ensure that the vibration response remains within acceptable limits by introducing effective damping in the system that reduces the sharpness of the resonance and lowers the peak values of alternating stresses to safe levels. It is worth mentioning here that active damping solutions are not covered by the paper.

Setting aside aerodynamic damping, which is beneficial in most cases but may become negative (i.e. exciting source) in the case of flutter, as already observed in 1956 by Goodman and Klumpp [12], the remaining sources of damping are connected to hysteresis dissipation within the material and to dry friction between the different components. In terms of material dissipation, coating the surface of the fan blade system with, for example, ceramic materials [13–16], or viscoelastic material [17–19] can effectively enhance the damping performance although it can also impact the aerodynamic efficiency. Due to the frequent inadequacy of various material and mechanical damping alternatives in enduring the challenging conditions within a gas turbine, friction damping emerges as the prevailing damping technique in aero-engines. Despite potential challenges such as fretting wear effects on the friction interface, which may raise maintenance concerns, it remains its prominence due to its resilience under high temperatures and complex loading conditions. Noteworthy is its capacity to provide substantially higher damping levels compared to material damping, with a potential increase ranging from 10 to 100 times, as emphasised in [20].

Friction damping has demonstrated its effectiveness in numerous industrial applications and is now widespread, particularly in turbomachinery where challenging operating conditions limit the feasibility of alternative damping sources. While introducing multiple contact interfaces within the system may be beneficial as it increases the damping sources, it also adds complexity in terms of modelling, simulation, and prediction of the dynamic behaviour. This is primarily due to the nonlinear nature of friction damping, the presence of intricate phenomena such as fretting wear, and the challenge of accurately modelling the friction. It represents numerous open questions that have been at the centre of many research studies over the past decades.

1.3. Contribution and organisation of the paper

This paper aims to review the current state of the art of friction damping in terms of modelling, design and testing. Although the applications are focused on turbomachinery, the methodologies and comments remain applicable to other fields where friction damping occurs. The recent review paper [21] provides an extensive review of numerical methods to predict vibration in bladed disks with friction joints. The current paper differs in that it mainly addresses the challenges of practical engineering aspects of friction dampers. Particularly, it includes a comprehensive evaluation of experimental capabilities and outcomes obtained from experimental tests, as well as a detailed section on design and optimisation strategies for friction damping, which have never been covered previously. The different topics addressed in the paper are summarised in Fig. 1 and include:

- A brief historical and technical description of the introduction of friction damping in turbine blade design (Section 2).
- A presentation of prominent numerical modelling methods for modelling contact interfaces of structural components, exploring recent advancements such as the incorporation of multi-scale analysis (Section 3).
- A section on numerical simulation techniques including general ideas on how to solve the nonlinear dynamic equations, reduced-order modelling methods and recent concepts such as nonlinear normal modes (Section 4).
- A comprehensive section on experimental works, including testing capabilities and challenges, model parameter estimation and model validation (Section 5).
- A comprehensive section on design and optimisation methods related to friction damping, aimed to provide new robust and efficient designs (Section 6).
- A section on current trends and future challenges in the study of friction damping (Section 7).

2. A brief history of the integration of friction damping in turbine blade design

The importance of friction damping in reducing the incidence of turbine failures was first mentioned in 1940, when Kroon [22] attempted to measure the material damping contribution as a function of stress, temperature and excitation frequency of blades, and stated that: *"Besides internal damping in the materials, there is a certain amount of damping caused by microscopic rubbing and impacting along the fits between rotor and blades and in the shroud connections"*. In 1946, Shannon [23], compared the order of magnitude of friction damping at the blade root with the internal material damping. While the different sources of damping depend on many factors, e.g. design of the blade root, preload, temperature, stress on the blade, etc, the comparison is still striking. The damping connected to friction was estimated to be 5 times greater than the one connected to internal material damping [24]. It should be noted that this estimate is related to a joint, i.e. blade root, which was not designed for the purpose of dissipating energy through friction. This gain can be enhanced when friction damping efficiency is targeted [20]. Yet, the contribution to the overall structural damping was significant. Current technologies exploit this mechanism by introducing friction contact interfaces in bladed disks to increase damping efficiency.

Fig. 2 depicts the progression of diverse friction dampers implemented on turbine blades, utilising images sourced from significant patents. The illustration serves a dual purpose. Firstly, it provides an estimation of the timeline for the introduction of various damping techniques. Even though the filing dates of these patents often do not align with the actual implementation of such devices in turbine designs, they still provide valuable and informative insights into the evolution of these technologies within the industry. Secondly, it offers a visual portrayal, though not exhaustive, of the varying adaptations of each damping mechanism. Complementary, Fig. 3 illustrates different damping solutions in real systems.

Although blade root attachments and shrouds were observed to contribute to structural damping [22], neither of them were purposely designed as friction damping devices. Blade root attachments responded to the technological need to connect the blades to the rotor in an era in which producing a blisk, i.e. an integrated bladed rotor, was not feasible. It also allowed the same blade casting to be re-used on rotors with a different number of blades. Blade roots come into different configurations, the most common being the "dovetail", the "fir-tree" and the "t-shape". Some of them are visible in the upper portion of Fig. 2.

Shrouds are integral protuberances found on each blade, interlocking at speed to form a ring that couples the blades and enhances the overall stiffness of the assembly. They were introduced to provide an
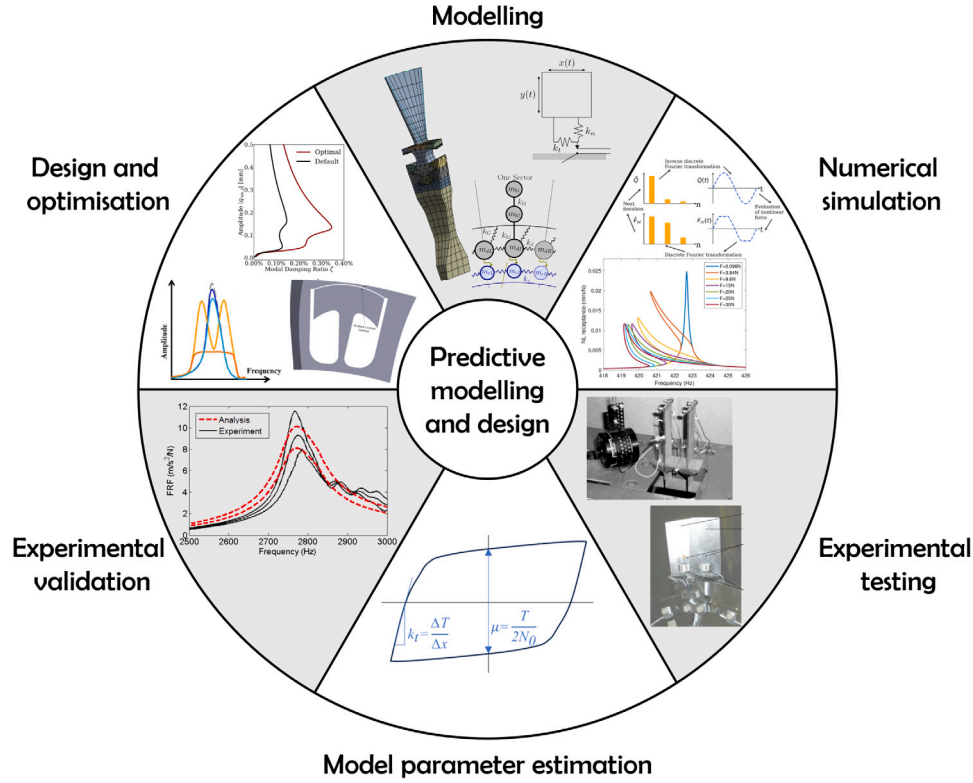
Fig. 1. Research topics related to the predictive modelling and design of friction dampers in turbomachinery.

elastic support at the mid-span of blades to prevent flutter. Initially, the same function was achieved by "tied blades", i.e. adjacent blades that were tied together by rods *"whose ends were screwed into threaded bushes set in the blade forms"* [28]. This technique was later discontinued due to the stress concentrations at the holes in the airfoils, and was replaced by snubbers or shrouds. In current terminology, snubbers usually refer to protrusions, integral to the blade airfoil, found at approximately two-thirds of the airfoil span, while "tip-shrouds" are found at the tip of the blade. The concept of "tied blades" also evolved into that of lacing wires as friction dampers, i.e. loose flexible rods which come into contact with the inner surface of the lacing holes within the turbine blade airfoil. In time, as shown in Fig. 2, other shapes of dampers placed mid-span on the blade airfoil were introduced. Such mid-span dampers may pass through holes, or may rest against protrusions integral to the airfoil. In both cases, the contact is ensured by the centrifugal force. The protrusions of adjacent blades may or may not come into contact. In the former case, a combination of snubber and mid-span damper is achieved. Both lacing wires and mid-span dampers are commonly used on last-stage blades of steam turbines. These blades are typically thin, long and flexible, making them particularly susceptible to substantial centrifugal and aerodynamic loads.

An external damper may also be placed in other positions along the blade. It may be positioned at the airfoil's tip, where it rests against blade covers or shrouds. Alternatively, one of the most common choices, especially in gas turbines, is to place it at the airfoil's root, against two adjacent inner platforms. This last configuration, which is more common with shroud-less shorter blades, has the advantage of not interfering with the aerodynamic flow. These dampers are usually referred to as underplatform dampers. The use of dual friction dampers, as proposed recently [29,30], involves coupling two separate dampers to the blade at different radial positions, offering enhanced damping and stiffening. However, careful consideration is required in determining the radial position to avoid disrupting the aerodynamic flow, akin to mid-span dampers. One proposed solution [30] involves placing one damper near the blade root, effectively replacing one lobe

of the disk sector. While this solution avoids flow interference, it may substantially increase stresses at the blade root-disk interface.

In the 1980s, blisks, an acronym for "Bladed Integrated Disks", were introduced as a response to the need for increased efficiency and reduced weight in gas turbine engines for aircraft and power generation. While they offer significant advantages in terms of aerodynamic performance and overall efficiency, they also present some challenges. Since the blisk is manufactured as a single piece, no inherent contact surfaces are available to dissipate energy via friction. For this reason, starting in the 1990s, split ring dampers were added to the annular air seal which is commonly used in gas turbine engines to prevent gas flow from one section of the engine to another [31] or, more generally, under the rim [32].

In all the above-mentioned cases, the rotation caused by the centrifugal load is responsible for the contact preload, while the relative motion necessary for friction dissipation is caused by the blades' vibration itself.

3. Numerical modelling of friction interfaces

3.1. An overview of modelling approaches

Predicting the damping resulting from friction in bladed disks requires modelling different components and their coupling through the contact friction interface, which is associated with many complex phenomena at different scales. When modelling mechanical components such as the bladed disk or dampers for dynamic studies, the emphasis is on deriving the structural mass, stiffness and damping matrices. These can be obtained analytically for lumped-parameter models in early-stage studies [33–35]. More recent analytical and semi-analytical models can be found in [36–40]. These models, characterised by a short simulation time, capture nonlinear dynamic behaviours and/or energy dissipation, and are well-suited for proof of concept. In practical applications, precise modelling of geometries and mechanical properties is essential for an accurate prediction of modal properties. In this
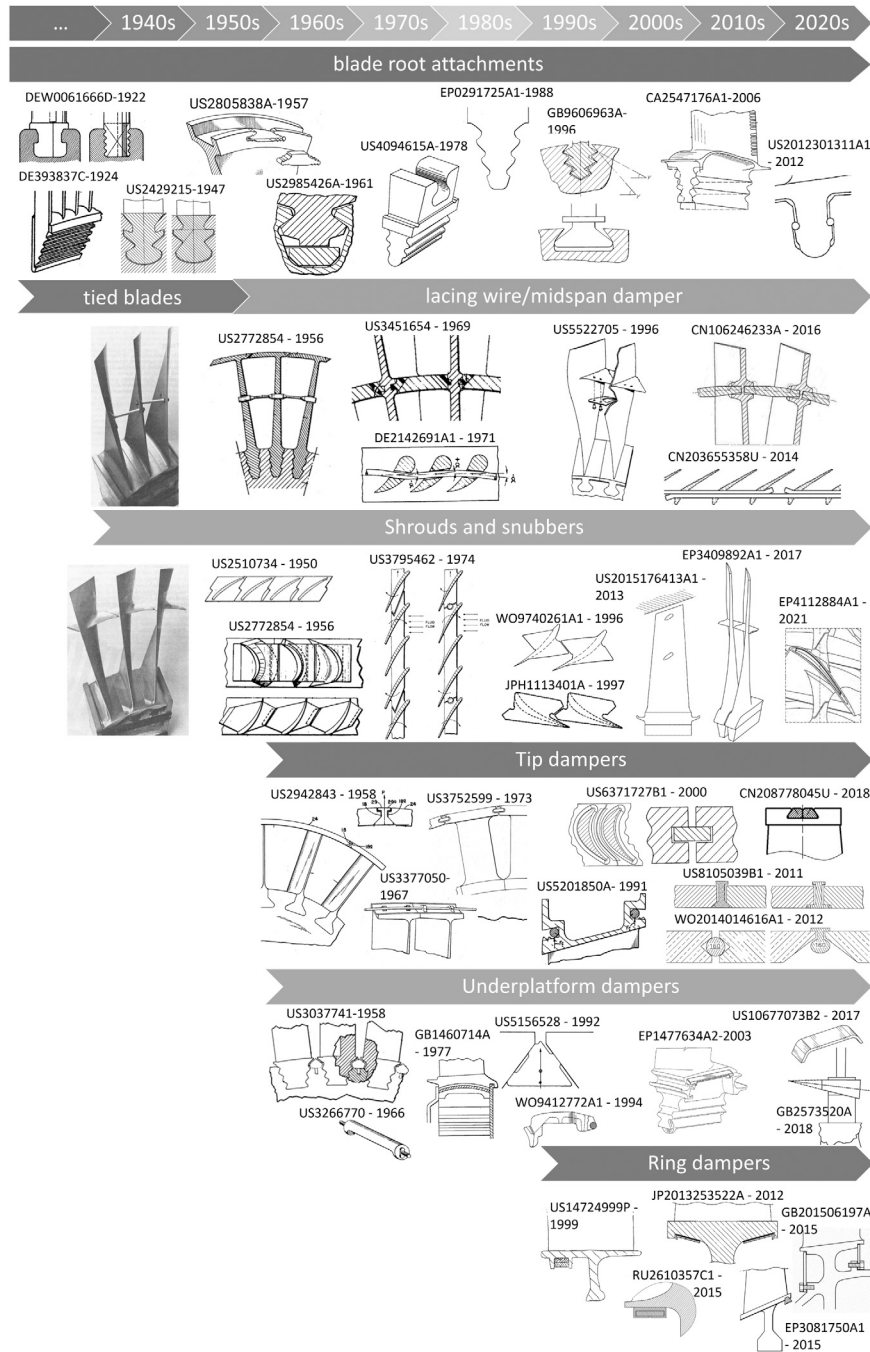
Fig. 2. Timeline representing the introduction of the different kinds of friction dampers in bladed disks.

context, full Finite Element Models (FEM) are usually employed to compute the structural matrices. With such a modelling approach, high-fidelity models can be produced, but they are computationally heavy on the other hand. When modelling bladed disk structures, preliminary studies usually consider the system to be perfectly cyclically symmetric to reduce computational cost while considering only a single sector. However, adapted strategies must be used to account for mistuning effects, which can have a significant impact on the system dynamics. More details on general reduction techniques and specific approaches dedicated to mistuning are given in Section 4.2.2. As an illustration, a lumped-parameter model of a bladed disk with a ring damper [35] and a high-fidelity FEM of a bladed disk with UPD [41] are displayed respectively in Figs. 4(a), and 4(b). The former has 8 DOF per sector

(2 for the blade, 3 for the disk and 3 for the ring damper) while the latter, with 30840 DOF per sector (14430 for the blade, 14628 for the disk and 1782 for the UPD), highlights the large size of realistic FEM and the need for model reduction, as will be developed in Section 4, to ensure affordable computational time.

Another challenge in modelling systems that include friction dampers lies in the representation of the contact friction interface. In this context, one is interested in modelling the normal loads, i.e. the non-penetration of the solids, and the tangential loads with a friction law, such as the Coulomb law, for example. Both are strongly non-linear leading to numerical difficulties when solving such problems. More advanced models include phenomena taking place at the contact interface, such as fretting wear.
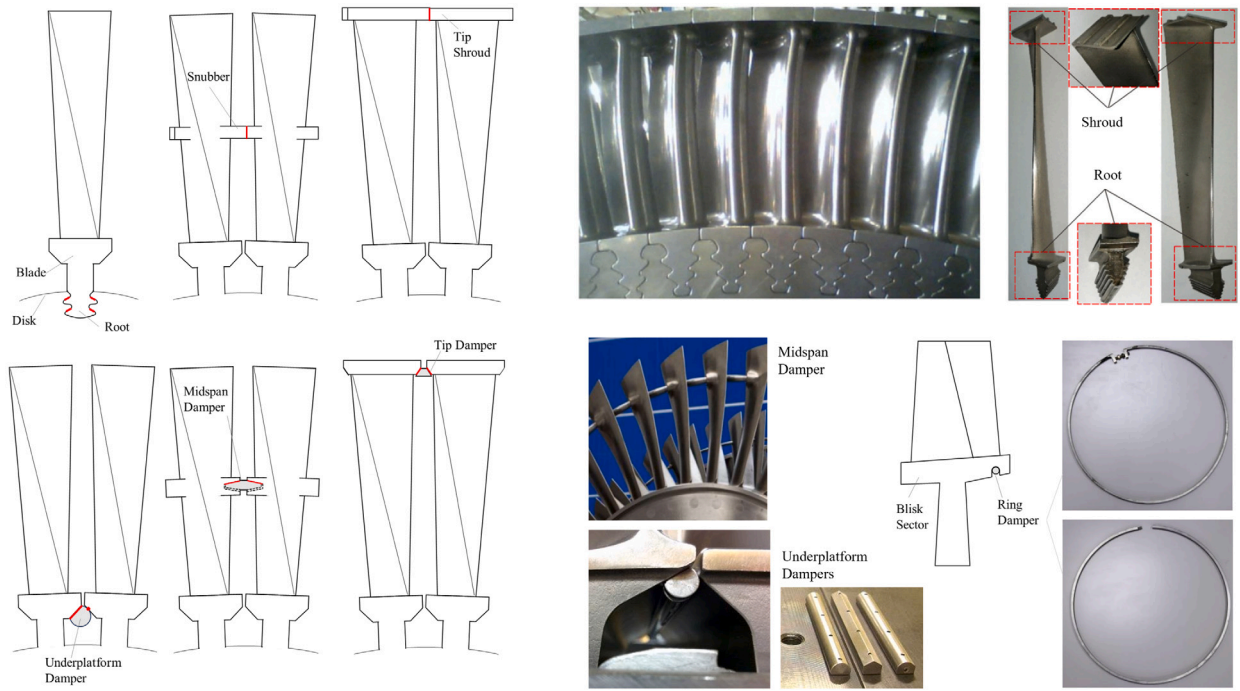
Fig. 3. In black and white, schematic representation of different kinds of damping solutions. Shrouds and roots (Photographs from [25]), Midspan dampers (©2020 Baker Hughes Company - All rights reserved, already published in [26]), Ring dampers [27].

(a)

(a) Full structure.

(b) Fundamental sector.

(d) Underplatform dampers.

(c) Fir-tree attachment.

(b)
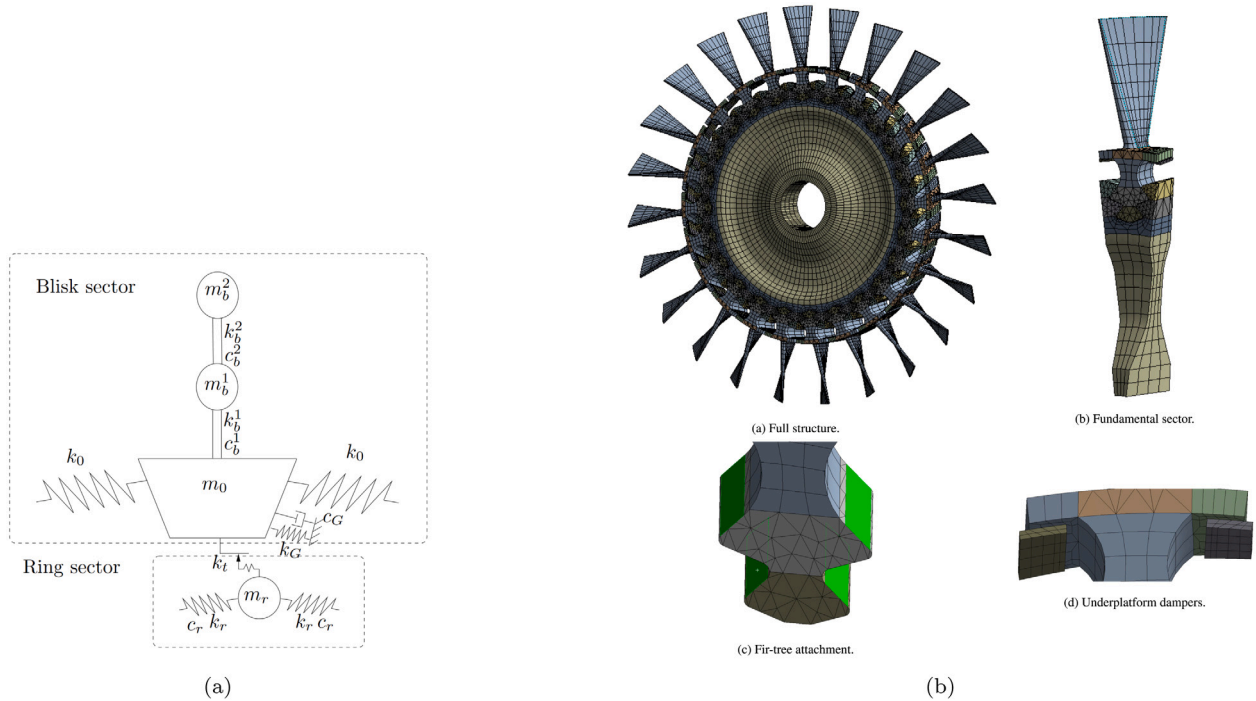
Fig. 4. (a) Lumped parameter model of a friction ring damper [35] and (b) high-fidelity FEM of the sector of a bladed disk with UPD [41].

This section is dedicated to a brief presentation of the main different friction interface models that exist and are used in the numerical modelling of friction damping for turbomachinery. It is worth mentioning here that the numerical modelling of contact interfaces, in general, constitutes a broad research domain, and turbomachinery applications represent only a small section of it. In such applications, the contact is highly loaded and vibrations are of small amplitudes. A commonly employed assumption is to decouple these two problems and analyse the dynamic behaviour around the static solution. For a general overview of contact modelling, one can refer to [42,43] and to [21] for application to bladed disks.

3.2. Analytical contact models

Analytical contact models were initially developed for static problems using the Hertz theory [42], primarily considering simple geometries and without accounting for frictional effects or interactions between surface asperities. For rough surfaces, the statistical approaches

based on analytical solutions are not able to track the local contact behaviour. Analytical models were subsequently expanded to account for various specific contact geometries and include frictional effects modelled as a Coulomb law [44,45]. Partial slip was later incorporated in [46,47]. While these methods have the advantage of being exact, they can only be used in very specific cases and are difficult to extend to complex interface geometries and/or more advanced friction laws. A more detailed review of analytical methods for contact friction modelling can be found in [48].

3.3. Macro-scale contact models

Finite element-based numerical methods have been developed to address dynamic contact problems across a wide range of structures and contact geometries. These methods gained widespread popularity and efficiency with the advancements and proliferation of computational capacity. Consequently, it became feasible to model the frictional contact interface and simulate its dynamic behaviour [43]. Nevertheless, to accurately capture contact dynamics, a highly refined mesh is essential, particularly in the presence of sharp strain gradients. This significantly increases computational time, rendering the method impractical for real-world applications. Alternatives based on the elastic half-space assumption have been proposed based on the use of Boundary Element Methods [49–51], zero-thickness elements [52] or thin-layer elements [53,54] to mesh only the contact elements. Even though nonlinear relations may be considered to model the friction law, the normal law is usually regularised with a linear-elastic unilateral law [55]. A major drawback of these methods comes from this regularisation, which is often too strong and tends to soften the friction contact effects. For these different reasons, these methods are not adapted for turbomachinery applications, where small vibrations with high contact pressure and change of contact status (impact, stick, slip) are experienced.

The most widespread strategy to model the friction contact interface in turbomachinery applications involves utilising a node-to-node contact formulation to define the interface's contact law between the two structures [33,56–58]. Such approaches discretise the contact surface by pairing a contact point from one solid with a contact point from the other solid. As the two points interact, it is assumed that the displacements remain sufficiently small, and that two points in contact can thus be considered to almost face-to-face during the vibrations. After establishing the pairing, the next step involves defining the contact law between the points to replicate the hysteresis-like behaviour, including both a normal law and a tangential law. These contact laws are usually referred to as contact models, or sometimes as friction elements. They are composed of additional stiffness and damping forces in the contact area. Depending on the case, macro-slip or micro-slip elements can be used [21]. Micro-slip elements give a smooth and progressive transition between the elastic deformation and the sliding contact [59,60]. However, such elements usually require the tuning of many parameters, making them difficult to use in practice. Such elements are mostly used when the normal load is constant over time [21]. Alternatively, the main drawback of using macro-slip elements is that for one contact point, the transition between sliding and sticking conditions is sharp. However, if the contact surface is discretised with many macro-slip elements, or if the hysteresis behaviour is reproduced implicitly with the contact law, then a smooth and progressive transition between the elastic deformation and the sliding contact can be reached for the contact surface [21,61–64].

In terms of contact models, classical options include the LuGre [65], Bouc-Wen [66], Iwan [67], Valanis [68], and Dahl [69] models. A full description and comparison of the different models can be found in [70]. The most commonly used contact element for turbomachinery is based on the Jenkins element, originally developed in [56,71] for a 2D problem. It was extended to 3D in [72] by coupling the movement in the two tangential directions to the contact surface, while considering a constant normal load. This was later expanded [57] to incorporate

variations in the normal load, accounting for possible loss of contact. Recent studies [73,74] focused on applying these advanced full 3D contact models. The latter additionally presents the Jacobian matrix for the contact model, required in many numerical methods for the computation of the dynamic response, as will be explained in Section 4.

In Fig. 5, three hysteresis loops are shown to illustrate the impact of the contact law. The total dissipated energy is represented by the area within the hysteresis loop. The first hysteresis loop corresponds to classic the Coulomb law, where the contact alternates between stick and slip conditions. The second loop represents a Jenkins element, which includes an elastic spring in addition to a Coulomb element. In this case, there is still a sharp transition between the stick and slip states. The third hysteresis loop depicts a typical microslip contact element such as the Valanis model. Here, we can observe a smooth transition between the two states, indicating micro-slip, i.e., partial slip on the contact surface. It is evident that the latter can describe more complex dissipative behaviour at the contact interface, but also requires more parameters to be explained.

The presented approaches are based on models that rely on multiple parameters, necessitating meticulous tuning for accurate predictions, which often requires expensive model updating techniques. The most popular method consists of updating the model parameters until the simulation fits experimental measurements [12,64,75–80], as will be detailed in Section 5. After this updating phase, the predictions can be reliable for the considered configuration [64]. However, this relies on the idea that the FEM with the contact model can accurately represent the real contact conditions, i.e. that there exists a set of model parameters that give a good fit with the experimental data. It is worth mentioning here that such approaches are applicable if the uncertainties, emerging from noise measurement or environmental variations for example, do not influence the system properties. In a context where uncertainties have a substantial impact, as shown in Section 6.2, more advanced updating methods must be employed (sensitivity-based, optimisation, Bayesian approaches, etc.) to consider the statistical aspect of the problem. More details can be found in [81]. Furthermore, conducting the necessary experiments can sometimes be challenging and/or costly. Finally, the updated parameters remain valid only for the considered scenario or structure, as they change quickly with the environment and geometry [82]. This poses a significant constraint during the design stage, particularly when no prior knowledge is available for contact modelling.

3.4. Multiscale contact model

More sophisticated modelling techniques have also been proposed to include more advanced phenomena taking place at the contact interface, such as wear [49,83], fretting [50,51,84,85], and the consideration of coating [13–16]. The methods described in the previous section only use a coarse description of the contact interface with a limited number of contact points and do not consider the microscale or mesoscale interface geometries. As examples, surface roughness affects the contact stiffness [43], while the mesoscale geometry and fretting wear significantly influence the distribution of normal pressure [86]. In this context, multiscale approaches have been developed to establish a connection between contact mechanics and dynamics [87,88]. To consider surface with microscale asperities, a compliant model incorporating a statistical distribution of asperities was developed [89]. It can assess the effects of the surface asperities in a statistically averaged sense while being more computationally feasible compared to the FE approach. With such an approach, the surface roughness and its impact on the effective contact surface are modelled and quantified. Thus, relations between the contact load and the real contact pressure or between the contact stiffness and the normal load are obtained. They are typically described by power laws. Such relationships can directly be included as a linear penalty stiffness [90] or a nonlinear penalty model [91] to solve the normal contact problem. Recently, fractal
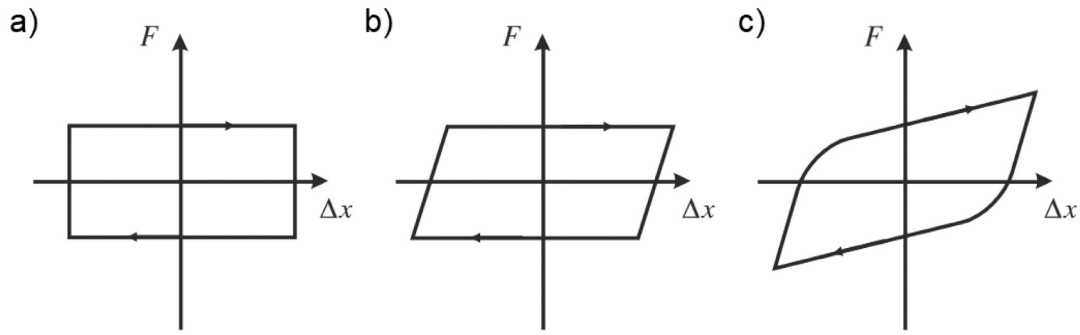
Fig. 5. Hysteresis curves for a Coulomb contact model (a), a Jenkins contact model (b) and a Valanis contact model (c) - Taken from [20].

and self-affine geometries have been employed to model more realistic roughness across different length scales [92]. The authors proposed a model to represent surface roughness using fractal geometry with a fractal dimension D. Using this model, the contact stiffness K_n is expressed as a function of the fractal dimension and the normal load P. They demonstrated that the contact stiffness is a function of a power law of the normal load, i.e. $K_n \propto P^\alpha$, where the power α depends on the fractal dimension D. This modelling allows for capturing the evolution of the first natural frequency and damping with respect to the contact pressure for a fan blade dovatial joint test case. Also, semi-analytical methods based on half-space theory were proposed to consider multiscale friction interface geometry that deals with surface roughness [93], mesoscale interface geometry [86,94] and fretting fatigue [85,93]. Semi-analytical methods discretise the contact interface to address the overall numerical challenge by analytically solving numerous elementary problems at smaller scales associated with each discretised element. These solvers combine macro- and micro-scale models. First, an initial quasi-static analysis is performed on the macro-scale model to compute the applied pressure and the shear traction fields [42,95]. Then, a micro-scale contact model is used to calculate the elastic deflections of the surface in the normal and tangential directions. Under the half-space assumption, this can be done with the Boussinesq and Cerruti potentials. The solver is speeded up with the projected conjugate gradient method [96] and a discrete-convolution Fast Fourier Transform (FFT). With such solvers, very refined contact meshes can be considered, allowing for the inclusion of surface roughness and profile in the simulations. These analytical solutions of contact properties are then incorporated into the nonlinear structural dynamics solver. Some studies, for example [86], demonstrate that the mesoscale surface geometry has a much greater impact on the nonlinear dynamic properties than surface roughness. An alternative multiscale framework was recently proposed in [97] for modelling the dynamics of bolted structures through zero-thickness elements to couple the effects of microscale roughness with the dynamic analysis of the system.

4. Numerical simulation

Using any of the modelling approaches mentioned in Section 3, the equation governing the dynamics of the whole system, including local friction joints, generally takes the form of the following ordinary differential equation:

$$\mathbf{M}\ddot{\mathbf{x}}(t) + \mathbf{C}\dot{\mathbf{x}}(t) + \mathbf{K}\mathbf{x}(t) + \mathbf{f}_{\mathrm{nl}}(\mathbf{x},\dot{\mathbf{x}},t) = \mathbf{f}_{\mathrm{e}}(t) \tag{1}$$

where $\mathbf{M}$, $\mathbf{C}$, $\mathbf{K}$ are the mass, damping and stiffness matrices of the system, respectively, and $\mathbf{x}$ the unknown DOF. $\mathbf{f}_e$ and $\mathbf{f}_{\mathrm{nl}}$ express the external excitation and nonlinear efforts, the latter corresponding to the nonlinear contact forces arising from the friction joints. The aim of this section is to present the general and most common ways to solve Eq. (1). Considering that in a realistic finite element modelling of an industrial structure, the number of DOF may be very large, some kinds of reduction techniques are required to simulate the dynamics in an

acceptable amount of time. Some of the reduction techniques existing in the literature were constructed from specificities offered by spectral methods. This section hence first introduces details on possible solution methodologies, with special attention paid to the harmonic balance method, before illustrating some recent reduction approaches adapted to this kind of problem.

4.1. Solving the nonlinear ODE

Two main approaches exist to solve Eq. (1): numerical time integration or methods that directly search for the stationary regime.

Numerical time integration techniques possess a primary advantage in their capability to handle diverse systems and nonlinearities without assumptions regarding the form or characteristics of the solution. These methods involve the resolution of Eq. (1) through a sequential iterative process starting with some a priori chosen initial conditions to simulate the evolution of the dynamics with time. The choice of initial conditions has a major influence on the solution reached by the solver as the scheme will naturally tend to stay within the same basin of attraction. It practically means that the solution to which converges the numerical integration depends on the initial conditions.

Integration methods are broadly categorised into explicit and implicit schemes.[1] Explicit schemes compute the current system response based on prior steps and often necessitate smaller time steps to ensure numerical stability [99]. For instance, the widely recognised Runge–Kutta algorithm [100] operates as an explicit scheme. In contrast, implicit schemes derive the current response based on both the present and previous steps. While most implicit schemes demonstrate unconditional stability in linear systems, they typically demand increased storage capacity and higher computational efforts compared to explicit solution strategies. There exist several implicit methods, such as for instance the Newmark scheme [101] or the Houbolt method [102]. A general review of numerical time integration can be found in [103] and some useful information for practical implementation in [104]. In [105] a series of time-marching methods tailored to friction-induced nonlinearities with a specific focus on turbomachinery applications was proposed.

If the objective is finding the solution (or at least *one* particular solution) describing the steady state reached after time, numerical time integration is not the best choice as it may require too great a computational effort for a system with a large number of DOF to calculate all the transient period. This justifies the limited use of these approaches in investigating nonlinear vibrations of structures with friction damping. The direct search for a static equilibrium state can be performed by a Newton–Raphson algorithm solving the equation $\mathbf{K}\mathbf{x}+\mathbf{f}_{\mathrm{nl}}(\mathbf{x}) = \mathbf{f}_{\mathrm{e}}$. In aero-engine applications, and more specifically in the simulation of structures with dampers, this step corresponds to solving

---

[1] There also exists a combination of both, known as the *Implicit–Explicit Method* [98].

for the pre-stressed structural state induced by centrifugal effects that apply normal forces on the different interfaces. In this expression, the possible linear part of the contact forces is implicitly included in the **K**-matrix. As the dissipation mechanism induced by friction depends on these normal forces, calculation of the pre-stressed state is therefore essential in the correct prediction of the underlying dynamics.

A direct search for a periodic steady state is possible by assuming a priori the periodic form of the solution and looking for only a solution of this kind. The shooting method, for instance, will iterate on the initial conditions and look for the periodicity condition to be satisfied after a single time period integration. Shooting techniques have been used widely in friction related applications, see for instance [106,107]. Another approach is to use a Galerkin procedure known as the Harmonic Balance Method (or HBM) that employs the Fourier basis as both base and weight functions. For this mean, the DOF $\mathbf{x}(t)$ are expanded on a Fourier basis and substituted in Eq. (1). The residual error is then orthogonalised (i.e. minimised) with respect to the same basis by projection. This results in the following algebraic system of equations to solve:

$$\mathbf{Z}(\omega)\hat{\mathbf{x}} + \hat{\mathbf{f}}_{nl}(\hat{\mathbf{x}}, \omega) - \hat{\mathbf{f}}_e = \mathbf{0} \qquad (2)$$

In this equation, $\hat{\mathbf{x}}$ are the unknown Fourier coefficients of the DOF, $\mathbf{Z}$ is the block diagonal multi-harmonic dynamic stiffness matrix function of the structural matrices ($\mathbf{M}$, $\mathbf{C}$ and $\mathbf{K}$) and also function of the frequency ω that defines the periodic solution, which is generally equal to the forcing frequency. The terms $\hat{\mathbf{f}}_{nl}(\hat{\mathbf{x}}, \omega)$ and $\hat{\mathbf{f}}_e = \mathbf{0}$ are the Fourier coefficients of the nonlinear forces and external forces, respectively, obtained during the projection step of the Galerkin procedure. The numerical evaluation of $\hat{\mathbf{f}}_{nl}(\hat{\mathbf{x}}, \omega)$ can be challenging. The most common approach is to use the alternating frequency/time (AFT) scheme [108] on regularised contact laws. These are required for convergence, although this inherently involves some discretisation errors and approximation. Another method, also based on frequency/time alternation, is the Dynamic Lagrangian Frequency Time (DLFT) [109]. It relies on a prediction–correction process to determine the contact state and associated forces. Because of this process, the DLFT can accurately verify non-regular contact laws and ensure non-interpenetration between the bodies in contact. A comparison between the DLFT formulation and a friction model based on normal and tangential stiffnesses is given in [110]. A detailed review of various strategies for handling nonlinear forces can be found in [21]. The HBM has been largely employed for its efficiency and robustness in solving for the periodic solution of nonlinear ODE, especially in the application of bladed disks with friction interfaces [35, 111–116].

Since several solutions may co-exist due to the nonlinear effects, the Newton–Raphson algorithm used to solve Eq. (2) may or may not converge towards (only) one of them, depending on the initialisation and accuracy of the descent direction used in the algorithm. To improve the latter, providing the solver with an analytical expression of the Jacobian matrix is particularly useful, see for example in [37] for the detailed expression in the case of a regularised Coulomb law. Numerical path continuation methods will provide convergence towards a particular solution and also make it possible to retrieve unstable ones. One can refer to [117–121] for different approaches and an explanation of their numerical implementation. By varying a parameter defined as the continuation parameter, for instance the rotational speed or the excitation frequency, each of these solutions will form a solution branch. In practical numerical solution procedures, one usually initiates the continuation scheme far from a resonant peak, in a region where nonlinear effects are negligible. Then, following and constructing step by step a solution branch as the continuation parameter varies, it is possible to detect possible bifurcations [122,123], switch to other solution branches [124–126] and assess their stability [127,128] in order to simulate a larger scope of possibly reached steady states.

4.2. Reduced order modelling

To conduct quantitative analyses on larger industrial numerical models, it has proved necessary to use model reduction techniques. Among these methods, one encounters classical Galerkin projection approaches including component mode syntheses that could be applied to any kind of structures, and some specific techniques relevant only to systems showing cyclic symmetry properties.

4.2.1. General approaches
Condensation. The simplest technique to reduce the size of an algebraic system with some nonlinear DOF (for instance Eq. (2)) involves using a condensation method. Particularly useful when the nonlinear effects are localised, this approach leverages the fact that only a small subset of the problem's DOF is affected by the nonlinear terms. The method partitions the unknown vector, $\hat{\mathbf{x}}$ in Eq. (2), into two parts and isolates the nonlinear DOF, those directly involved in the term $\hat{\mathbf{f}}_{nl}$ from the purely linear DOF. By a simple matrix inversion, it then becomes possible to express the linear DOF in terms of the nonlinear DOF. This form is substituted into the other part of the equation to find a new, significantly reduced-size algebraic equation whose size is equal to the number of nonlinear DOF in the problem. In cases where the nonlinear terms are expressed in terms of relative variables, as in most friction problems in which laws involve a node-to-node contact formulation, it is also possible to condense the relative DOF. These straightforward condensation techniques have, for example, been used in [32,41,129–135] for bladed disk finite element models.

Note that these condensation methods do not involve approximation: they simply entail rewriting equations to streamline the nonlinear solver. Conversely, the Galerkin projection approaches mentioned later on are approximations that involve information loss during the transition to the reduced model.

Galerkin projection. The primary idea behind the Galerkin projection reduction method is to seek an approximate solution to the dynamic problem as a linear combination of a reduced-size basis relative to the initial space. This involves expressing $\mathbf{x}(t)$ as $\mathbf{x}(t) = \boldsymbol{\Phi}\mathbf{q}(t)$ in the equation of motion (1) and then projecting the resultant onto the reduced space. The classical reduction on a linear modal basis is part of these Galerkin methods. The form of the resulting equation is similar to the un-reduced equation, allowing for the use of previously described solution-seeking and periodic solution methods to find $\mathbf{q}(t)$, and then to backtrack to $\mathbf{x}(t)$. The primary challenges lie in choosing the reduction base $\boldsymbol{\Phi}$ and computing the projected nonlinear terms on the new base $\boldsymbol{\Phi}^{\mathrm{T}}\mathbf{f}_{nl}(\boldsymbol{\Phi}\mathbf{q}, \boldsymbol{\Phi}\dot{\mathbf{q}})$. Poor handling of the reduced nonlinear efforts assessment may result in overestimation or underestimation of the nonlinear effects, leading to a flawed behaviour of the reduced model. The direct approach to compute these nonlinear forces involves simply projecting the nonlinear term onto the reduction basis, akin to the treatment of linear matrices in the system. This method may require manipulating large quantities when the number of DOF is substantial. Sometimes, a spectral substitution technique can be employed to replace this nonlinear term with a previously calculated nonlinear mode, see [37].

To build a reduced base through linear transformation, linear modes can be associated with their modal derivatives [136], companion modes (or dual modes) [137], or even nonlinear modes (see [138,139] for more details on their interpretation and calculation). It may also be possible to use constraint modes [140], hybrid modes [141], or a single dominant mode supplemented with static stiffness matrix compensation [142]. When adopting nonlinear modes, the change of variables between the bases remains linear, but the amplitude of the additional modes changes with frequency. The modal deformation is then evaluated at each frequency iteration from a backbone curve representing the pre-calculated nonlinear mode. This nonlinear modal synthesis, initially proposed in [143], was later extended to non-conservative
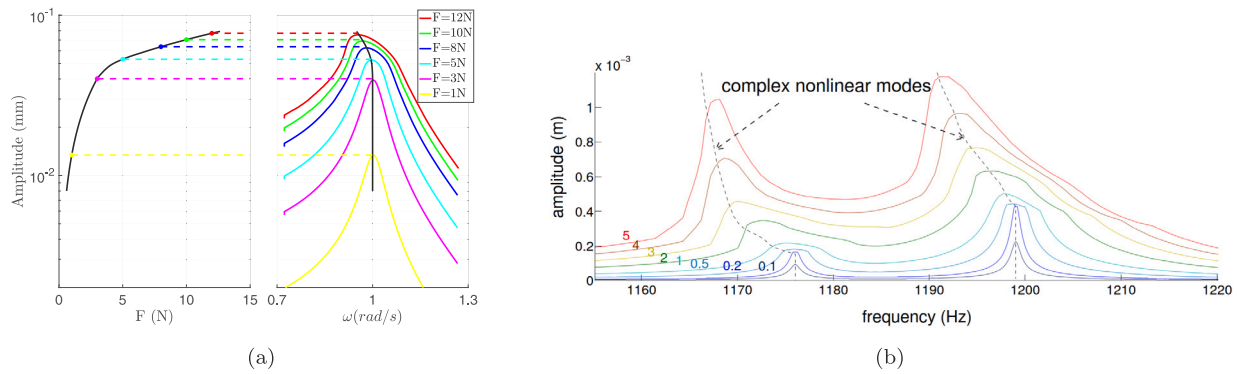
Fig. 6. Nonlinear modes and FRFs for different forcing amplitudes: (a) FEM of a fan system [146] and (b) lumped parameter model of a mistuned structure, adapted from [147].

systems [111] and was further developed by Krack et al. for the calculation of nonlinear modes with multiple harmonics [144]. These two approaches, developed within a framework of synthesis with a single nonlinear mode, were generalised to a multi-mode synthesis without assuming mode orthogonality in [37]. One of the limitations of these methods is that the projected nonlinear forces are substituted without coupling via other modes, preventing the ability to simulate internal resonances. A relatively similar approach introduced "response-dependent nonlinear modes" to enhance the projection basis [145]. It proposes a structural modification using the Dual Modal Space method to reduce the computational effort in evaluating nonlinear effects. The complex nonlinear modes defined in [111] represent a pseudo-periodic solution of the autonomous system (1), that is, with $\mathbf{f}_e = \mathbf{0}$, yet allowing for dissipative nonlinearities, contrasting with the nonlinear (real) normal modes [139].

The calculation of nonlinear modes can also be useful to avoid frequency forced responses simulations and save computation time as they can depict the loci of the resonant response for a given energy input without having to simulate an entire solution branch. Recent studies have been dedicated to this concept, showcasing its efficiency in analysing systems of both academic and industrial complexity. For example, nonlinear modal analysis has been applied to simulate the response of turbines with underplatform dampers [36], blisks with ring dampers [135] and fan blade systems with dovetail joints [146]. The relationship between nonlinear modes and forced nonlinear frequency response is illustrated in Fig. 6(a) for a FEM of a fan system with dovetail joints and in Fig. 6(b) for an academic model of a mistuned system with blade root friction. For a given excitation forcing level, the vibration amplitude corresponding to the forced resonance response can be identified through the knowledge of the nonlinear mode.

Component mode synthesis. Component Mode Synthesis (CMS) reduced order models are particularly adapted to structures composed of several components (or sub-structures) assembled at interfaces [148,149]. Each sub-structure can be reduced using the above-mentioned techniques and coupling at interfaces is accounted for by adding static modes, associated with the nodes retained within the interface of each sub-structure, to the global reduction basis. The number of dynamic modes retained is chosen based on a conventional frequency criterion. After this reduction, only generalised coordinates of the reduced substructures and the DOF associated with the nodes within interfaces remain. Depending on the boundary conditions applied to the interface while treating a separate sub-structure, CMS approaches can be classified into free [150,151], fixed [152,153] or hybrid interface methods [154,155]. An assessment of these techniques for assembled structures with friction interfaces can be found in [156]. The Craig–Bampton method [153] is known as one of the most popular fixed interface CMS approaches because of its efficiency. Its extension to account for nonlinear effects incoming from frictional interfaces in bladed disks was performed in [129] by adding complex nonlinear normal modes, computed with a fixed interface, to the reduction basis of the blade sub-structure.

Interface reduction. CMS approaches present a significant limitation for structures with a high mesh density at the interfaces as they result in a reduced model that maintains an excessive number of physical coordinates linked to sector boundaries. To overcome this issue, given the assumption that the model retains an excess of information, double component modal synthesis approaches have been devised [157] to filter out the dynamics of the interfaces and retain only the necessary information according to the calculation requirements. It is based on the concept of interface mode [158]. For this purpose, after reassembling the complete structure via the boundary nodes (which have been retained so far in the Craig–Bampton procedure) to form the reduced mass and stiffness matrices of the entire system, the sub-blocks corresponding to the boundaries are then extracted from the reduced matrices, and the corresponding modes are computed. The reduction of the interfaces is performed by selecting certain eigenvectors used as a reduction basis for the boundary degrees of freedom. This selection can be based on a frequency criterion, retaining only the modes whose frequencies are of the same order as those of the fixed-interface modes preserved for the creation of the super-elements [153]. These retained modes are sometimes referred to as partial interface modes [159] or branch modes [160]. Combining a nonlinear component mode synthesis and reduction of the cyclic symmetry interface, Joannin et al. [129] simulated efficiently nonlinear forced responses of a realistically meshed bladed disk with friction nonlinearities.

The general technique mentioned above is well suited when the interface forces acting between sub-structures are linear. Other methods were developed especially to reduce frictional interfaces that require a high level of discretisation to capture singularities, see for instance [149,161,162]. More recently, adaptive component mode synthesis [163] has been proposed and validated for fan blade systems through a reformulated equation of motion by introducing an internal penalty variable depending on the online contact condition. In recent years, reduction techniques of increasing complexity [164–168] have been introduced, aiming to exploit the piecewise linearity of friction states (i.e., stick, slip, and lift-off). Despite the reduced size of the system, the computation of nonlinear forces is still performed in full-space, resulting in substantial online computational costs, especially for high-fidelity modelling of joints requiring a large number of contact nodes. To address this drawback, hyper-reduction techniques have emerged [32,168,169], which evaluate nonlinear forces in the reduced space, further decreasing the computational burden.

4.2.2. Approaches specific to rotationally cyclic structures

The cyclic symmetry of bladed disks can also be used to reduce the size of the problem to solve. The original method that simplifies the analysis of cyclic symmetric structures primarily stems from the work of Wildheim [170] and Thomas [171], extending the study conducted in [172], where the structures considered were infinitely long linear chains of identical substructures. For more in-depth insights, a reference such as [173] discusses the transformation from complex cyclic components to real cyclic components.

The general method for obtaining the equation of motion in a cyclic basis involves applying a change of variables between physical DOF and cyclic components (via a discrete spatial Fourier transform) and relies on the concept of continuity between sectors. With a partitioning of physical DOF into internal and boundary ones, it may be possible to retain only the structural matrices of the reference sector in the equation of motion projected into the cyclic basis. After projection, partitioning, and imposition of boundary conditions, the resulting structural cyclic matrices are block-diagonal (due to the orthogonality of the Fourier basis). By this means, all the physical quantities of a cyclically symmetric structure can be described using a cyclic basis with cyclic components defined over the reference sector and a harmonic index, or spatial wave number, often called *nodal diameter*. In a linear and perfectly tuned system, the change to cyclic coordinates allows decoupling the system by each nodal diameter.

Nonlinear forces introduce coupling among the different nodal diameters via higher time or space harmonics and very few procedures exist to reduce the nonlinear dynamics of a cyclically symmetric structure. Most studies on this subject, for example [173,174], solve the complete nonlinear system without using the advantages offered by cyclic periodicity. In 2004, Petrov [175] assumed the displacement of a cyclically symmetric structure subjected to wave type excitation to have the same form as the excitation. He then achieved reduction by reducing the complex dynamic stiffness matrix arising from the HBM application. This assumption has been employed in the literature, among other things, for studies on the influence of contact zones [176] or wear [85] on the system's dynamics. In practice, depending on the form of the external excitation, it is possible that not all the cyclic components will be coupled by nonlinear forces. The method developed in [177] theoretically demonstrates which cyclic components will actually be coupled when the structure is subjected to a waveform excitation. Focusing only on the corresponding harmonics then further reduces the size of the system to be solved while removing the restrictive assumption imposed by the solution's form.

Given the highly specific issue posed by blade mistuning in the context of turbomachinery, several reduction approaches that deal with the effect of mistuning have been developed [178–184]. Furthermore, the consideration of both nonlinearities and mistuning within numerical simulations remains a major challenge that no existing technique appears to effectively address. Hence, the development of new methods to tackle this challenge has been identified by Castanier and Pierre [3] as one of the significant endeavours for bladed disk design, and this has been the subject of recent research [37,185–189].

5. Experimental testing

Due to the complex nature of dry friction, the dynamic design of friction-damped turbine blades still relies heavily on experimental verification. Numerical models (see Section 3) used during the design phase rely on assumptions/approximations[2] and thus need tuning against experimental evidence, often gathered on purposely developed test rigs. These test rigs are a vital part of the research in the friction damping field, as they offer experimental evidence in a controlled laboratory environment which is used not only to tune, but also to validate the numerical models later used as design tools. Over the years, different research groups across the globe have designed, produced, calibrated and tried out a large number of rigs. The main purpose of this section is to highlight the key challenges common to these test rigs, review the solutions adopted, and discuss the trends and key developments.

The experimental work related to friction-damped structures subjected to dynamic loading can be classified into three main categories:

1. Test setups that concentrate on the **contact mechanics of individual interfaces**, with the goal of estimating calibration parameters required for contact models.
2. Test setups designed to replicate the **dynamics and/or mechanics of gas turbine components**, with the aim of validating numerical models and assessing the effectiveness of specific friction dampers.
3. Test setups that pursue **both** objectives above, involving the monitoring of structure dynamics while simultaneously observing the contact interfaces.

Section 5.1 focuses on the first kind of test rigs, while Section 5.2 focuses on the second and third kind of test rigs.

5.1. Contact interface characterisation

The ability to accurately predict the dynamics of friction-damped structures is hindered by the challenge of integrating suitable models for contact interfaces. As discussed in Section 4, numerical models typically aim at reproducing the hysteresis-like behaviour observed at the contact, by introducing additional stiffness and damping parameters. Such parameters are often formulated in terms of tangential and normal contact stiffness, k_t and k_n, and friction coefficient μ. While the normal contact stiffness k_n is typically estimated using analytical and/or numerical formulations [46,190,191], k_t and μ are estimated starting from hysteresis curves (see Fig. 7) measured in controlled conditions on purposely developed test rigs. Hysteresis measurement and contact mechanics represent extensive research fields. This section focuses on the test rigs developed to target turbomachinery applications, where specific materials and operating conditions are of interest. In detail, this section will focus on the latest efforts of research groups active in the field. Additional notable works, related to other applications (e.g. bolted joints [192–194], brake squeal [195,196], static metal seals [197], torsional fretting [198], low and ultra-low friction systems [199]), share some features with the presented test rigs but are beyond the scope of the present review.

5.1.1. The test rigs

In gas turbine applications, obtaining hysteresis data is crucial for various materials and combinations, spanning a broad spectrum of temperatures, normal load, amplitudes within slipping regimes, and considerations related to the running time and wear-dependent properties. To address these requirements, these test rigs were specifically designed for measuring hysteresis properties within a nominal contact zone or area. The gathered data were subsequently integrated into finite element models appropriately scaling the contact stiffness information. Since the nominal contact area is here used as a "representative unit", its configuration should be meticulously controlled, incorporating not only general features such as material, presence of coating, etc., but also specific details such as the applied normal load, the surface finish of the contact region, the spectrum of slippage amplitudes, the frequencies of cyclic loading and the contact area nominal extension. This last feature can be numerically evaluated for flat-on-flat interfaces only, while it is theoretically zero for hemispherical-on-flat interfaces and a simple line for cylinder-on-flat interfaces.

All these test setups have a set of shared objectives:

- to apply a normal load N between a pair of specimens;
- to generate tangential loading either via controlled displacement or controlled force on one side of the contact;
- to measure the tangential resisting force T on the opposite side;
- to measure the relative displacement between contact surfaces.

Although the objective remains constant, the design choices vary among the different rigs. An initial comprehensive examination of these test rigs is available in [200]. Table 1 seeks to revise this review with the most recent contributions, emphasising crucial aspects related to

---

[2] Approximations are also introduced by certain solution techniques, as discussed in Section 4. However, these will not be addressed further in this paper.
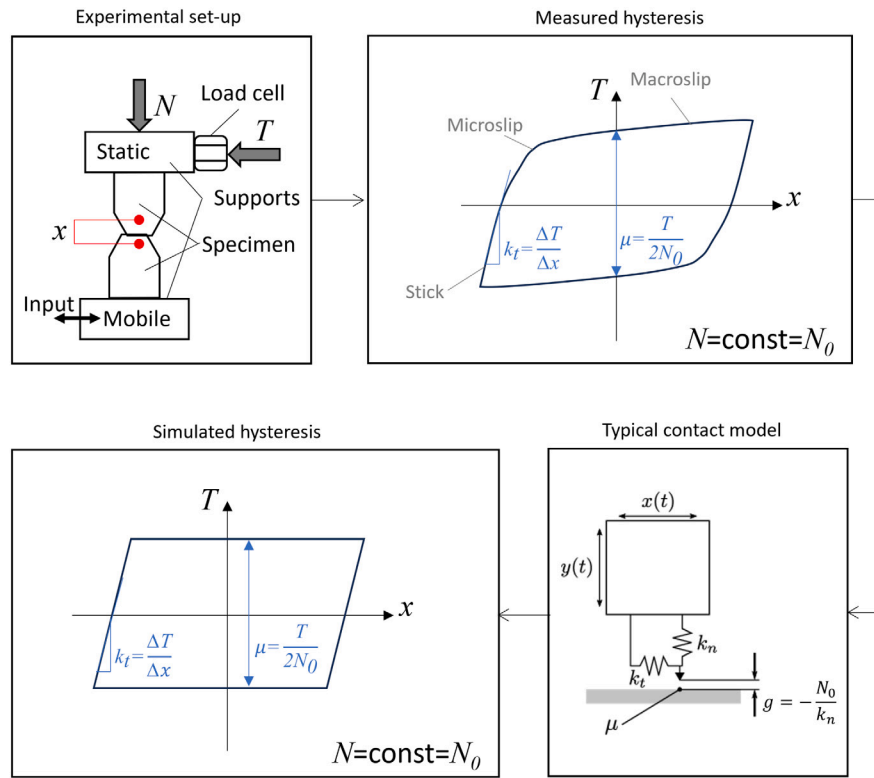
Fig. 7. Graphic representation of the link between a measured and simulated hysteresis cycle.

Table 1
Main features of the test rigs dedicated to the experimental characterisation of contact interfaces for turbomachinery applications.

References	[201]	[202]	[59,203]	[204]	[205]
Contact configuration	Flat-on-flat	Flat-on-flat	Flat-on-Flat Cylinder-on-Flat	Flat-on-flat	Sphere-on-flat
Nominal contact area	Square [1–1.4] mm^2	Two rect. patches [25–100] mm^2	Two rect. patches [5–50] mm^2	Two rect. patches [6,18] mm^2	Sphere radius: 6 mm
Nominal contact pressure/load	<500 MPa	[20–200] MPa	[1–30] MPa	[1–35] MPa	<4700 N
Frequency	<200 Hz	<10 Hz	<300 Hz	<80 Hz	<2 kHz
Sliding amplitude	< 100 μm	[20–500] μm	< 150 μm	< 50 μm	<2 mm
Temperature	<800 °C	<900 °C	<1000 °C	Room temperature	Room temperature
Tangential Excitation	Shaker	Hydraulic actuator	Shaker	Piezoelectric actuator	Shaker
x measurement	Two LDVs	DIC	Two LDVs	One LDV	One LDV
T measurement	Piezo force transducer	Strain force transducer	Piezo force transducer	Strain force transducer	Piezo force transducer
N application	Pneumatic actuator	Hydraulic actuator	Deadweights	Piezoelectric actuator	Piezoelectric actuator
N measurement	-	-	-	Strain force transducer	Strain force transducer
Temperature application/control	Furnace	Not disclosed	Induction with thermocouple feedback	-	-

measurement and motion techniques. It should be noted that, over the years, some of the research groups have designed different generations of test rigs. In this instance, the earlier versions (fully described in [200]) have been omitted, as they have been surpassed by their successors.

Effectively producing and measuring hysteresis cycles pose a series of challenges which have been faced in different ways by the different research groups. In the following a few of these challenges are analysed, highlighting the pros and cons of each adopted solution.
The selection of contact interface geometry significantly influences contact parameters and the dispersion of estimated results. The sphere-on-flat contact is less susceptible to uncertainty, making it suitable for

exploring test rig functionality and assessing the impact of variables such as normal load variation [205]. However, as the focus shifts to interfaces commonly found in turbomachinery friction dampers, a natural progression to "flat-on-flat" and "cylinder-on-flat" contacts is anticipated. The "flat-on-flat" interface, a prevalent choice, is notably influenced by surface morphology and aligning systems. While many test rigs for flat-on-flat interfaces employ a rigid aligning system, the strategy presented in [203] advocates a "self-aligning" system. In this setup, the specimen with two contact tracks is free to rotate around two axes, unaffected by factors other than the normal load, providing a condition closer to the actual working environment. The choice between a rigid or self-aligning system depends on the test's

purpose [206]. For more repeatable tests, a rigid setup is preferred, while a self-aligning system is recommended for testing complex and larger interfaces. An essential consideration highlighted by various research groups is the design of flat-on-flat contact interfaces. Both the mobile and fixed contact surfaces should have the same width along the sliding motion direction. Failure to meet this condition may result in the shorter specimen wearing a groove within the wider one, leading to a hardening effect in the hysteresis [203].

Tangential excitation is crucial for inducing relative motion between specimens and, consequently, generating friction force. Closed-loop actuation mechanisms, whether force or displacement-based, are commonly employed. The shaker is the preferred choice for high-frequency measurements; however, careful dynamic design of the test rig structure and its joints must be consistently conducted to ensure that the resonance frequencies of the rig are well above those of the measurements.

The application of the normal load N is intricately tied to the test rig's purpose. Stable application of a constant normal load, with built-in measurement capability, can be achieved using actuators or simple deadweights. Rigs operating under a constant normal load, with the goal of attaining high contact pressure, often opt for pneumatic or hydraulic actuators [201,202]. For rigs designed to apply a normal load varying harmonically around a mean value, a piezo actuator is the preferred choice [204,205].

Accurately measuring the contact force T (and N in [204,205]) involves not only selecting suitable force sensors but also ensuring a smooth force transfer, while preventing potential compensation or misalignment issues arising from the test rig structure. Piezo-based force transducers are the preferred choice for test rigs aiming to achieve higher frequency measurements. These sensors are affected by the volatility of the electric charge, posing challenges in attaining long-term stable measurements. This is not a limiting factor if the goal of the measurement is related to assessing properties such as contact stiffness or dissipated energy (i.e. area of the cycle), as an incorrect assessment of the mean value of T would not change the result. The correct assessment of the mean value of T becomes essential when considering the presence of multiple static equilibria under the same nominal conditions, as further discussed in Section 6.2.1. Measurement of the normal force N is accomplished through a strain force transducer. This selection is justified by the superior long-term stability of strain force sensors compared to piezo-based force transducers. This stability is crucial for accurately capturing the stable mean force value. It is important to note that the softer structure of the strain force transducer comes with a limitation in suitability for high-frequency measurements. The force-transfer mechanism from the contact to the load cell(s) is another crucial aspect, as discussed previously. Various structural approaches, such as elastic beams, three-claw stabilisers, and tripods, have been employed to ensure high stiffness, perfect alignment, and the transfer of forces without introducing spurious components.

Measuring the relative displacement at the contact x is crucial for accurately capturing hysteresis and subsequently estimating the tangential contact stiffness k_t. There appears to be a consensus among various research groups favouring techniques such as Laser Doppler Vibrometers (LDV) or Digital Image Correlation (DIC). Both methods ensure an adequate resolution when measuring within a low displacement range, i.e. [0.1–2] μm, typically corresponding to a fully stuck condition, a prerequisite for estimating tangential contact stiffness. The necessity for high-precision measurement techniques is underscored by a comparison between DIC and a linear variable differential transformer in [202]. Additionally, the definition of "relative displacement" itself is noteworthy. In certain test rigs, only the displacement of the moving specimen is measured, assuming the compliance of the test rig connected to the fixed specimen is negligible. While this approach may be suitable for specific test rig architectures, it is not universally applicable, as demonstrated in [202]. Opting for a differential measurement, either with DIC or using two LDVs positioned as close as possible to the contact, appears to be the safest choice.

The effect of wear has been observed in all test rigs, to various degrees. In detail, hysteresis properties exhibit a significant dependence on overall slipping time, closely tied to the wear of the contact zones. Some research groups incorporate within their measurement protocol, besides μ and k_t which can be recorded as a function of the number of cycles, other wear-related parameters, e.g. the possibility of measuring the wear volume history of the same pair of specimens with a negligible perturbation to the wear processes [203].

The influence of frequency does not appear to be significant, particularly within the 20–100 Hz range. While higher frequency measurements offer advantages for assessing wear, they also bring about a greater influence of the test rig itself. As the frequency increases, the signals tend to become more disrupted, posing challenges for accurate evaluation.

Real time contact state detection is a recent focus of research in the field of single interface testing. Recent works have used ultrasound [207] and total internal reflection [208] to detect in real time the effective contact area and contact state of non-transparent and transparent samples respectively using the test rig detailed in [201].

5.1.2. An overview of published results

Several rigs have been designed, constructed, and used over the years to measure hysteresis cycles of friction contacts. A quantitative comparison of results is not always possible due to the large variety of test conditions (contact interface geometry, materials, temperature, etc.), and the fact that the influence of each variable on the contact parameters is not known with precision. Nevertheless, a number of common features and trends have been observed and are summarised below:

- **Hysteresis Shape.** A positive slope of the macroslip portions of the hysteresis cycles depicted in Fig. 7 (unexplained by a Coulomb-type friction model) is often observed. Furthermore, the macroslip portion of the cycles may exhibit fluctuations, which stem from interactions among wear scars, often traceable to a ridge being formed at each end of a multi-cycle test run [198].
- **Friction Coefficient**. This parameter exhibits remarkable stability, as consistent outcomes are observed when testing the same material on various rigs. Results from the Polito-Imperial round robin on steel-on-steel specimens [209] showed variations within a 15% range. Generally, for flat-on-flat interfaces in steel-on-steel and other materials used in turbomachinery, μ ranges from 0.4 to 0.8 at room temperature, with most values falling within the [0.6–0.7] range [198,201,202,210]. At temperatures exceeding 200 °, μ decreases to [0.2–0.3] [200,201,211]. No major influence of parameters such as worn area of contact or normal load have been observed.
- **Contact stiffness**. The k_t values are much more scattered, with discrepancies up to 70% between the same experiment on different rigs [209]. Nevertheless, a dependency on the worn area A_w, rather than the commonly practiced nominal area, has been evidenced in [209] for flat-on-flat contacts. This relation has been here confirmed using the results published in [204], as evidenced in Fig. 8. A further confirmation of this dependence is given by the fact that k_t was observed to gradually increase during the test due to the expanding worn contact area. Normalised contact stiffness k_t/A_w, is notably lower in hysteresis loops with macroslip than in fully stuck hysteresis loops measured at lower displacement amplitudes. This decrease in loops with macroslip is attributed to a reduced time for the ageing of asperity contacts at higher velocities, indicating a velocity dependency [209].
- **Harmonic variation of normal load**. The use of a harmonic normal force results in non-uniform energy dissipation, leading to a rougher worn surface, while under constant normal force, the worn surface tends to flatten. This variation also influences the evolution of contact parameters, which exhibit a continuous
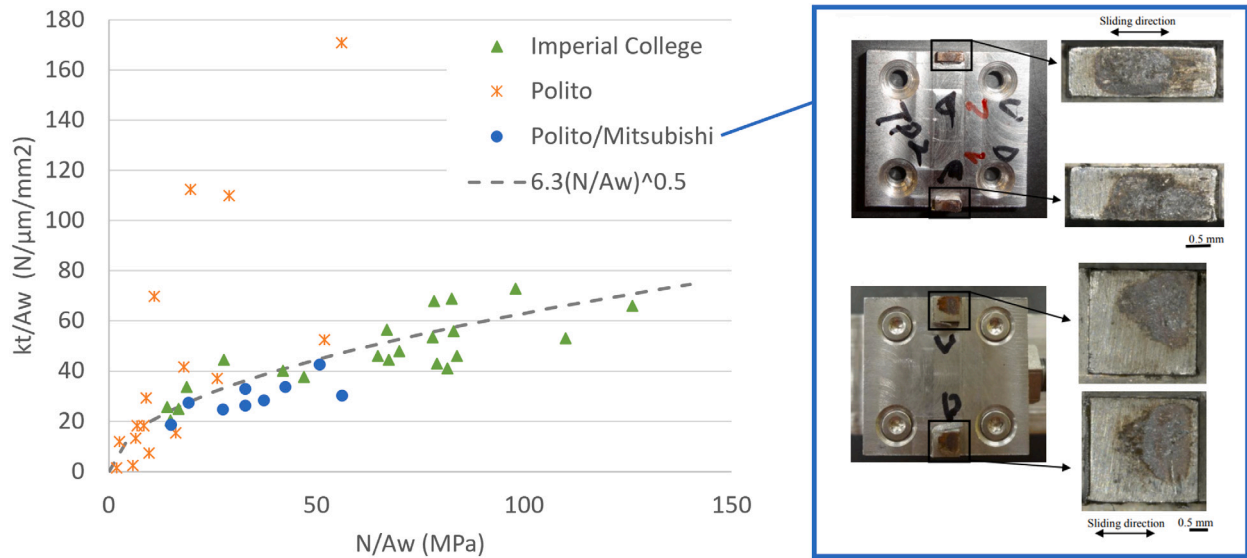
Fig. 8. Tangential contact stiffness k_t normalised by the worn area A_w versus N/A_w.
Source: Adapted from [209] with the addition of results from [204].

Table 2
Main contributions found in the literature on experimental characterisation of friction damping devices for turbine disks.

Friction damping device	References
Blade root	[9,12,75,76,78,112,213–222]
Underplatform damper	[63,88,216,223–232] [62,64,79,212,233–243]
Mid-span damper	[244–246]
Tip damper	[247,248]
Blade shroud	[87,249–259]
Ring damper	[260]

evolution due to the fluctuations in interface conformity [205]. While the normal load is typically constant for shrouds and blade roots when the rotational speed of the disk is constant, this investigation is particularly relevant in the case of dampers [212]. Here, the inclined contact surface, combined with the damper kinematics, produces a harmonic variation of both tangential and normal contact forces even at constant disk rotational speed.

5.2. Friction damping devices

This section is devoted to test setups designed to replicate, in a controlled environment, the dynamics and/or mechanics of gas turbine components. Test setups that include friction damping elements such as dampers and shrouds are commonly employed to validate numerical models or assess the effectiveness of a particular damping device. Table 2 provides an overview of key references detailing the construction of these test setups and the corresponding outcomes. The references are categorised based on the type of friction damping device investigated by the test rig.

5.2.1. Common features and challenges

While the forthcoming sections will highlight variations, these test setups share common objectives:

- to ensure normal preload at the contact;
- to provide excitation and/or enforce appropriate kinematics;
- to measure relevant quantities, either on the blade(s) and/or at the contact.

The execution of these tasks may differ based on the test rig configuration, whether rotating or non-rotating, leading to distinct challenges. Several examples for each task are discussed below.[3]

- **Normal preload at the contact** may be provided by the centrifugal effect in rotating test rigs, as in real working conditions, but often the scale of laboratory testing in terms of disk dimension and rotational speed results in contact pressures which are below those actually experienced in operating conditions. Non rotating test rigs provide the contact preload often using deadweights; in this case the resulting pressure distribution may be different from the one provided by centrifugal load.

- **External excitation** is typically provided in non-rotating test setups utilising a shaker. This choice offers flexibility to explore a broad range of excitation levels from full stick to gross slip. Despite its widespread adoption, the shaker is not free from drawbacks. Since the shaker needs to be mechanically attached to the structure, it is almost impossible to avoid some sort of interaction between them. Depending on a number of factors such as the location and kind of stinger, excitation level etc., the structure under scrutiny may physically push back against the shaker attachment, producing non-fundamental harmonic content in the force measured by the load cell, entailing the need for specific shaker models at the validation stage [261,262]. Another important point to consider when selecting the test rig configuration is the mode shape of the structure. The kinematics in a non-rotating setup, where a complete disk is not represented (e.g., two blades with an interposed damper), are limited to pure In-Phase and Out-of-Phase modes. While this does not constitute a limitation if the purpose of the test rig is validation, it does prevent the direct assessment of the friction damping performance in an extensive set of working conditions. In contrast, classical rotating rigs often employ air jets on blades for excitation. While this may not induce a full-slip situation in all cases, it allows for exploring additional inter-blade phase angles [263]. The preferred choice in newly designed rotating set-ups is piezoelectric actuators, as in [264], which, compared to air-jets ensure a better control on the amplitude of excitation. An additional, less common test set-up, comprises a complete disk in a non-rotating configuration,

---

[3] This discussion is not exhaustive, and a comprehensive overview is provided in subsequent sections for each specific damping device.
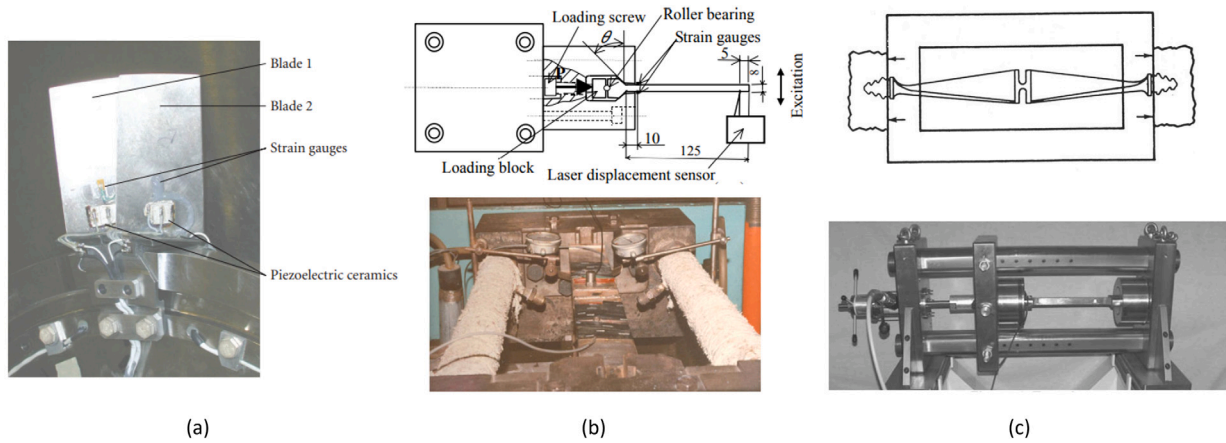
Fig. 9. Test set-ups used to investigate blade root damping. (a) Rotating configuration from [112]. (b) Non-rotating single blade configurations from [78] (preload from loading screw) and [265] (preload from thermal shrinkage). (c) Non-rotating double blade configurations from [213,214].

Table 3
Features of test set-ups focusing on blade root damping.

References	Set-up	Preload	Excitation	Measured Quantities
[12]	Non-rotating	Clamps	Vibrating table	Dissipated Energy
[75]	Non-rotating	Spring-loaded wires	Shaker	Blade dynamic response η
[76]	Non-rotating	Loading screw	Vibrating table	Blade dynamic response η
[213]	Non-rotating	Thermal Shrinkage	Strikers	Blade dynamic response δ
[214]	Non-rotating	Hydraulic cylinder	Impulse Hammer Resonance Electromagnet	Resonance frequency η, Q
[112]	Rotating	Centrifugal effect	Piezo actuator	Dynamic response ζ
[216]	Rotating	Centrifugal effect	Piezoelectric exciters	Dynamic response ζ
[78]	Non-rotating	Loading screw	Shaker Platform	Dynamic response ζ
[265]	Non-rotating	Thermal Shrinkage	Shaker	Dynamic response η
[217]	Non-rotating	Hydraulic cylinder	Hydraulic cylinder	Load–Stress curve
[218]	Non-rotating	Hydraulic cylinder	Impulse Hammer Resonance Electromagnet	Dynamic response
[219,220]	Non-rotating	Loading screw	Impulse Hammer Shaker	Dynamic response
[80] [221]	Non-rotating	Hydraulic cylinder	Shaker	Contact parameters η
[222]	Non-rotating	Hydraulic cylinder	Shaker + Electromagnet	ζ

where the excitation is given by electromagnets, generating a travelling wave.

• **Measurement of relevant quantities** includes the dynamic response of the structure and, less frequently, the force–displacement hysteresis at the contact. Dynamic response measurements are easily obtained with accelerometers or laser scanning in non-rotating setups. Rotating rigs, often placed in spin-pits under vacuum, are less accessible, making tip-timing and strain gauge measurements more common. Force–displacement hysteresis measurements are currently feasible only in non-rotating rigs.

5.2.2. Blade root

Table 3 summarises the main features of all the test set-ups designed to investigate blade root damping. Three main **architectures** can be identified and are represented in Fig. 9 and are closely connected with

the strategy used to ensure the **preload** at the contact. In rotating set-ups [112,216] the load is guaranteed, as in real conditions, by the centrifugal effect. Non-rotating test set-ups can be further differentiated into single or double blade configurations. Statically pulling a single blade does introduce an additional source of damping due to the contact between the blade and the pushing/pulling device. One strategy involves the minimisation of this damping contribution: in single blade test set-ups the preload may be guaranteed by thin pulling wires loaded with springs [75] in an effort to avoid the disruption of the blade root motion during slip, or by loading screws. Such screws are equipped with strain-gauges [76,78] or load cells [219,220] to measure the load. The load is transferred to the test piece via a small diameter bearing to obtain a uniform load distribution. An alternative non-rotating architecture comprises a dummy blade where a root attachment is machined at both ends thus creating a symmetric arrangement [80,214,217,221] or two blades welded at the tip [213]. The symmetry of the architecture, the equivalence of loads and joint kinematics ensures a load application

very similar to the real operating conditions. In this case, preload is typically obtained using a hydraulic cylinder. An alternative idea, valid for both single [265] and double-blade [213] arrangements, involves providing an initial mismatch between the contact surfaces at the blade root that is removed by thermal expansion. The preload is then obtained through thermal shrinkage.

Two main kinds of **excitation** can be found in these test rigs:

- Harmonic/resonance excitation. This excitation is typically provided through a shaker or using a vibrating table. In the second case there is a reduced risk of introducing an additional damping/stiffness contribution through the shaker attachment. Other non-contact methods include electromagnets. In rotating set-ups the preferred choice is piezoelectric actuators.
- Impulse excitation, i.e. hammer test, is typically employed when evaluating free decay response. One limitation of hammer tests is that the maximum achievable level of excitation is typically lower than that obtained with other excitation devices [214]. Depending on the specific structure, the preload at the contact and the direction of excitation, such excitation levels may [266,267] or may not [214] be sufficient to trigger slip of the interfaces.. A new excitation system presented in [222], proposes the use of power-to-release and classical electromagnets to detach a shaker and pushrod from the specimen after reaching steady-state high frequency vibration.

All friction joints modify the dynamic response of the system. They are part of/attached to through two contributions [218,221]:

- they introduce an additional stiffness, which is maximum in full stick regime and decreases as the joint starts to slip
- they introduce damping, which is null in full stick regime and increases as the joint starts to slip

Given the position of the blade root joint, the first contribution is less significant and often masked by the stiffening effect of the centrifugal load on the blade. Blade root damping, on the other hand, has been recognised since the 1940s [22,23] and represents the target measured quantity of most of the test set-ups detailed in Table 3. The results were initially given in terms of empirical observation, expressed as logarithmic decrement δ, in order to be easily compared with other sources of damping, such as material damping and aerodynamic damping (or excitation) [24] and/or to include the presence of the root joint in the damping matrix **C** without the need for modelling the contact. With time, this and other damping measures were introduced and related to relevant design quantities of the blade root such as stress at key locations, centrifugal load, root geometry, temperature, etc. As of today, there is no unified quantity to represent damping. One of the most common measures is the loss factor η which is defined as the ratio of energy dissipated in unit volume per radian of oscillation to the maximum strain energy per unit volume. The loss factor η may be obtained through the half power method as shown in Fig. 10. In order to clarify the contribution of each work detailed in Table 3, the relation between η and the various damping-related quantities is given below:

$$\eta \approx \frac{\Delta f}{f_n} \approx \frac{\delta}{\pi} \approx 2\zeta \approx \frac{1}{Q} \tag{3}$$

where δ is the logarithmic decrement damping, ζ is the damping ratio and Q is the quality or Q-factor. It should be noted that Eq. (3) is valid within a 5% error for $0 < \eta < 0.3$ [268], while more complex relations, e.g. $\eta = 2\zeta\sqrt{1 - \zeta^2}$, hold outside of that range. As will be apparent from Fig. 10, the experimental set-up and its **exciting source** may guide the way results are presented. As an example, test rigs with harmonic excitation [75,76], typically rely on the half-power method to estimate damping (η), while those test set-ups which use impulse excitation/vibratory decay tests resort to logarithmic decrement δ computation [213] or to the Hilbert Transform to estimate η [214].

Nevertheless, Eq. (3) may be used to offer an estimate of the quantities which have not been directly measured.

In [75,76], the effect of slip at the root on the dynamic response of blades was quantified through the loss factor η. A compressor and a fan blade, both equipped with a dovetail root were investigated respectively. In both cases various experiments were conducted by adjusting the centrifugal loads to replicate scenarios ranging from a completely clamped blade (high load, no slip at the root) to situations with decreasing loads that induced different degrees of slip. Similar conclusions which can be summarised below were drawn:

1. Loss factors decrease rapidly with an increase in centrifugal load.
2. Higher levels of excitation result in greater friction damping for low centrifugal loads, but this dependence diminishes with increased centrifugal loads.
3. Loss factors plateau at moderate centrifugal loads, gradually approaching non-friction damping levels, indicating a tendency for minimal slip at the root.

Confirmation of points 1–3 can be found in [214,265], where η is plotted against vibration amplitude for varying centrifugal loads. Further support for point 2 is presented in [216] and in [213], where a nearly linear relationship between the logarithmic decrement δ and vibration amplitude at the blade tip is evidenced. However, recent experiments [221] demonstrate the damping-dynamic displacement/excitation relationship over a broader displacement range. For low excitation levels corresponding to the full stick condition, damping remains approximately constant and aligns with the material's intrinsic damping η_0, as corroborated in [78,216], which compared η and ζ values for bonded and un-bonded root joints. As the root starts to slip, damping increases to a maximum with rising displacement, consistent with observations in [75,76], but subsequently asymptotically decreases to η_0. It is noteworthy that this decrease corresponds to joint interfaces in advanced gross-slip, a condition rarely encountered in practical working conditions.

Other relevant measured quantities include the stress on a key location on the disk sector [217] or at the (dummy) blade root section [78], and the friction-dissipated energy [12]. Regardless of the measured quantity, several works try to replicate measured results with a model which includes friction. All contact models, as detailed in Section 5.1, require calibration parameters, i.e. friction coefficient μ and, when implemented, normal and tangential contact stiffness k_n and k_t. Such values are either tuned on the basis of the experimental results [75,76], identified with a purposely developed numerical technique which compares measured frequency and damping with those obtained from a FE model [80], or measured through a separate contact fretting test set-up replicating the material and geometry of a single lobe of a blade root joint [12,78].

5.2.3. Blade friction damper

Table 4 summarises the main features of all the test setups designed to investigate blade friction dampers, here defined as separate objects, unlike shrouds or roots, which are integral to the blade. Depending on their position, they may be classified as 'underplatform', 'midspan', or 'tip' dampers. Nevertheless, the features of the test rigs used to investigate their performance can be applied to all these types of dampers. Test rig architectures can be subdivided into rotating and non-rotating. Non rotating rigs can be further classified depending on the number of blades employed. A total of five main test rig architectures can be identified in Table 4 and are represented in Fig. 12:

- Two Blades (2B): by far the most common non-rotating test rig architecture, comprising two blades with an interposed damper.
- Single Blade (1B): a single blade is in contact with (i) a ground damper, (ii) two dampers, one on each side of the blade. The other side of the dampers is in contact with a stiffer structure called a dummy blade/platform, which may be equipped with force sensors to measure contact forces, as in [238].
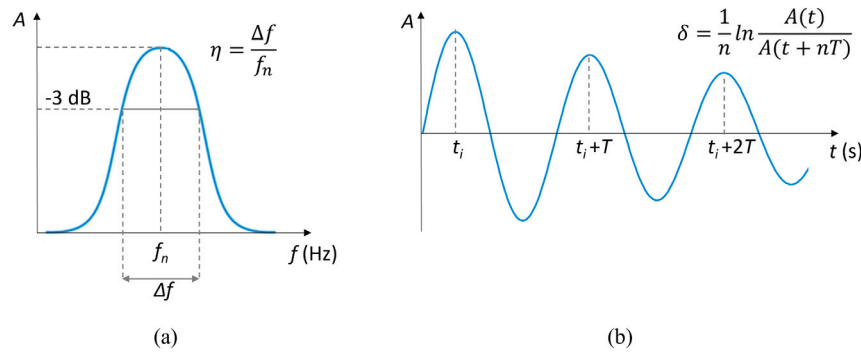
Fig. 10. (a) Graphical representation of the half-power method to estimate the loss factor η (b) Graphical representation of the logarithmic decrement method to estimate parameter δ.

Table 4
Features of test set-ups focusing on blade friction damper.

References	Set-up	Preload	Excitation	Measured Quantities
[63,88,225,228,229] [64,234,237,248,269]	Non-Rotating 2B	Deadweights	Shaker	Dynamic response
[62]	Non-Rotating 2B	Deadweights	Air jets	Dynamic response
[247]	Non-Rotating 2B	Deadweights	Electromagnet	Free decay
[240,241]	Non-Rotating 2B	Compressed Air	Shaker	Dynamic response
[232,236,239]	Non-Rotating 2B	Deadweights	Shaker	Dynamic response Damper kinematics
[223]	Non-Rotating 1B	Deadweights	Shaker	Dynamic response
[227]	Non-Rotating 1B	Deadweights	Air jets	Dynamic response
[220,238,242,246]	Non-Rotating 1B	Deadweights	Shaker	Dynamic response Contact forces Damper-plat kinematics
[79,212,235,270,271]	Non-rotating 0B	Deadweights	Piezo actuators	Contact forces Damper-plat kinematics
[233]	Non-Rotating Disk	Deadweights	Magnets	Dynamic response
[226]	Rotating	Centrifugal Effect	Air jets	Dynamic response
[224,231]	Rotating	Centrifugal effect	Magnets	Dynamic response
[216,230]	Rotating	Centrifugal effect	Piezo exciters	Dynamic response
[243–245]	Rotating	Centrifugal effect	Acc/Deceleration	Dynamic response

- No Blade (0B): the damper is in contact with two dummy platforms. One platform is connected to a piezo actuator to reproduce the platform kinematics; the other dummy platform is connected to a set of force sensors to measure contact forces.
- Non-rotating Disk.
- Rotating Disk.

While in rotating rigs (RD), the preload is naturally ensured by the centrifugal effect, non-rotating setups (2B, 1B, 0B) face the challenge of ensuring a realistic contact pressure distribution. For solid dampers (i.e., prismatic dampers), the most common method involves using wires pulled by deadweights. This requires machining holes in the dampers, typically located at their centre of mass, to replicate the pull of the centrifugal load. This methodology, despite its widespread use, may not be representative of real working conditions, as further discussed below. In some cases, to achieve optimal contact pressure aligned with operating conditions without increasing deadweights, the damper or platform contact surface is machined to localise the contact. The impact of the effective contact surface on the results will be further analysed below. Wires and deadweights are impractical for strip dampers. In this case, the preload is guaranteed by a purposely developed compressed air system [269], as illustrated in Fig. 12(a), which loads the strip without any contact, mimicking the effect of the centrifugal force. In this case, a measure of the preload and its distribution is achieved using a calibration system based on a pressure-sensitive film.

The excitation depends on the test rig architecture and its goal. In non-rotating setups, with one or more blades present (1B, 2B), a shaker is the most common choice to provide dynamic excitation. In 2B configurations, typically only one blade is excited and transfers energy to the other blade through the damper and the base. In [241], both blades are equipped with a shaker to ensure that both are equally excited and their motion has equal amplitude. Permanent magnets are used to excite rotating [224,231] and non-rotating [233] disk configurations. This technique, like piezo exciters on rotating configurations, ensures the ability to trigger different Engine Order excitations. Non-rotating 0B configurations employ piezo actuators to input the desired kinematics to one of the dummy platforms. It is important to note that the 0B configuration, unlike all others, does not need dynamic excitation, as the purpose of the rig is to investigate damper mechanics. In this sense, non-rotating 0B configurations share more similarities with single-contact test arrangements as described in Section 5.1. The **measured quantities** are closely aligned with the two primary objectives of these test rigs, as discussed in Section 5:

- to validate numerical models incorporating dry friction dampers,
- to assess the effectiveness of a specific damper configuration.

Both of these aims can be pursued by considering the dynamics of a bladed arrangement and/or the contact mechanics of the damper. Model validation to some extent is feasible with all the test rigs outlined in this section, as it is possible to replicate the test rig configuration
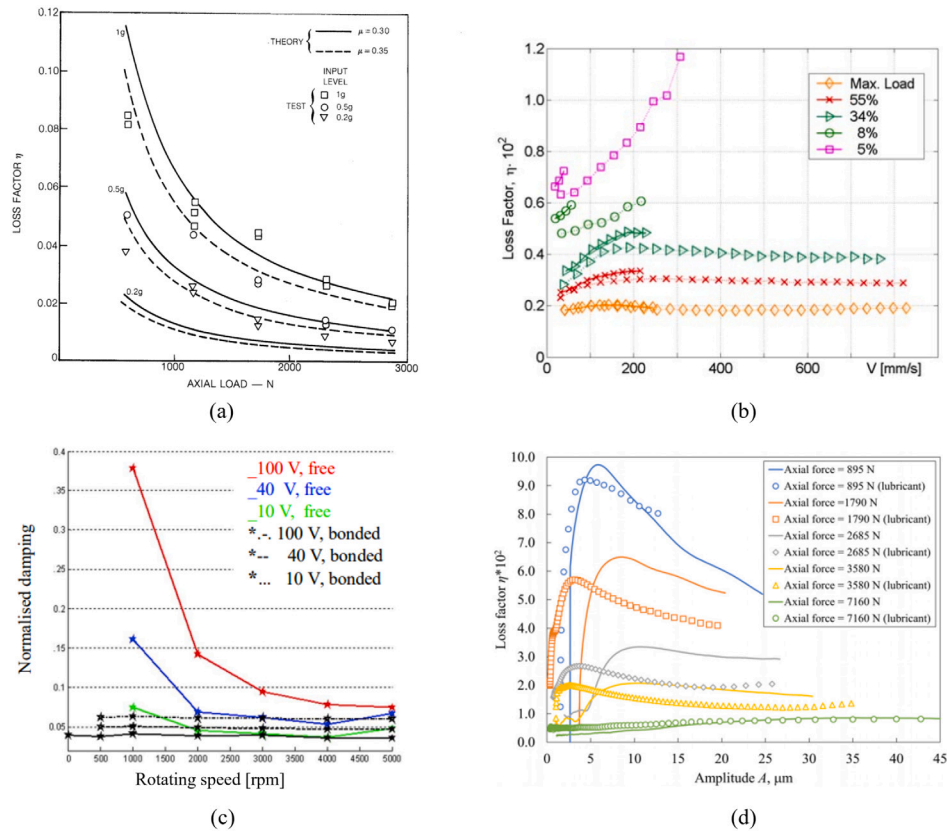
Fig. 11. Damping measurement as a function of (a) centrifugal load [76], (b) amplitude of the response [214], (c) rotational speed [216], and (d) amplitude of displacement [221].
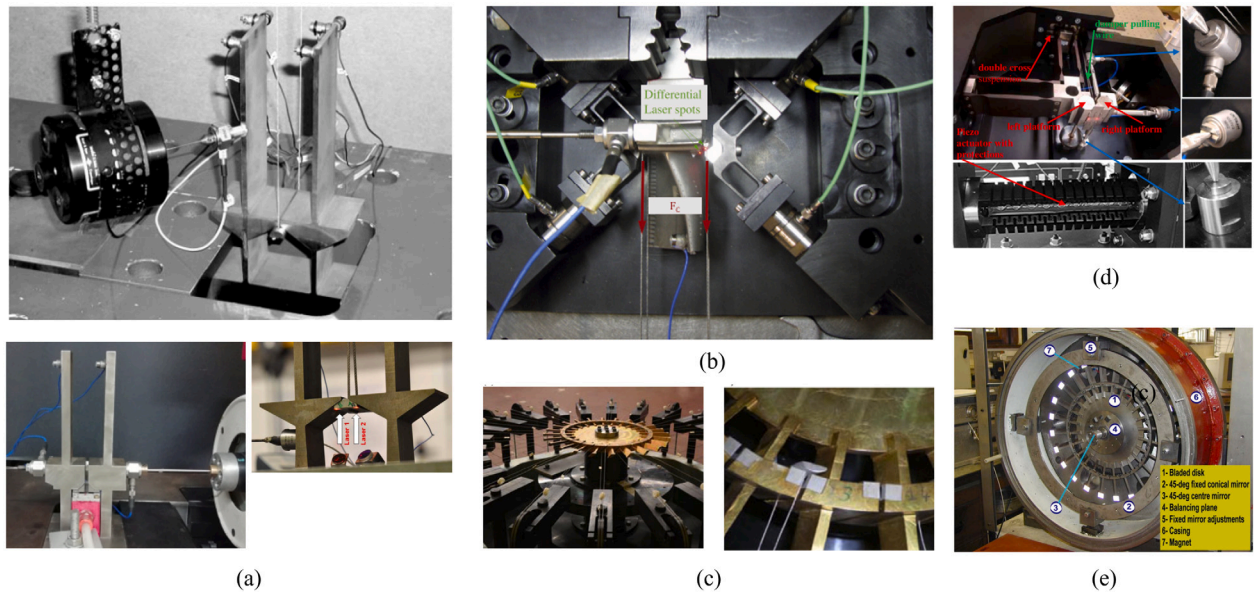

Fig. 12. Test set-ups used to investigate underplatform dampers (a) Non-rotating Blade–Damper–Blade (BDB) configuration with preload from deadweights-wires system pulling a solid damper [64,229] and with preload from compressed air pushing a strip damper [241] (b) Non-rotating Platform–Damper–Blade (PDB) configuration [242]. (c) Non-Rotating full disk configuration. (d) Non-rotating Platform–Damper–Platform configuration [212] (e) Rotating rig [231].
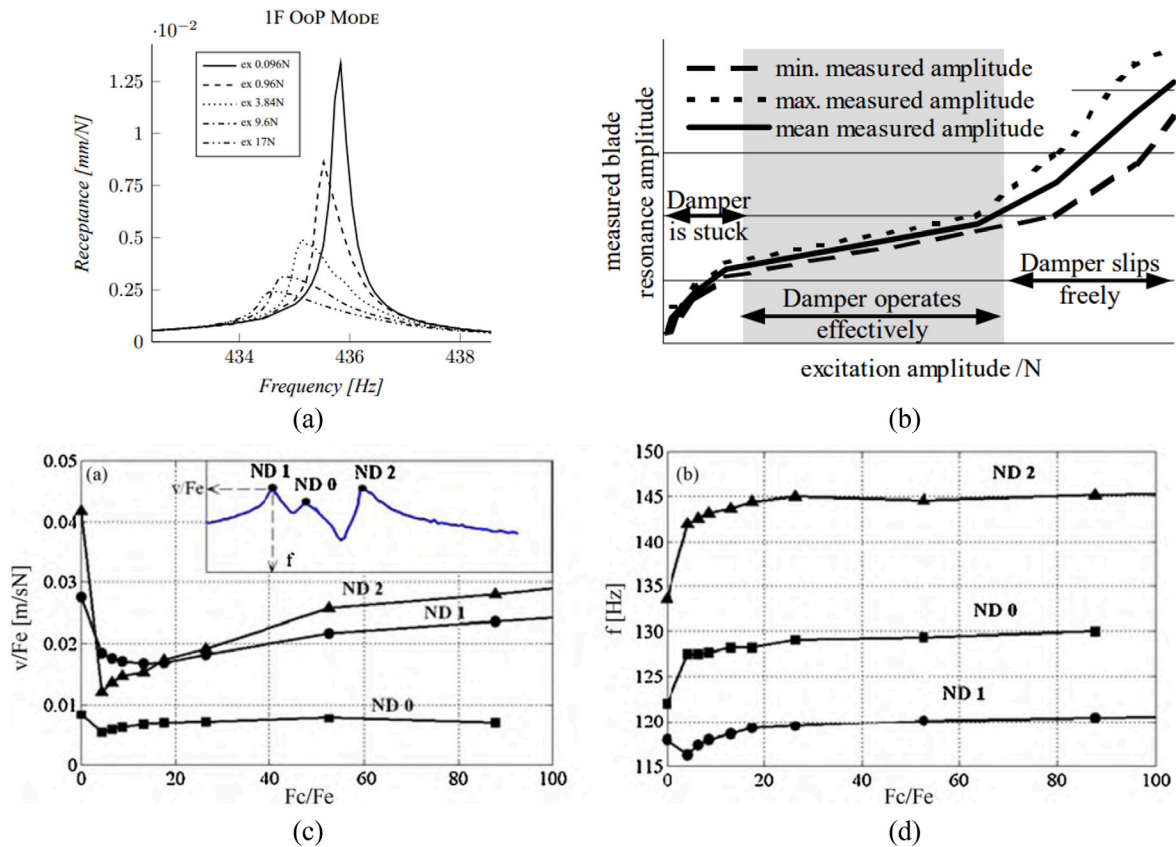
Fig. 13. (a) Frequency response Functions for increasing levels of excitation from [64] (b) Damper performance curve from [88] plotting amplitude of vibration vs. excitation level (c) Damper performance curve from [233] plotting receptance vs. damper preload over excitation level (d) Damper performance curve from [233] plotting frequency of response peak vs. damper preload over excitation level.

in a numerical environment and reproduce either the blade dynamic response and/or the hysteresis cycles of the damper/blade interface.

The effectiveness of the damper, however, can only be quantified under specific conditions that depend on the test rig architecture. For instance, non-rotating 2B configurations offer only In-Phase and Out-of-phase modes of vibration, while non-rotating and rotating disk setups can be driven to assess any desired Engine Order excitation. Non-rotating 1B configurations test the damper effectiveness with platform kinematics that are very specific and seldom encountered in real working conditions. However, in their most recent version [238,242], they provide the most comprehensive level of model validation, encompassing both blade dynamics and damper contact mechanics. In [220], the contact forces at the blade–platform interface reconstructed from the measurements were directly applied to a finite element model of the blade, thus bypassing the need for a contact model. The resulting blade response was then compared with the measured counterpart.

All of these points are summarised in Table 5. The analysis of the experimental evidence gathered on the test rigs described in this section yielded cross-confirmations and comparable results on several key points, as outlined below.

- **Assessment of damper effectiveness** Blade friction dampers introduce stiffness and damping contributions that depend on the excitation level [272], which in turn triggers varying degrees of slip at the contact interfaces. One common method to evaluate damper performance is to fix the preload (corresponding to a given rotational speed) and adjust the dynamic excitation applied to the bladed array. At low excitation levels, the damper remains fully stuck to the platforms, contributing maximum stiffness but zero damping. As excitation levels increase, slip at the interfaces occurs, leading to increased damping and decreased stiffness contributions. With further increase in excitation, the damper may

begin to slip freely or detach, resulting in a frequency response function resembling that of a free, unbounded bladed system (i.e., without a damper). Results are often presented by displaying the Frequency Response Functions for increasing excitation levels (Fig. 13(a)) and/or by plotting the maximum amplitude and frequency of each curve against the excitation level (Fig. 13(b), (c), (d)). These plots, known as performance curves, aim to summarise damper effectiveness across a wide range of operating conditions. It is noteworthy that the appearance of the damper performance curve may vary depending on the convention used. For example, in Fig. 13(b), where the x-axis is linearly correlated with the excitation level, a fully stuck damper is depicted on the left side and a freely slipping damper on the right. The opposite is true for Fig. 13(c)–(d), where the x-axis represents the preload on the damper relative to the excitation level. Another important distinction lies in the measurement of the blade(s)' dynamic response. In some cases (Fig. 13(b)), the blade(s)' response is directly represented through vibration amplitude, resulting in a continuous increase from full stick to free slip. It is essential to note that the gradient with which the amplitude increases over excitation (i.e. the slope of the curves in Fig. 13(b)) is at its minimum when the damper is operating effectively, as highlighted by the shaded area in Fig. 13(b). An alternative method to represent the blade(s)' response is through receptance (Fig. 13(a) and (c)), i.e., the response normalised by the excitation level. In a linear system, the performance curve would appear as a flat line, as the response would increase linearly with the excitation level. However, in a friction-damped system, the curve exhibits a minimum when the damper operates at maximum efficiency. Similarly, damper effectiveness can be investigated at the mechanics level, independent of the blade dynamics response. In

studies such as [212,235,238,246], the contact force on the right side of a damper is measured, leveraging the fact that the damper has a unique contact on the right side. The damper equilibrium is then reconstructed, assuming the damper inertial forces are negligible (Fig. 14(a)). Relative platform-damper kinematics are measured using a differential laser vibrometer at both contact interfaces (Fig. 14(b)), along with relative platform–platform kinematics. For example, as illustrated in [79], to replicate pure blade In-Phase vibration, the relative platform kinematics are vertical (Fig. 14(c)). It can be demonstrated that the total energy dissipated by the damper equals the sum of the areas of the hysteresis cycles at the two contact interfaces (Fig. 14(d)–(e)), which in turn is equal to the platform–platform equivalent hysteresis cycle. This cycle is obtained by plotting the relative platform displacement (directly imposed in these types of test rigs [79,212,235]) against the corresponding component of the contact force at one of the two interfaces (Fig. 14(f)). The shape of the platform-damper hysteresis cycles differs from that shown in Fig. 11 due to the continuous variation of the normal load on the interfaces. Analysing the platform-damper hysteresis cycles allows assessment of the contact state at the different interfaces during the vibration period and provides a direct estimation of the contact parameters k_t and μ.

- **Effect of the damper shape and platform kinematics** The behaviour and effectiveness of a damper are influenced by various factors, including its mass, geometry, and rigid body motion, which, in turn, depends on the kinematics of the platforms, such as the mode of vibration. Some of these test rigs have been used to compare the performance of different types of dampers. A notable example involves solid dampers, characterised as rigid prismatic objects that may be cylindrical, wedge-shaped, or asymmetrical (flat on one side and cylindrical on the other). In [248], the performance of these three types of dampers, positioned at the tip of the blades, was compared under In-Phase and Out-of-Phase modes of vibration. The asymmetrical damper demonstrated superior performance in reducing the response level in both cases, while the cylindrical one consistently showed the least effectiveness (Fig. 15(a)). The reason for the cylinder's lack of performance lies in its kinematics, particularly in the In-Phase mode of vibration, where it involves substantial rotation and minimal slip, as demonstrated in [271] and further illustrated in Fig. 15(b). Wedge-shaped dampers exhibit significant energy dissipation for the Out-of-Phase mode because the damper slides without rotating, as demonstrated in [239] through DIC measurements (Fig. 15(c)) and in [232] through Laser Vibrometer measurements. However, in the In-Phase mode, the wedge damper loses effectiveness due to lift-off of the contact interfaces [232,239]. This is reflected in Frequency Response Functions that exhibit a softening behaviour with jumps. The relationship between damper kinematics and dissipated energy has been further elucidated in the investigation of asymmetric dampers with different platform angles and depth of cut [270]. Further considerations on the variability of experimental results, both due to surface finishing and to solution multiplicity inherent to frictional behaviour are discussed thoroughly in Section 6.2.1.

5.2.4. Blade shroud

Table 6 summarises the main features of all the test setups designed to investigate blade shrouds. Three main test rig **architectures** can be identified in Table 6 and are represented in Fig. 16. These configurations are analogous to those described in Section 5.2.3 with the same names. In detail, non-rotating setups may involve either two blades (2B) coupled through a shroud or one blade (1B) coupled to one or two dummy shrouds, which may be instrumented with load cells to measure contact forces. A non-rotating disk configuration is

also presented in [250], where only two of the blades are loaded, excited, and monitored. In shrouds, the **preload** at the contact is provided by the untwisting due to the centrifugal effect. The same mechanism can be reproduced in rotating setups, while other strategies must be adopted for non-rotating ones. There is not a unique and widespread solution as in test rigs investigating blade roots or dampers. D'Ambrosio et al. [250], in their 1B non-rotating configuration, connected the dummy blade under investigation to a system composed of a blade spring and a steel ball rubbing against a support mounted on a controlled XY table, which is used to charge the contact. The normal and tangential loads are measured by means of a load cell mounted on the fixed block. The advantage of this system is that, since the spring stiffness in the direction of contact is low, it provides a high sensitivity to normal load, thus enabling exploration of a wide range of values. On the other hand, the position and direction of the contact are not representative of realistic working conditions. In 1B configurations, one possible solution is to ensure preload by pushing the dummy shrouds against the blade through deadweights [87,255], or using a screw-driven lift [257]. Other solutions [252] involve a load disk that integrates the dummy shrouds. A moment is applied to the disk, which then rotates and ensures contact with the blade. A similar solution adopted by [259] rotates the blade rather than the support holding the dummy shrouds. These solutions have the advantage of providing a static moment on the blade as in real operating conditions. In [254], the preload is obtained by mounting interference between the two blades and later estimated using strain gauge measurement. In [256], the preload is not provided as the goal of the analysis is to verify the dynamic performance of shrouds undergoing impact as well as friction.

Similar to Section 5.2.3, the most common **excitation** in non-rotating rigs is through a shaker, while in rotating setups, air jets and permanent magnets are used.

The **measured quantities** in this case always include the dynamic response of the blade. Similarly to the previous section, the response is typically presented as a function of frequency for different levels of excitation and preload at the contact. In some specific cases, additional information on the shroud kinematics and on the exchanged contact forces is made available.

A synthesis of noteworthy insights derived from the analysis of the experimental findings is presented below:

- **Comparison with numerical predictions and contact interface detection:** The measured responses are typically compared to numerical predictions, which have become increasingly complex as computational capabilities and model features have improved over the years. Model improvements usually involve the representation of the contact interface. In [249], only resonance frequencies are compared, and the computed counterpart is obtained by imposing a full stick condition on a subset of the nominal contact area. In [230,250,255,258], the complete response is computed, and the importance of a fine discretisation of the contact interface, representative of the effective rather than nominal contact conditions, is emphasised to achieve successful experimental–numerical matching. The influence of the effective contact interface area is further investigated in [257], where changes in contact surfaces were periodically detected over millions of cycles and linked to alterations in the measured hysteresis loops and vibration characteristics.

- **Influence of normal load:** Different works [87,252,254] highlighted the influence of normal load on the shrouds, showing that a decrease in normal load tends to increase damping and limit maximum alternating stresses. However, it was shown in [87] that an excessive reduction in normal load may trigger contact separation and therefore a sharp and sudden increase in blade stress. If the loss of contact is intermittent, on the other hand,
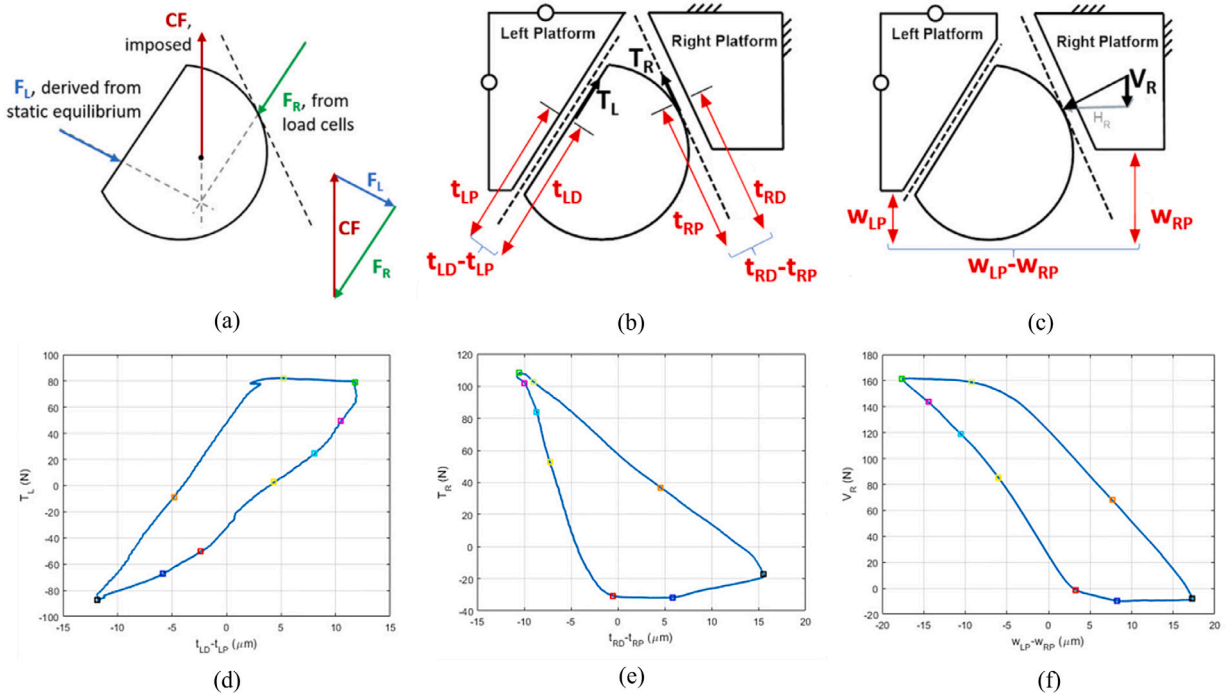
Fig. 14. (a) Procedure to reconstruct damper equilibrium (b) Procedure to measure/reconstruct damper–platform hysteresis at contact interfaces (c) Procedure to assess the platform–platform equivalent hysteresis for ideal In-Phase motion (d) Measured damper–platform hysteresis at flat-on-flat contact interface for curved-flat damper (e) Measured damper–platform hysteresis at cylinder-on-flat contact interface for curved-flat damper (f) Measured platform–platform equivalent hysteresis for curved-flat damper.
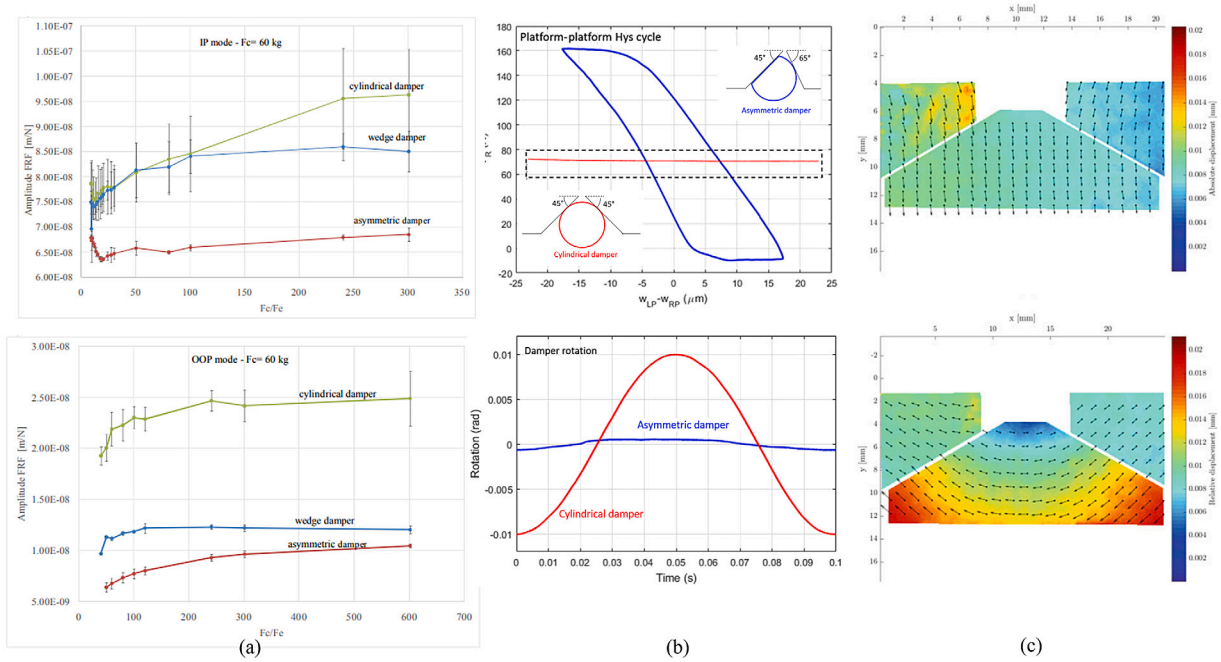
Fig. 15. (a) Damper performance curves for asymmetrical, cylindrical and wedge-shaped dampers for In-Phase and Out-of-Phase modes of vibration from [248]. (b) platform–platform hysteresis cycle and damper rotation for asymmetrical and cylindrical dampers for In-Phase platform kinematics from [271]. (c) Wedge-shaped damper kinematics using DIC measurements for In-Phase and Out-of-Phase modes of vibration from [239].

several repeated impacts (i.e., chattering) will introduce additional damping, which will manifest as a response function with an irregular shape [230].

- **Influence of shroud geometry and Engine Order Excitation:** As in the case of friction dampers, different contact angles and relative kinematics at the contact may trigger different contact states as shown in [273] and further exemplified in Fig. 17.

5.2.5. Blisk friction ring damper

Designing and commissioning a whole rotating test rig is complex and expensive. There are very few experimental studies on the testing of friction ring dampers in a rotating blisk. The only known experiment on the topic was designed and conducted at the École Centrale de Lyon [112,260], which characteristics are given in Table 7. They tested a high-pressure compressor blisk using a friction ring damper in a rotating test rig. The test rig was developed earlier in a study by [112]

Table 5

Friction Damper Test Rig Configurations vs Usability of Experimental Evidence.

Test rig configuration	Model validation	Assessment of Damper effectiveness
Non-rotating 0B	Damper mechanics	Any Engine Order excitation, bending modes only
Non-rotating 1B	Damper mechanics Blade dynamics	Only one condition/mode similar to 90° inter-blade phase angle
Non-rotating 2B	Blade dynamics	In-phase and Out-of-phase modes
Non-rotating Disk Rotating	Blade dynamics	Any Engine Order excitation
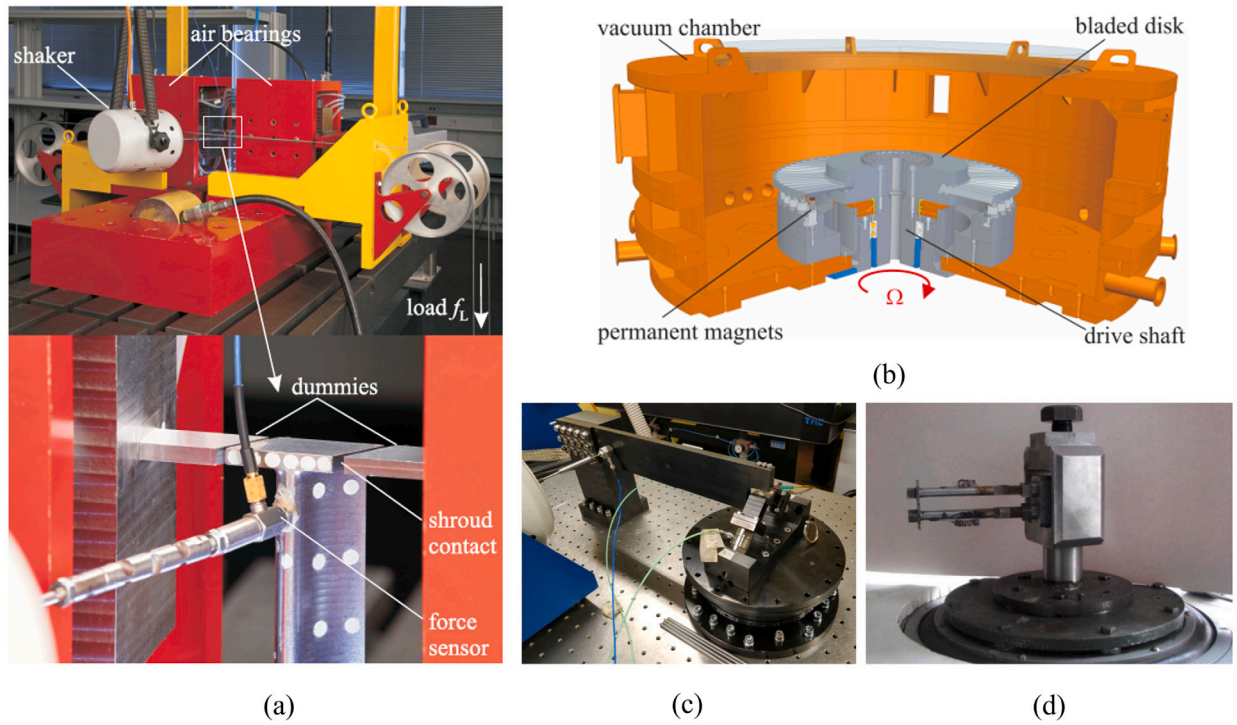
Fig. 16. Test set-ups used to investigate bladed shrouds (a) Non-rotating 1B configuration with two dummy shrouds and (b) rotating configuration from [255]. (c) Non-rotating 1B configuration with one dummy shroud from [257]. (d) Non-Rotating 2B configuration from [254].

Table 6

Features of test set-ups focusing on blade shrouds.

| References	Set-up	Preload	Excitation	Measured Quantities
[249,251,258]	Rotating Disk	Centrifugal Effect	Air Jets	Dynamic Response
[87]	Non-rotating 1B	Deadweights	Shaker	Dynamic Response
[250]	Non-Rotating 1B	Preloaded spring	Shaker	Dynamic Response Contact forces Relative Displacements
[250]	Non-rotating Disk (2B)	Loading Screw	Shaker	Dynamic Response
[252]	Non-rotating 1B	Load Disk	Shaker	Dynamic Response
[254]	Non-rotating 2B	Mounting interference Strain gauge	Shaker	Dynamic Response
[256]	Non-rotating 2B	–	Shaker	Dynamic Response
[259]	Non-Rotating 1B	Blade rotation	Shaker	Dynamic Response Contact forces
[255]	Non-rotating 1B	Deadweights	Shaker	Dynamic Response
[255]	Rotating Disk	Centrifugal Effect	Permanent magnets	Dynamic Response
[257]	Non-Rotating 1B	Blade rotation	Shaker	Dynamic Response Contact forces Relative displacement
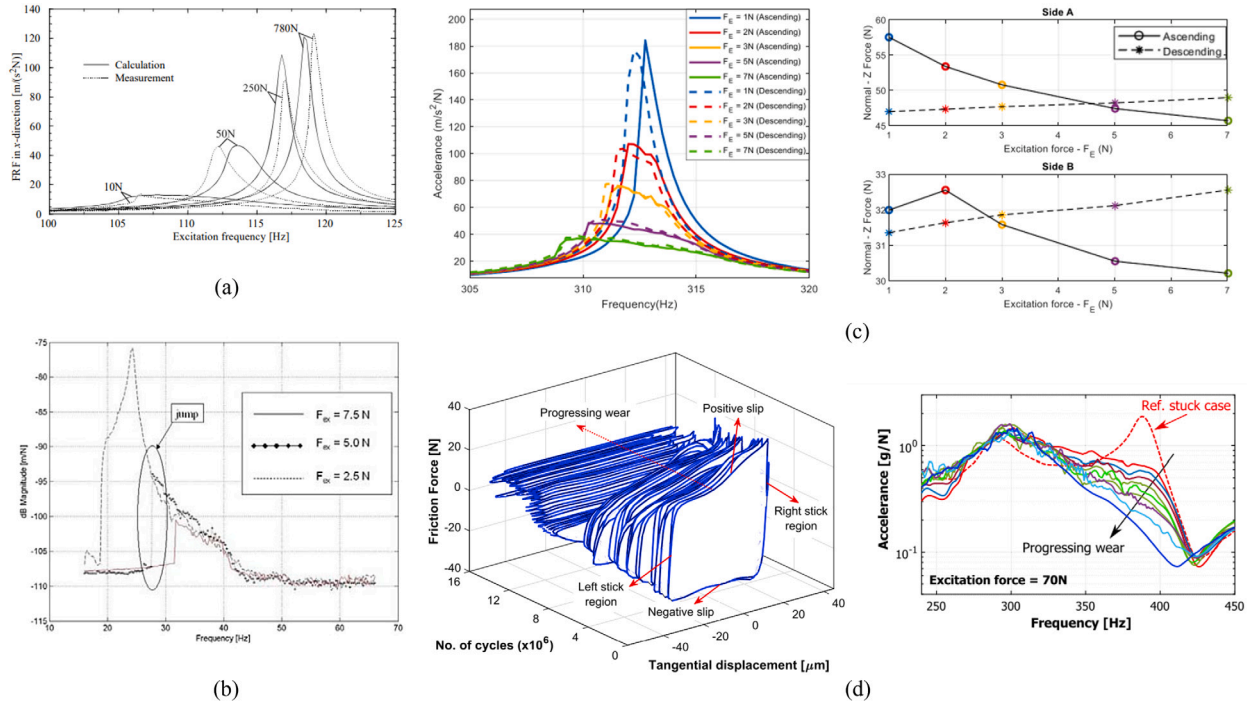
Fig. 17. (a) Measured vs. simulated nonlinear response of shrouded blade for different preload levels from [87]. (b) Nonlinear response of shrouded blade exhibiting jump phenomenon from [250]. (c) Variability of the nonlinear frequency response and corresponding values of the static component of one of the contact forces from [259]. (d) Hysteresis loops at the shroud-dummy contact recorded for increasing degrees of wear and corresponding frequency response from [257].
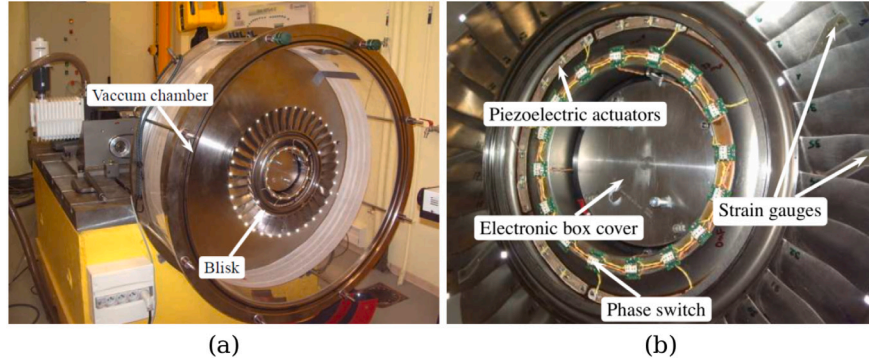

Fig. 18. Experimental set up of a rotating blisk with a friction ring damper [260].
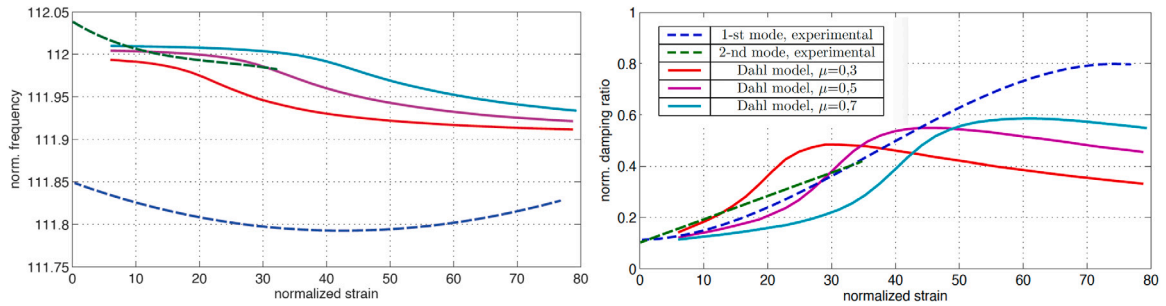

Fig. 19. Experimental testing results of a rotating blisk with a friction ring damper [260].

to investigate friction damping blade attachment. Fig. 18 shows the experimental setup used in the study. The rig is powered by an electric motor that can rotate at a maximum speed of 5000 rpm. Fig. 18(b) illustrates the use of 24 piezoelectric plates, split into 8 groups, as an excitation system to facilitate precise control for exciting targeted modes. The vibration measurement system comprises 12 semiconductor

strain gauges, with 8 attached to the suction side of the blades and the remaining 4 on the disk. The frequency–strain and damping–strain curves at different rotating speeds were obtained from experimental forced responses using a nonlinear modal identification technique. The test results are used to validate the nonlinear numerical simulation results. The comparison between experimental and numerical results
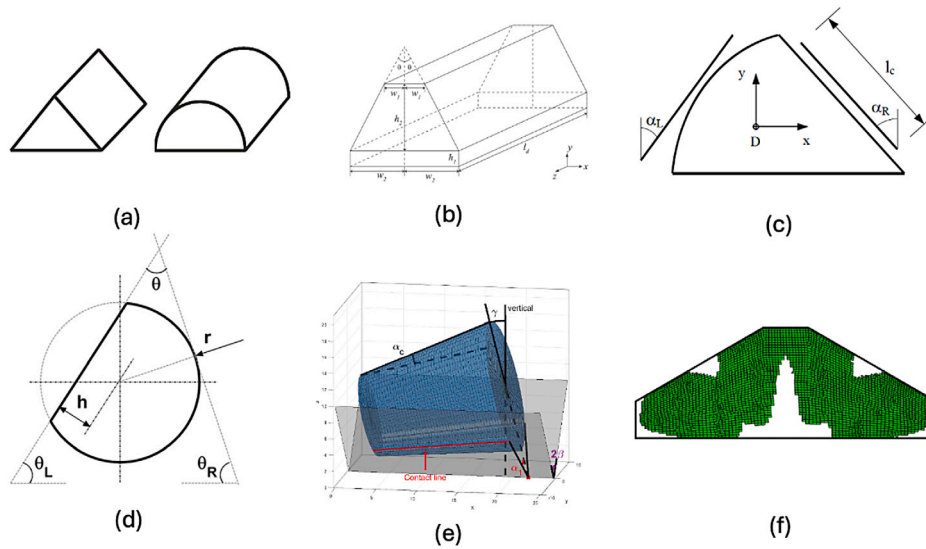
Fig. 20. Different geometries of UPDs: (a) Wedge-shaped and cylindrical underplatform damper from [274] (b) Modified wedge-shaped underplatform damper from [275]. (c) Semi-cylindrical underplatform damper from [276]. (d) Asymmetrical underplatform damper from [272]. (e) Conical underplatform damper from [277]. (f) Topology optimised underplatform damper from [278].

is illustrated in Fig. 19. It can be observed that the damping ratio and resonant frequency obtained from the numerical simulation are consistent with the experimental results at the same order of magnitude. The damping ratio trend obtained from the numerical simulation at a friction coefficient of 0.5 corresponds well with the curve derived from the experimental findings at lower strain levels. However, when the strain level exceeds 50, the difference between the numerical and experimental results becomes noticeable. The results in [112] also exhibit similar outcomes. These observations indicate that the current numerical technique is relatively dependable for the prediction of nonlinear friction damping.

6. Design and optimisation of friction dampers

In the last two sections, the numerical and experimental techniques for the simulation and testing of dynamical systems with friction interfaces were reviewed. This section focuses on advances in terms of the design and optimisation of friction dampers in turbomachinery. The primary objective of design and optimisation is to enhance the performance and robustness of friction damping under various operational conditions, considering diverse sources of uncertainty. This involves modifying structural features such as mass, shape, interface, or material properties.

6.1. Structural design and optimisation

6.1.1. Underplatform damper (UPD)

The initial investigations, conducted in [34,279,280], aimed to explore the impact of non-geometric parameters (including friction coefficients, excitation level, and contact normal force) on resonance peak frequency and response levels in turbine blades. These studies underscored the significance of such parameters in the damping performance of wedge-shaped friction dampers. A similar sensitivity study was also performed by Krack et al. [36] considering uncertainties in the friction coefficient, the excitation level and the linear damping. Panning et al. [61,229,274] were the first to numerically investigate the influence of contact geometry of both cylindrical and wedge-shaped friction dampers on damping effectiveness by parametrically varying both the geometry of blade–platform and dampers. This confirms the experimental findings detailed in Section 5.2.3 and demonstrates how effective numerical models can be in the design phase, i.e. avoiding costly experimental campaigns. The geometry of the wedge-shaped and cylindrical damper is shown in Fig. 20(a). Zucca et al. [276] were among the first to model the semi-cylindrical friction damper (shown in Fig. 20(c)) which had been in use in the turbomachinery industry since the 1980s. This shape, as pointed out in the study, ensures full contact between the damper and the blade–platform over the flat damper side when the relative platform angle changes during blade vibration (i.e. self-adjusting). Their numerical investigation made it possible to link the damper kinematics (i.e. lack/presence of rotation) to its stiffening and damping capabilities. This investigation was further developed by Gastaldi et al. [210,272,281], who parametrised the semi-cylindrical damper shape in terms of its angles and depth of cut (see Fig. 20(d)) and proposed pre-optimisation maps which forecast, without the need for numerical iterative computations, the combination of design parameters that will lead to undesirable behaviours such as rotation and jamming for In-Phase and Out-of-Phase modes. More recent works focus on choosing, among the pre-optimised damper configurations, the best fit for a specific blade [38,40,282]. In [283], the coupling between a blade and a semi-cylindrical damper is optimised by considering a design space defined by ten geometric parameters. Among these parameters, three are allocated for the damper. Two surrogate models are introduced and compared, both capable of significantly reducing the computational time needed for a regular design of experiments (DOE) factorial sampling by several orders of magnitude.

Other options to avoid damper rotation have been explored. As shown in Fig. 20(e), Denimal et al. [277] proposed a conical underplatform damper to avoid the rolling phenomenon of traditional wedged-shaped dampers for In-Phase modes through geometric compliance, leading to a better damping performance in both In-Phase and Out-of-Phase mode when compared to classical wedged and circular dampers. In the context of high-fidelity optimisation, Yuan et al. [275] introduced a surrogate-based optimisation approach to enhance the damping performance of a modified wedge-shaped underplatform damper. The geometrical parameterisation of the damper is shown in Fig. 20(b). The study was intended to optimise the shape of the wedge-shaped friction dampers to achieve minimal resonance frequency shift and maximum friction damping. Recently, Denimal et al. performed a further topology optimisation of an underplatform damper [278] where the internal structure of the wedged damper is optimised under stress constraints imposed on the contact interface. One of the topologically optimal dampers is shown in Fig. 20(f). In addition to the design of the damper geometry itself, a simplified and parametric beam model with only one turbine blade and damper was then developed to study
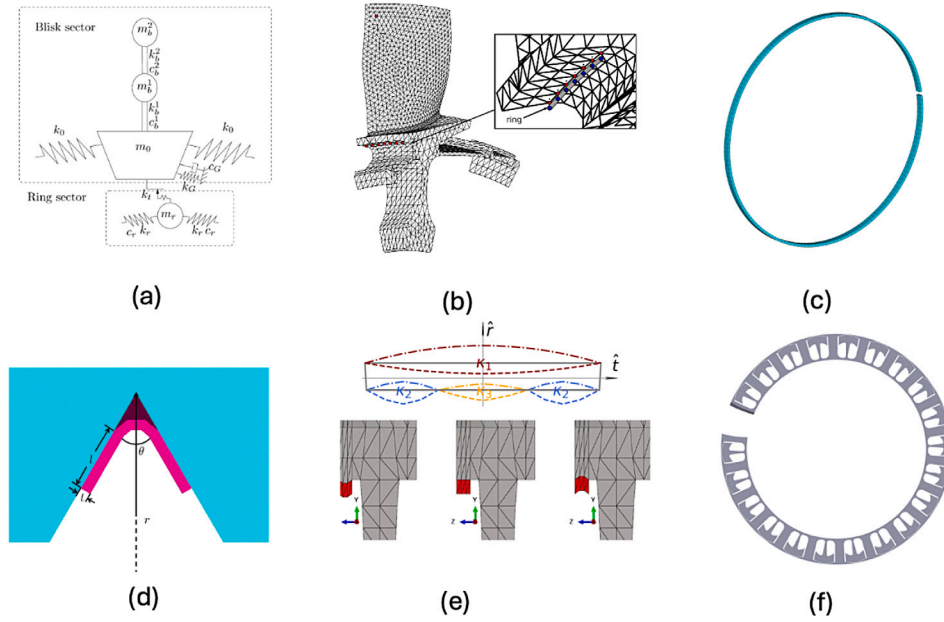
Fig. 21. Different friction ring damper models: (a) Ring damper represented by Lumped parameters from [35]. (b) Ring damper represented by 3D beam from [131]. (c) Open ring damper with rectangular cross section from [133]. (d) Ring damper with V shape cross section from [134]. (e) Ring damper with varying top and bottom surface geometry from [135,285]. (f) Multiple sectors composed tuned ring damper where each sector includes a casing and a slender oscillator that rubs against its casing from [286].

Table 7
Features of test set-ups focusing on ring dampers.

References	Set-up	Preload	Excitation	Measured Quantities
[260]	Rotating	Centrifugal effect	Piezo actuator	Dynamic response

the influence of platform position and angle of generic friction damper on the nonlinear modal properties [284]. The study indicated that the optimal configuration of the frictional damper can be achieved when the contact angle is around 20° to 30°. The vertical position of the platform to place the damper is highly mode-dependent. Quaegebeur et al. [189] optimised the intentional mistuned pattern of UPDs to reduce both the 1st flexural and torsional modes. An optimal mistuning pattern was identified considering aerodynamic constraints and the negative random mistuning effects on the vibration response. However, the identified mistuned UPD is mode-dependent and may be sensitive to the veering region in lower nodal diameters.

6.1.2. Friction ring damper

The initial studies for friction ring dampers were performed using lumped parameter models, as shown in Fig. 21(a) [35,287]. The impact of both the ring damper mass and the rotational speed on the nonlinear forced frequency response [35] and damped nonlinear normal modes [287] were revealed. The studies indicate that these parameters significantly influence damping properties, as they can alter the centrifugal force applied to the friction interface, resulting in a change in friction limits and stick–slip behaviour on the interface. Results demonstrate that when the damper mass increases or when the rotational speed increases, the amplitude of the resonant peaks changes indicating the existence of an optimal damper mass that should be carefully tuned. A full FEM of the blisk with a simplified ring was then considered in [131], modelling the ring damper using 3D-beam elements as shown in Fig. 21(b). The authors emphasised the significant role of ring thickness in friction damping, concluding that there is an optimal ring thickness for maximising friction damping, which is consistent with earlier investigations in [35]. A full high-fidelity FEM including both the blisk and the ring damper was developed in [132] as a case study to validate a novel reduced order modelling method. In the studies [132,288], the impact of a non-dimensional parameter ρ,

which is a function of the friction coefficient, normal contact pressure, and forcing level, was evaluated in the context of a nonlinear dynamic response. The sensitivity of the resonance peak and friction damping to the non-dimensional parameter ρ was investigated over a wide range, showing that the friction damping efficiency is proportionally correlated to the non-dimensional parameter, highlighting that it is crucial to control the normal contact load for the optimal design of friction ring dampers. In terms of design and optimisation, the shape of friction ring dampers has been the main focus as it directly impacts the normal contact pressure. Using a similar blisk FEM shown in [132], a parametric study was carried by Tang and Epureanu [134] to assess the damping effectiveness of a V-shaped friction ring damper, whose geometry is shown in Fig. 21(d). To enhance the robustness of the friction damper, a comprehensive sensitivity analysis was conducted in [134] to investigate the influence of geometric parameters, including the angle, length, and thickness of the wedge shape, on the nonlinear dynamic response of the blisk. The location of the ring damper was also studied over a wide variation of ρ to find the optimal placement. In the recent studies [135,285], the top and bottom surface geometries of the friction ring damper were numerically optimised using damped nonlinear modal analysis. The parameterisation of the surface geometry and some examples are shown in Fig. 21(e). It was found that the variation of the contact interface geometry significantly impacts the normal pressure distribution and initial contact conditions, leading to a large variation in the resonant frequency and damping ratio. It was demonstrated that, by taking an optimal geometry, the vibration response at resonance can be reduced by about 50%.

The concept of tuned vibration absorbers can be integrated into the design of friction damper to enhance the damping effects. The idea of the concept is to allow for substantial energy transfer between the blisk and the ring damper by matching the natural frequencies of the ring damper with a specific resonance frequency of the disk. This tuning can greatly amplify friction damping. The theoretical work of this concept was first proposed in [133]. As shown in Fig. 21(c), an open ring damper with a rectangular cross-section was studied for this concept. The concept was further extended in [286] where a pioneering design for a fully tuned friction ring damper was proposed. The design of the ring damper is shown in Fig. 21(f). It is composed of a casing used to hold the system in place and a slender oscillator

that rubs against its casing. It enables the internal friction interface to be loaded with a targeted constant normal load, leading to a substantial improvement in damping properties. It was numerically studied using a high-fidelity FE model based on the geometry of the NASA rotor67 [286], demonstrating good effectiveness of this innovative design across various parameters, with the most significant reduction observed in the presence of substantial geometric mistuning, attributed to the absence of one of its sectors. This study also highlighted that a change in the topology or architecture of the damper can drastically improve the damping properties of friction ring dampers. It also shows some robustness even if the tuning is not perfect. By having a mistuned damper, any blisk mode can be targeted and wide frequency ranges can be targeted with the ring damper, even blade-dominated modes that are usually not targetable with those dampers. Similarly to the study in [189] applied to UPD, it appears that mistuned friction dampers have generally positive effects on friction damping and its robustness regardless of the type of damper. Despite numerous numerical investigations on the design of friction ring dampers, to the best of the authors' knowledge, no work with rigorous optimisation studies has been conducted for friction ring dampers, and this may be the topic of future research.

6.1.3. Shroud and snubber damping

There are very few studies on the design and optimisation of shroud and snubber damping. One of them was conducted by Wang et al. [273] using normalised slip load and the orientation of the interface as two critical design parameters. The other main parameter to control the friction damping of the shroud is the normal load on the friction interface as indicated in experimental studies [87,252,254]. There will be an optimal normal load to maximise the friction damping while avoiding loss of contact.

In summary, the previous design studies of friction dampers focused mainly on the shape and surface geometries of the damper to improve the damping performance. For underplatform dampers, different geometries were explored to avoid the rolling motion of the damper during the in-phase mode. For friction ring dampers, in addition to the exploration of different shapes, the mesoscale surface geometry was considered as a design parameter, showing a significant impact on the damping performance due to its influence on normal pressure distribution. Innovative designs such as tuned friction mass dampers were explored to increase relative motions between the blisk and the damper. However, experimental verification and rigorous optimisation studies are lacking for friction ring damper designs. For both ring and underplatform dampers, the intentional mistuning design of the friction damper was explored, showing improvement in friction damping.

6.2. Robust design and uncertainty quantification

Another crucial aspect in the design of friction dampers is ensuring performance robustness under various sources of uncertainties. One of the main uncertainties comes from the modelling of the friction interface. In this subsection, we will first present the variability of experimental measurements observed during the contact interface characterisation and friction damping device testing. This will be followed by a review of related numerical studies on robust design and uncertainty quantification.

6.2.1. Experimental observation of the variation

Experimental measurements often encounter variability and/or lack of repeatability, meaning that the same nominal experimental conditions may produce different measured reference quantities. While some variability is inherent in all experimental observations, an additional factor arises when considering contact friction: the non-uniqueness of the solution. As shown in Section 3, for turbine applications, the contact friction model is usually parametrised using a few variables that can be obtained experimentally using fretting test rigs [84,203,290] as shown

in Section 5.2. However, current contact models are not yet capable of capturing the complexity of frictional phenomena. This results in a large observed variability of the contact parameters. Fig. 22 gives an example of the variation of measured coefficient of friction and contact stiffness from the 1D friction test rig presented in [84], showing that both contact parameters follow a Gaussian distribution in Test 5 with a standard deviation of 0.23% and 3.77% respectively. It can also be observed that there is a larger variation of the mean values of coefficient of friction and contact stiffness among the four tests, highlighting that it is not possible to represent the contact behaviour using a unique set of contact parameters.

In addition to the variation of contact parameters themselves, the initial contact conditions of the friction damping device may lead to a large variation in the damping performance. If a portion of the contact interface in friction damping devices remains permanently stuck during vibration (i.e., microslip of the contact interface), the dynamic behaviour and the friction damping contribution depend on the initial conditions, leading to different static force equilibria. This phenomenon was initially theorised numerically [227] and later experimentally observed [242,246,269]. In [242,246], the same experimental nominal conditions (preload, excitation level) resulted in different frequency response functions on the blade for underplatform and midspan dampers, respectively. In both cases, the observed variability was linked to differences in the static component of the measured contact forces.

Furthermore, flat-on-flat contact interfaces may further amplify variability in damper performance because the nominal contact area may differ from the actual one due to surface imperfections such as roughness and waviness. While this effect is present in all friction damping solutions (e.g., roots, shrouds), it is particularly pronounced in the case of friction dampers. This is because different damper kinematics, such as increased rotation, may be triggered by different support conditions. As shown in Figs. 20 and 21, flat-on-flat contact interfaces are often used for most friction damper designs. In [60], it was observed that numerical predictions of the dynamic response of blades with wedge dampers, assuming a uniform pressure distribution on the grid of contact points on the nominal contact area, failed to match experimental observations. This discrepancy encompassed both the reduction in response amplitude and the difference in frequency (i.e., overall stiffness and damping contribution). As shown in Fig. 23(a), the experimental–numerical agreement significantly improved when the actual pressure distribution was estimated using a Fuji Prescale pressure film and was replicated in numerical simulations. Similar findings were obtained when investigating the damper mechanics of asymmetric underplatform dampers [289]. In that case, a practical solution to minimise damper rotation, ensure an adequate level of damping, and reduce variability was to remove the central portion of the damper's flat surface to ensure contact at the outer edges, as illustrated in Fig. 23(b). A recent study [243] analysed the dynamic response of an industrial high-pressure turbine-bladed disk with wedge dampers measured from engine tests. The study revealed that accurately modelling realistic contact bedding patterns, derived from observations of worn components, significantly improved the agreement between frequency response predictions and engine data, as illustrated in Fig. 23(c). Furthermore, an important implication is that numerical predictions are not unique but rather accompanied by an uncertainty band attributable to contact sensitivity. The studies in [231,291] also compare the dynamic response from experimental testing and numerical models, concluding that the discrepancy obtained comes mainly from the insufficient modelling of the friction interface. Delaune et al. [292] performed a study to investigate the effects of uncertainties associated with fretting wear, showing that it can significantly change the variation of the vibration response.

In summary, as observed in Section 6.2.1, the main source of discrepancy between the experimental and numerical simulation results comes from friction interface modelling. Firstly, current contact models
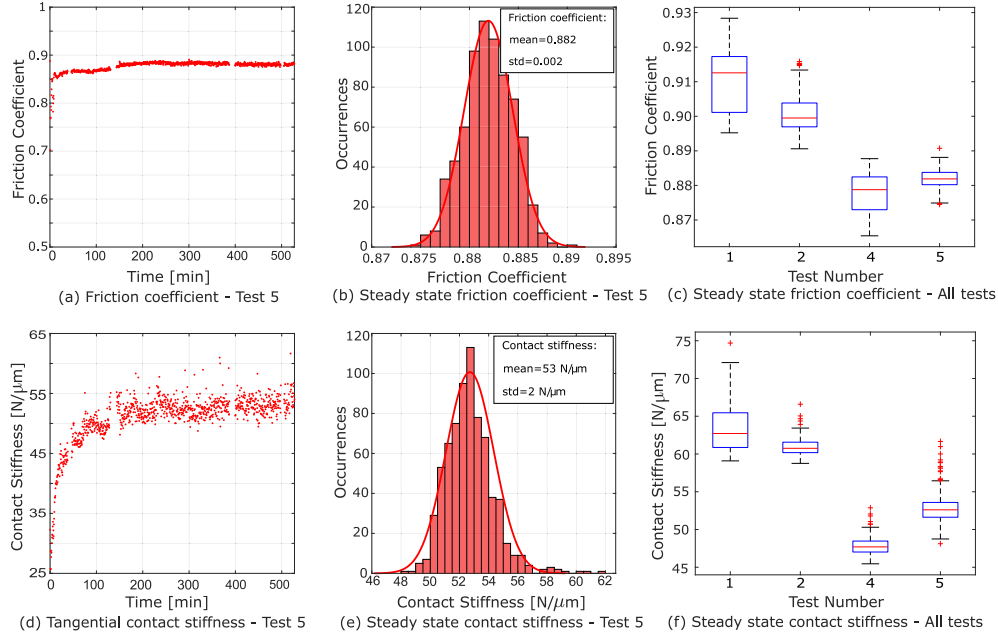
Fig. 22. (a,d) Evolution in time of μ and k_t; (b,e) Statistical distribution of steady state μ and k_t (values after 200 min); (c,f) Boxplots of steady state μ and k_t; Tests 1 and 2 were conducted at a relative displacement of 14μm, and tests 4 and 5 at 22μm [275].
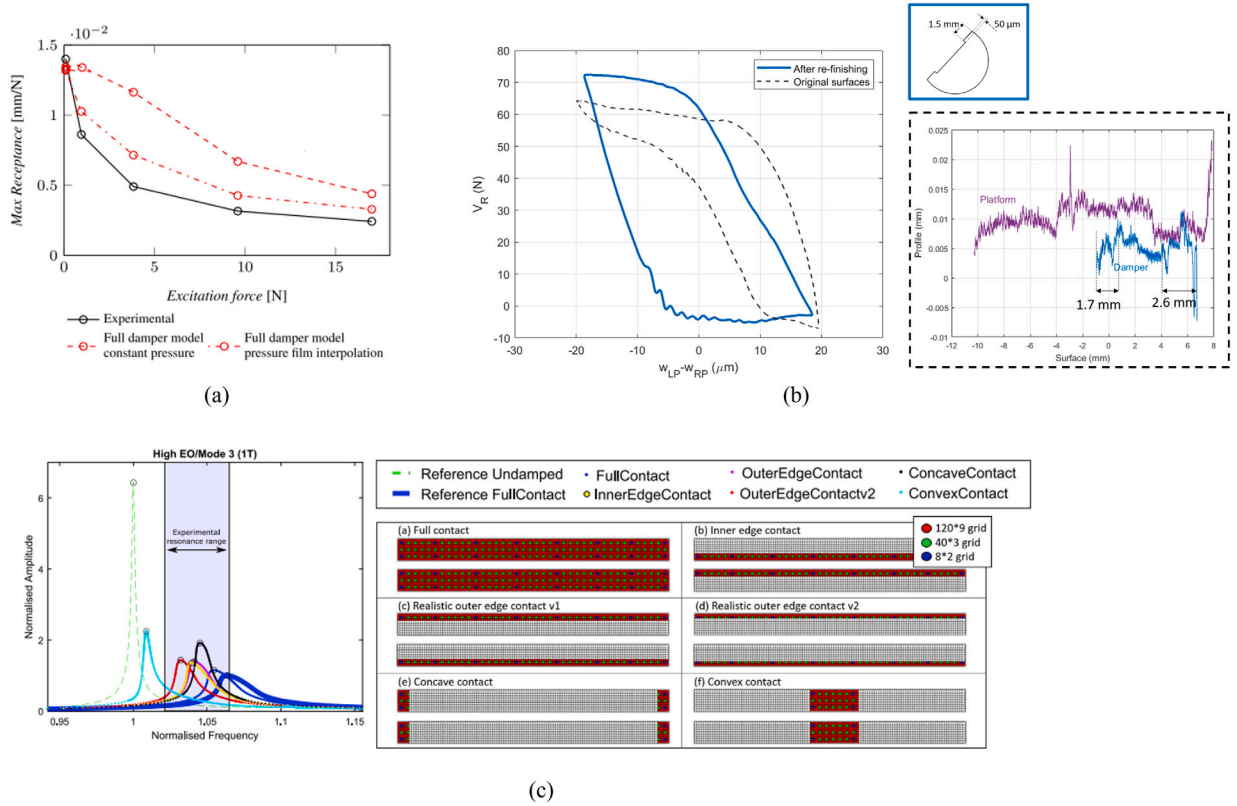

Fig. 23. (a) Damper performance curve for Out-of-Phase mode of vibration: measured vs simulated results using different hypotheses on contact pressure distribution [236] (b) (Left) Measured In-Phase platform–platform hysteresis of an asymmetrical underplatform damper with two different flat surface finishings; (Right) In black, profilometer results for damper flat surface and corresponding platform insert and, in blue, schematic representation of re-finishing process for damper flat surface. Adapted from [289]. (c) Simulated frequency response function for bladed disk with wedge dampers under different contact point distribution hypotheses and comparison with experimental results. Adapted from [243].

are not yet able to fully capture the contact friction behaviour from experiments, which leads to contact parameter variability. Furthermore, the inevitable deviation of surface geometry from the nominal condition, due to manufacturing and finishing tolerances can significantly impact contact pressure distribution leading to a very different dynamic response. Finally, the inability to control the initial position of friction dampers which is a result of the centrifugal loads arising from disk rotation, can change the contact pressure distribution greatly and thus influence the dynamic response. In addition, uncertainties may also arise from environmental conditions during operation such as the variation of temperature which may change the friction coefficient [293], and the evolution of material and contact properties over the structure's lifespan, for example, due to the progression of wear [85,294] and the influence of creep [295].

6.2.2. Robust and reliability based design studies

Considering the various sources of uncertainties highlighted in the experimental observation, it is imperative to identify and address the primary uncertainties in the system to enhance numerical predictions, as demonstrated in previous studies [82]. Petrov [296], using a sensitivity approach and reconstructing the probability density functions of forced frequency response, demonstrated the substantial impact of uncertainties in the friction coefficient on the nonlinear dynamic response of turbine blades. The impact of contact parameters on the variation of the dynamical response was further confirmed by Krack et al. [297] through a reliability analysis of a blisk with shroud coupling. To further understand the uncertainties related to the contact parameters, an advanced multi-scale modelling approach was developed in [294] considering surface roughness, waviness and fretting wear of the contact interface. However, the related robust design and optimisation of the approach have not yey been carried out due to the high computational expense.

More recently, Yuan et al. [275] performed a robust optimisation of the geometry of the wedge-shaped underplatform damper considering manufacturing variability. The performance robustness of the damper is defined as the sum of the variance of two simulated parameters, namely resonance amplitude and resonance frequencies. A new optimisation approach taking into account the non-uniqueness of friction forces was proposed for the computation of dynamic response boundaries for turbine bladed disks with contacts [298,299] and midspan dampers [300]. The computation of frequency response variability was further enhanced using a nonlinear-mode-based approach [301].

Sun et al. [284] conducted a stochastic analysis of nonlinear modal properties, considering variations in the contact angle and the relative position of the damper to the platform. Monte Carlo simulations together with Sobol analysis were used to evaluate the global sensitivity of each geometrical parameter. Yuan et al. [275] propagated the uncertainties from friction interface parameters in the dynamical response of bladed disk systems from an underplatform damper. The stochastic dynamic response obtained through numerical uncertainty propagation closely aligns with the experimental results of the nonlinear dynamic response. The key findings of their investigation are depicted in Fig. 24. It is worth noting that the phase instead of frequency is used in the study to facilitate the construction of data-driven models for numerical propagation. The majority of the experimental data points lie within the 90% confidence interval identified from the stochastic model considering the uncertainties from contact parameters. It illustrates that the stochastic dynamic response can improve the predictivity of the physical model by taking into account the main sources of uncertainty.

In terms of friction ring dampers, the robustness of their shape design was studied using a 3D full-scale compressor in [285]. The variation in the manufacturing process was taken into account and uncertainties were propagated using Kriging-based surrogate models. The uncertainties associated with friction dampers can also give rise to mistuning effects, resulting in substantial variations in their impact on the dynamic response [189]. This depends on the potential deliberately

introduced mistuning pattern. Yuan et al. [86] proposed a methodology to quantify the influence of mesoscale interface geometry variation on the nonlinear dynamic response, showing that the edge radii and surface bumpiness can have significant effects on the nonlinear modal properties of fan blade systems. In [302,303], the boundary of the steady-state response was determined using two different numerical approaches for wedged friction dampers. A criterion that determines the periodic response boundaries according to the limit tangential force was proposed.

The different studies presented previously have demonstrated the significant impact of friction contact uncertainties on the nonlinear dynamic response for aero-engine structures with friction interfaces, highlighting the importance of taking into account the uncertainties in the design stage. Most of the current uncertainty and robust design studies are related to underplatform dampers using relatively simplified models. There are very few works focusing on the robust design of the blade root damping and friction ring dampers due to the high computational cost of manipulating the variation of high-fidelity models and associated nonlinear simulations. Classical Monte Carlo simulation methods are often used for uncertainty propagation but they become very expensive for high-fidelity models. To overcome this limitation, Butlin et al. [304,305] proposed a new approach based on the principle of Maximum Entropy for the prediction of the response variability of friction-damped turbine blades. The proposed approach can make the prediction two orders of magnitude faster than the classical Monte Carlo simulation. It was also validated against the experimental database through a representative turbine blade test rig. More efforts are needed in the development of such methods as well as data-driven modelling techniques to improve the efficiency of the uncertainty propagation of such nonlinear large-scale models. The other challenge for uncertainty quantification is that there is not sufficient experimental data available on the characterisation of friction interfaces at different scales. More experimental testing will be needed to create the database for supporting uncertainty quantification and robust design studies.

7. New trending topics

7.1. New friction damper designs

New concepts of friction dampers in turbomachinery have been emerging in recent years to enhance and control friction damping for multi-operational conditions and multi-modes in a passive, active or semi-active manner. Coupling the traditional dry friction dampers with electrical units, novel materials and energy transfer concepts have been explored to control the normal pressure or relative tangential displacement on the friction interface. This section introduces innovative concepts for the next-generation design of friction dampers.

7.1.1. Shunted piezoelectric damping

The piezoelectric material can be actively or passively coupled with friction dampers to improve damping performance. The key concept of shunted piezoelectric damping is to distribute piezoelectric material on the surface of the friction damper [306,307] to dissipate the strain energy stored in the friction damper or blisk itself through a shunted impedance. A similar idea was also investigated in [308] but without the friction ring damper. This damping technique can be used to suppress the vibration for both disk–dominated modes and blade-dominated modes [309].

Programmable shunted circuit parameters, combined with a reliable dry friction damping structure, are a very robust damping technique for an aero-engine operating at variable working conditions where the normal force deviates from the design value. The effective working range can be extended up to 2.6 times [307] by matching piezoelectric damping and dry friction regarding the working state and excitation level. Using programmable synthetic impedance [310] or
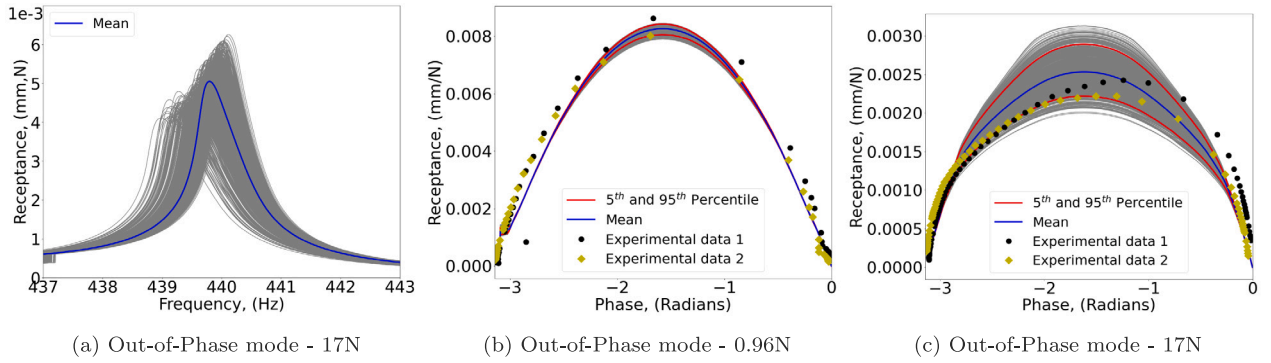
(a) Out-of-Phase mode - 17N　　　　(b) Out-of-Phase mode - 0.96N　　　　(c) Out-of-Phase mode - 17N

Fig. 24. (a) Randomly generated FRFs of the turbine blades with underplatform damper at the excitation level of 17 N; (b,c) Comparison of stochastic dynamic phase response and experimental data at the excitation level of 0.96 *N* (linear case) and 17 *N* (nonlinear case) [275].
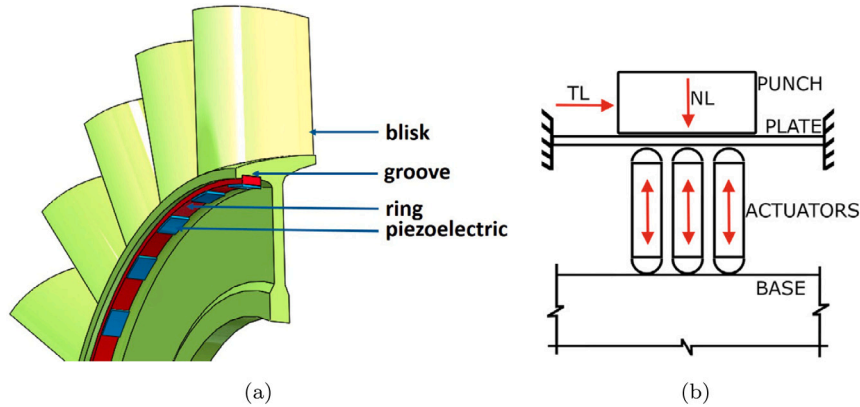

(a)　　　　　　　　　　　　　　　　　　　　(b)

Fig. 25. (a) Illustration of piezoelectric ring damper [307]; (b) Conceptual design of contact normal load distribution using piezoelectric actuation [313].

the self-adaptive shunted circuit (e.g. the synchronised switch damping circuit [311]), also leads to vibration mitigation robust to variable working conditions. Fig. 25(a) depicts an illustration of a piezoelectric ring damper, showcasing how damping is imparted through both the friction damper and the piezoelectric damping mechanism. Furthermore, the proposed piezoelectric network can be used to mitigate the amplification effects of the mistuned blisk by distributing piezoelectric patches in an optimal topology [312]. It will facilitate the creation of electric energy pathways between sectors, promoting the dissipation of vibrational energy.

7.1.2. Normal pressure-controlled friction damper

The effectiveness of friction damping is primarily governed by the critical friction threshold between two surfaces, which is predominantly influenced by the normal load and coefficient of friction. Recent research efforts have been made to adjust the local normal loading of the friction damper by inputting a control voltage to the distributed piezoelectric materials based on the inverse piezoelectric effect. Wu et al. [314] explored this concept to mitigate the steady-state vibration of the structure by controlling the second harmonic time-varying normal force and revealed a 20% increase in damping compared with the optimal constant normal force. To remove the additional mass brought by the actuators that limits their application prospects in the aerospace field, macro-fibre-composites can be applied to control the normal force of the friction dampers as studied in [315]. Recently, Lasen et al. [313,316] introduced a proof-of-concept experimental campaign aiming for a turbine underplatform damper. Its conceptual design is shown in Fig. 25(b). The pressure distribution due to the normal load (noted NL in Fig. 25(b)) can be altered using a series of piezoelectric actuators leading to different hysteretic behaviour and frequency responses. This conceptual design of normal load control has

been applied to a 1D friction test rig in [313] demonstrating that the stiffness, energy dissipation, and friction limit can be altered through the manipulation of actuation pattern and/or input voltage. Such a control mechanism allows for customising the interface behaviour to achieve the optimal damping performance of the assembled structure. The principal challenge of piezo-based damping technologies is the installation and maintenance of piezoelectric materials.

7.2. New modelling and simulation techniques

7.2.1. Full data-driven models for contact modelling and simulation

Recent developments in numerical modelling and simulation have emphasised the adoption of data-driven techniques for the modelling and simulation of contact laws. These techniques avoid the expensive trial-and–error process of tuning the contact model parameters. However, using these approaches presents some challenges, such as requiring a large data set and dealing with the difficulty in obtaining friction information. In [317], artificial neural networks (ANN) are used on experimental data for the reconstruction of the normal contact force from the displacement and velocity. In the context of control applications, Dong et al. [318] suggested a method to address friction modelling by incorporating a deep Gaussian process for compensation. In [319], ANN is used to predict the friction force based on the normal load, relative velocity and material properties derived from different elementary experimental benchmarks. Finally, in [320], ANN is used to reduce the computational cost and replace the AFT procedure in the computation of the nonlinear dynamic response.

7.2.2. Multi-physics simulations

Recent endeavours have focused on incorporating and coupling with other physical phenomena to enhance predictions and integrate

additional design technologies. As an illustration of piezoelectric coupling, Wu et al. [321] introduced the concept of the Nonlinear Modal Electromechanical Coupling Factor (NMEMCF). The paper outlines a numerical strategy for incorporating piezoelectric coupling into nonlinear dynamic computations using the HBM. This approach was validated through testing on a beam structure with a piezo patch, demonstrating its effectiveness in achieving high damping levels. Properly considering piezoelectric coupling is the initial stage of the numerical design of piezoelectric damping, as discussed in Section 7.1.1. In [322], thermal coupling is considered and a numerical strategy to integrate it into the simulations is presented. In the proposed modelling, the friction coefficient depends on the temperature, an unknown variable within the problem, alongside the displacements, and the former is different for each contact point. In the context of aerodynamic coupling, in [323], a fully-coupled Fluid–Structure Interaction solver able to deal with nonlinear effects of both structural and fluid domains is presented. It is based on the HBM and a serial coupling strategy where the structural and fluid problems are solved alternatively.

7.3. New experimental techniques

In earlier studies, the investigation of contact interfaces was carried out independently from the study of friction-damped turbomachinery components. However, recent advancements have led to the integration of these two approaches. Consequently, two types of experimental evidence, relating to the same test case, such as dynamic response and contact behaviour (e.g., hysteresis or relative contact kinematics), are now available. This integration enables a more comprehensive validation process and facilitates pinpointing deficiencies in the model with greater precision.

Another recent trend involves heightened focus on the actual contact area, which may deviate from the nominal one derived solely from the geometry of the contact interface. Initially, this was accomplished by scanning the contact surfaces and modelling the particular case under examination [236,289]. Subsequently, common wear patterns were analysed [243] to inform numerical models, enabling the generation of not just one specific response but rather a statistical distribution of responses. Recent studies used ultrasound [207] and total internal reflection [208] methods to actively monitor both the true contact area and the actual contact conditions in real time. In addition, in [257] the periodic recording of the effect of wear on the dynamic response evolution has been observed, while simultaneously monitoring the evolution of the contact interface and the dynamic response.

To improve the efficiency of experimental testing, nonlinear modal testing has been actively explored to capture only the amplitude-dependent resonance response of the system instead of the whole FRF at different force amplitudes. Phase lock control methods based on the extended periodic motion concept were developed to obtain the amplitude-dependent modal properties and were used to validate a turbine blade component test with frictional contacts [324]. Recently, velocity feedback-based nonlinear modal testing was proposed to remove the requirement of a controller [325]. In addition, control-based-continuation [326,327] and response-controlled testing methods [328, 329] are promising alternatives which can also be applied to predict autonomous dynamical responses such as limit cycle oscillations due to friction interfaces. Recently, an experimental test rig for friction saturated limit cycle oscillations was developed for the validation of the numerical prediction methods of turbine blades where an adjustable velocity feedback loop was instrumented [330].

8. Conclusions

This review offers an in-depth look at recent progress in friction damping for turbomachinery. The discussion encompasses numerical modelling, simulation, experimental testing, design methodologies, and optimisation studies, providing insights into cutting-edge techniques and key discoveries. By identifying gaps and suggesting future research directions, this review serves as a valuable resource. Potential research avenues for each topic are given next.

- **Modelling and simulation.** Numerical contact and friction models require enhancement to incorporate various modelling scales and additional physics affecting contact dynamics, which necessitates maintaining computational efficiency and improving current simulation techniques. An ongoing challenge lies in calibrating contact model parameters, often based on limited experimental data and valid only under specific operating conditions. Future endeavours should strive for a systematic methodology for parameter calibration. Furthermore, numerical resolution methods could aim for greater realism with fewer model reduction approximations and more intricate finite element models. Addressing complex phenomena such as mistuning, multi-physics effects, and uncertainties promises more accurate predictions. This progress can be facilitated by computational solution improvements that rely on parallel computing, such as the use of a parallel HBM [331] or parallel model refinement [332]. Both methods offer significant potential for computational speedups and could provide even greater benefits when applied to more realistic models. Another strategy involves data-driven modelling techniques, which emphasise the need for extensive experimental data while avoiding reliance on traditional modelling efforts to account for uncertain multi-physics behaviour. Hybrid analytical and data-driven modelling techniques represent a promising research area. These approaches require further detailed investigation to fully leverage the potential benefits of recent rapid advancements in artificial intelligence algorithms and computing power.

- **Experimental investigation.** Some of the possible topics of future experimental investigation include a thorough campaign on the effects of wear and surface finishing on contact conditions and dynamic response, the contact characterisation of new coatings and materials, including additive manufactured ones and measurement techniques targeting real time contact condition monitoring. Novel experimental techniques to monitor local contact conditions, and improve the efficiency of the testing are needed to investigate the effects of the variation of multi-scale surface geometries, and fretting wear. More experimental test rigs are needed for friction ring dampers to validate numerical modelling of different designs. Additionally, given the increasing interest in the digital twin concept and the expansion of online monitoring capabilities, more full-scale engine test rigs should be envisioned. This would ensure realistic working conditions, and data collection that accounts for statistical variability, enabling robust model validation and providing large datasets for data-driven modelling.

- **Design and optimisation.** The design of friction dampers can still be improved by taking into account the interface geometries at various scales, long-term fretting wear effects and other physics couplings. This can help to expand the design space and increase the reliability of the dampers. Novel designs of friction dampers can be explored by controlling the normal load distribution on friction interfaces to further optimise damping performance across different operational conditions. This can be achieved by leveraging advances in electric controlling systems, material development, and new manufacturing techniques. The damping robustness of structures should be improved further by considering the uncertainties associated with initial preloading position, contact parameter characterisation, and surface geometries. Robust and statistically relevant strategies must be developed to characterise and propagate uncertainties into the nonlinear dynamic response of structures with multiple contact

interfaces. The future research direction for designing and optimising friction damping should consider integrating novel manufacturing capabilities and mechanically or tribologically tailorable materials. These manufacturing and material technologies will expand the design possibilities and provide more practical options across different scales. Additionally, this will necessitate the development of more efficient and innovative robust topological optimisation methods, which will involve combining the rapid advancements in artificial intelligence technologies.

CRediT authorship contribution statement

Jie Yuan: Writing – review & editing, Writing – original draft, Investigation, Conceptualization. **Chiara Gastaldi:** Writing – review & editing, Writing – original draft, Investigation, Conceptualization. **Enora Denimal Goy:** Writing – review & editing, Writing – original draft, Investigation, Conceptualization. **Benjamin Chouvion:** Writing – review & editing, Writing – original draft, Investigation, Conceptualization.

Declaration of competing interest

The authors declare that they have no known competing financial interests or personal relationships that could have appeared to influence the work reported in this paper.

Data availability

No data was used for the research described in the article.

Acknowledgements

References

[1] D. Ewins, Control of vibration and resonance in aero engines and rotating machinery–An overview, Int. J. Press. Vessels Pip. 87 (9) (2010) 504–510.

[2] E. Seinturier, Forced response computation for bladed disks industrial practices and advanced methods, in: Lecture Series-Von Karman Institute for Fluid Dynamics, vol. 2, 2007, p. 5.

[3] M.P. Castanier, C. Pierre, Modeling and analysis of mistuned bladed disk vibration: Current status and emerging directions, J. Propuls. Power 22 (2) (2006) 384–396.

[4] J. Yuan, F. Scarpa, G. Allegri, B. Titurus, S. Patsias, R. Rajasekaran, Efficient computational techniques for mistuning analysis of bladed discs: A review, Mech. Syst. Signal Process. 87 (2017) 71–90.

[5] B. Lee, Self-sustained shock oscillations on airfoils at transonic speeds, Prog. Aerosp. Sci. 37 (2) (2001) 147–196.

[6] F. Zhao, J. Nipkau, M. Vahdati, Influence of acoustic reflections on flutter stability of an embedded blade row, Proc. Inst. Mech. Eng. A 230 (1) (2016) 29–43.

[7] F. Zhao, N. Smith, M. Vahdati, A simple model for identifying the flutter bite of fan blades, J. Turbomach. 139 (7) (2017) 071003.

[8] M. Vahdati, G. Simpson, M. Imregun, Mechanisms for wide-chord fan blade flutter, J. Turbomach. 133 (4) (2011) 041029.

[9] A.V. Srinivasan, Flutter and resonant vibration characteristics of engine blades, J. Eng. Gas Turb. Power 119 (4) (1997) 742–775.

[10] L. Fathyunes, M.A. Mohtadi-Bonab, A review on the corrosion and fatigue failure of gas turbines, Metals 13 (4) (2023) 701.

[11] N. Mukhopadhyay, S. Ghosh Chowdhury, G. Das, I. Chattoraj, S. Das, D. Bhattacharya, An investigation of the failure of low pressure steam turbine blades, in: Failure Analysis Case Studies II, Elsevier, 2001, pp. 211–223.

[12] L.E. Goodman, J.H. Klumpp, Analysis of slip damping with reference to turbine-blade vibration, J. Appl. Mech. 23 (3) (1956) 421–429.

[13] K. Cross, W. Lull, R. Newman, a.R. Cavanagh, Potential of graded coatings in vibration damping, J. Aircr. 10 (11) (2004) 689–691.

[14] S. Patsias, C. Saxton, M. Shipton, Hard damping coatings: An experimental procedure for extraction of damping characteristics and modulus of elasticity, Mater. Sci. Eng. A 370 (1) (2004) 412–416.

[15] O.T. Easterday, An Experimental Characterization of Damping Properties of Thermal Barrier Coatings at Elevated Temperatures (Ph.D. thesis), Air Force Institute of Technology, 2011.

[16] Y. Chen, J. Zhai, Q. Han, Vibration and damping analysis of the bladed disk with damping hard coating on blades, Aerosp. Sci. Technol. 58 (2016) 248–257.

[17] L. Rouleau, O. De Smet, J.-F. Deü, Vibration prediction of rotating composite fan blades comprising viscoelastic damping treatments, J. Sound Vib. (2022) 117135.

[18] B. Manayil Santhosh, M. Tufekci, L. Salles, F. Scarpa, J. Yuan, Flutter mitigation of turbofan blades using viscoelastic patches, in: Proceedings of ISMA 2022-International Conference on Noise and Vibration Engineering and USD 2022-International Conference on Uncertainty in Structural Dynamics, 2022.

[19] J. Yuan, G. Allegri, F. Scarpa, Buffeting mitigation using carbon nanotube composites: A feasibility study, Proc. Inst. Mech. Eng. G 227 (9) (2013) 1425–1440.

[20] S. Bograd, P. Reuss, A. Schmidt, L. Gaul, M. Mayer, Modeling the dynamics of mechanical joints, Mech. Syst. Signal Process. 25 (8) (2011) 2801–2826.

[21] M. Krack, L. Salles, F. Thouverez, Vibration prediction of bladed disks coupled by friction joints, Arch. Comput. Methods Eng. 24 (2016) 589–636.

[22] R.P. Kroon, Turbine-blade vibration due to partial admission, J. Appl. Mech. 7 (4) (1940) A161–A165.

[23] J.F. Shannon, Vibration Problems in Gas Turbines, Centrifugal and Axial Flow Compressors, Reports and memoranda, H.M. Stationery Office, 1948.

[24] J.R. Schnittger, The stress problem of vibrating compressor blades, J. Appl. Mech. 22 (1) (1955) 57–64.

[25] X. Guo, J. Zeng, H. Ma, C. Zhao, L. Qu, B. Wen, Dynamic characteristics of a shrouded blade with impact and friction, Front. Mech. Eng. 15 (2) (2020) 209–226.

[26] E. Ferhatoglu, S. Zucca, D. Botto, J. Auciello, L. Arcangeli, Nonlinear vibration analysis of turbine bladed disks with Midspan dampers, J. Eng. Gas Turb. Power 144 (4) (2022).

[27] A. Balakirev, B. Bolotov, A.K. Golovkin, M.S. Nikhamkin, N. Sazhenkov, L. Voronov, I.B. Konev, Experimental evaluation of the efficiency of gas turbine engine parts damping with dry friction dampers using laser vibrometer, in: Proc. of the 29th Congress of the International Council of the Aeronautical Sciences. ICAS 2014, 2014.

[28] E.K. Armstrong, Recent blade vibration techniques, J. Eng. Power 89 (3) (1967) 437–444.

[29] J. Man, X. Bian, W. Zeng, W. Yan, D. Qiao, Experimental investigation of the dynamic response of a flat blade with dual dry friction dampers, Energies 16 (21) (2023) 7401.

[30] J. Man, B. Xue, X. Bian, W. Yan, D. Qiao, W. Zeng, Experimental and numerical investigations on the dynamic response of blades with dual friction dampers, Aerospace 10 (12) (2023) 977.

[31] M.A. Niemotka, J.C. Ziegert, Optimal design of split ring dampers for gas turbine engines, J. Eng. Gas Turb. Power 117 (3) (1995) 569–575.

[32] S. Baek, B. Epureanu, Reduced-order modeling of bladed disks with friction ring dampers, J. Vib. Acoust. 139 (6) (2017) 061011.

[33] J.H. Griffin, Friction damping of resonant stresses in gas turbine engine airfoils, J. Eng. Power 102 (2) (1980) 329–333.

[34] K.Y. Sanliturk, D.J. Ewins, R. Elliott, J.S. Green, Friction damper optimization: Simulation of rainbow tests, J. Eng. Gas Turb. Power 123 (4) (1999) 930–939.

[35] D. Laxalde, F. Thouverez, J.-J. Sinou, J.-P. Lombard, Qualitative analysis of forced response of blisks with friction ring dampers, Eur. J. Mech. A Solids 26 (4) (2007) 676–687.

[36] M. Krack, S. Tatzko, L. Panning-von Scheidt, J. Wallaschek, Reliability optimization of friction-damped systems using nonlinear modes, J. Sound Vib. 333 (13) (2014) 2699–2712.

[37] C. Joannin, B. Chouvion, F. Thouverez, J.-P. Ousty, M. Mbaye, A nonlinear component mode synthesis method for the computation of steady-state vibration in non-conservative systems, Mech. Syst. Signal Process. 83 (2017) 75–92.

[38] C. Gastaldi, M.M. Gola, Platform-centered reduction: A process capturing the essentials for blade-damper coupled optimization, J. Eng. Gas Turb. Power 143 (8) (2021).

[39] M.M. Gola, A general geometrical theory of turbine blade underplatform asymmetric dampers, Mech. Syst. Signal Process. 191 (2023) 110167.

[40] C. Gastaldi, M.M. Gola, Convergence-free mapping of non-linear damper-blade performance, Mech. Syst. Signal Process. 208 (2024) 111062.

[41] S. Quaegebeur, B. Chouvion, F. Thouverez, Nonlinear dynamic analysis of three-dimensional bladed-disks with frictional contact interfaces based on cyclic reduction strategies, Int. J. Solids Struct. 236–237 (2022) 111277.

[42] K. Johnson, Contact Mechanics, Cambridge University Press, UK, 1985.

[43] P. Wriggers, T.A. Laursen, Computational Contact Mechanics, vol. 2, Springer, 2006.

[44] E. M'Ewen, XLI. stresses in elastic cylinders in contact along a generatrix (including the effect of tangential friction), Lond. Edinb. Dublin Philos. Mag. J. Sci. 40 (303) (1949) 454–459.

[45] G.M. Hamilton, L.E. Goodman, The stress field created by a circular sliding contact, J. Appl. Mech. 33 (2) (1966) 371–376.

[46] R.D. Mindlin, H. Deresiewicz, Elastic spheres in contact under varying oblique forces, J. Appl. Mech. 20 (3) (1953) 327–344.

[47] C. Cattaneo, Sul contatto de due corpi elastici: Distribuzione locale deglisforzi, Rendiconti dell'Accademia nazionale dei Lincei 6 (1996) 342–349.

[48] M. Brake, Contact modeling across scales: From materials to structural dynamics applications, J. Struct. Dynam. 1 (2021) 49–135.

[49] G. Sfantos, M. Aliabadi, A boundary element formulation for three-dimensional sliding wear simulation, Wear 262 (5–6) (2007) 672–683.

[50] T.W. Kim, S.M. Moon, Y.J. Cho, Prediction of fretting wear using boundary element method, Tribol. Int. 44 (11) (2011) 1571–1576.

[51] L. Rodríguez-Tembleque, R. Abascal, M. Aliabadi, Anisotropic fretting wear simulation using the boundary element method, Comput. Model. Eng. Sci. (CMES) 87 (2) (2012) 127–156.

[52] V. Kaliakin, J. Li, Insight into deficiencies associated with commonly used zero-thickness interface elements, Comput. Geotech. 17 (2) (1995) 225–252.

[53] C. Desai, M. Zaman, J. Lightner, H. Siriwardane, Thin-layer element for interfaces and joints, Int. J. Numer. Anal. Methods Geomech. 8 (1) (1984) 19–43.

[54] M. Mayer, L. Gaul, Segment-to-segment contact elements for modelling joint interfaces in finite element analysis, Mech. Syst. Signal Process. 21 (2) (2007) 724–734.

[55] G. Vermot Des Roches, Frequency and Time Simulation of Squeal Instabilities. Application to the Design of Industrial Automotive Brakes (Ph.D. thesis), Ecole Centrale Paris, 2011.

[56] B.D. Yang, M.L. Chu, C.H. Menq, Stick-slip-separation analysis and non-linear stiffness and damping characterization of friction contacts having variable normal load, J. Sound Vib. 210 (4) (1998) 461–481.

[57] B.D. Yang, C.H. Menq, Characterization of 3D contact kinematics and prediction of resonant response of structures having 3D frictional constraint, J. Sound Vib. 217 (5) (1998) 909–925.

[58] D.J. Segalman, D.L. Gregory, M.J. Starr, B.R. Resor, M.D. Jew, J.P. Lauffer, N.M. Ames, Handbook on dynamics of jointed structures, 2009, Sandia National Laboratories, Albuquerque.

[59] C. Gastaldi, M.M. Gola, An improved microslip model for variable normal loads, in: Proceedings of the 9th IFToMM International Conference on Rotor Dynamics, Springer International Publishing, Cham, 2015, pp. 169–179.

[60] L. Pesaresi, J. Armand, C. Schwingshackl, L. Salles, C. Wong, An advanced underplatform damper modelling approach based on a microslip contact model, J. Sound Vib. 436 (2018) 327–340.

[61] L. Panning, W. Sextro, K. Popp, Spatial dynamics of tuned and mistuned bladed disks with cylindrical and wedge-shaped friction dampers, Int. J. Rotating Mach. 9 (3) (2003) 219–228.

[62] E. Cigeroglu, N. An, C.H. Menq, Forced response prediction of constrained and unconstrained structures coupled through frictional contacts, ASME J. Eng. Gas Turb. Power 131 (2) (2009) 022505–022505–11.

[63] C.M. Firrone, D. Botto, M.M. Gola, Modelling a friction damper: Analysis of the experimental data and comparison with numerical results, in: Volume 3: Dynamic Systems and Controls, Symposium on Design and Analysis of Advanced Structures, and Tribology, ASMEDC, 2006.

[64] L. Pesaresi, L. Salles, A. Jones, J. Green, C. Schwingshackl, Modelling the non-linear behaviour of an underplatform damper test rig for turbine applications, Mech. Syst. Signal Process. 85 (2017) 662–679.

[65] C.C. De Wit, H. Olsson, K.J. Astrom, P. Lischinsky, A new model for control of systems with friction, IEEE Trans. Autom. Control 40 (3) (1995) 419–425.

[66] Y.-K. Wen, Method for random vibration of hysteretic systems, J. Eng. Mech. Div. 102 (2) (1976) 249–263.

[67] D.J. Segalman, A four-parameter Iwan model for lap-type joints, J. Appl. Mech. 72 (5) (2005) 752.

[68] M. Iranzad, H. Ahmadian, Identification of nonlinear bolted lap joint models, Comput. Struct. 96 (2012) 1–8.

[69] P.R. Dahl, Solid friction damping of mechanical vibrations, AIAA J. 14 (12) (1976) 1675–1682.

[70] A.T. Mathis, N.N. Balaji, R.J. Kuether, A.R. Brink, M.R. Brake, D.D. Quinn, A review of damping models for structures with mechanical joints, Appl. Mech. Rev. 72 (4) (2020) 040802.

[71] C.-H. Menq, P. Chidamparam, J. Griffin, Friction damping of two-dimensional motion and its application in vibration control, J. Sound Vib. 144 (3) (1991) 427–447.

[72] K. Sanliturk, D. Ewins, Modelling two-dimensional friction contact and its application using harmonic balance method, J. Sound Vib. 193 (2) (1996) 511–523.

[73] S. Yajie, H. Jie, S. Yingchun, Z. Zigen, Forced response analysis of shrouded blades by an alternating frequency/time domain method, in: Turbo Expo: Power for Land, Sea, and Air, vol. 42401, 2006, pp. 865–872.

[74] M. Afzal, I.L. Arteaga, L. Kari, An analytical calculation of the Jacobian matrix for 3D friction contact model applied to turbine blade shroud contact, Comput. Struct. 177 (2016) 204–217.

[75] D.I.G. Jones, Vibrations of a Compressor Blade With Slip at Root, Tech. Rep. AFWAL-TR-80-4003, Air Force Wright Aeronautical Laboratories, Air Force Systems CommandWright-Patterson AFB, 1979.

[76] A.V. Srinivasan, D.G. Cutts, S. Sridhar, Turbojet Engine Blade Damping, Tech. Rep. CR 165406, United Technologies Research Center, East Hartford, CT, 1981.

[77] T. Cameron, J. Griffin, R. Kielb, T. Hoosac, An integrated approach for friction damper design, J. Vib. Acoust. 112 (1990) 175–182.

[78] K. Asai, S. Sakurai, T. Kudo, N. Ozawa, T. Ikeda, Evaluation of friction damping in dovetail root joints based on dissipation energy on contact surfaces, in: Volume 6: Structures and Dynamics, Parts A and B, ASMEDC, 2009.

[79] C. Gastaldi, T.M. Berruti, M.M. Gola, A novel test rig for friction parameters measurement on underplatform dampers, Int. J. Solids Struct. 185 (2020) 170–181.

[80] H. Dastani, D. Botto, M. Glorioso, Experimental and numerical investigation of contact parameters in a dovetail type of blade root joints, Appl. Sci. 11 (24) (2021) 12008.

[81] S. Bi, M. Beer, S. Cogan, J. Mottershead, Stochastic model updating with uncertainty quantification: An overview and tutorial, Mech. Syst. Signal Process. 204 (2023) 110784.

[82] J. Yuan, A. Fantetti, E. Denimal, S. Bhatnagar, L. Pesaresi, C. Schwingshackl, L. Salles, Propagation of friction parameter uncertainties in the nonlinear dynamic response of turbine blades with underplatform dampers, Mech. Syst. Signal Process. 156 (2021) 107673.

[83] J.F. Archard, W. Hirst, The wear of metals under unlubricated conditions, Proc. R. Soc. Lond. Ser. A. 236 (1206) (1956) 397–410.

[84] A. Fantetti, L. Tamatam, M. Volvert, I. Lawal, L. Liu, L. Salles, M. Brake, C. Schwingshackl, D. Nowell, The impact of fretting wear on structural dynamics: Experiment and simulation, Tribol. Int. 138 (2019) 111–124.

[85] E. Lemoine, D. Nélias, F. Thouverez, C. Vincent, Influence of fretting wear on bladed disks dynamic analysis, Tribol. Int. 145 (2020) 106148.

[86] J. Yuan, L. Salles, D. Nowell, C. Schwingshackl, Influence of mesoscale friction interface geometry on the nonlinear dynamic response of large assembled structures, Mech. Syst. Signal Process. 187 (2023) 109952.

[87] W. Sextro, The calculation of the forced response of shrouded blades with friction contacts and its experimental verification, in: Turbo Expo: Power for Land, Sea, and Air, American Society of Mechanical Engineers, 2000.

[88] J.a. Szwedowicz, M. Kissel, B. Ravindra, R. Kellerer, Estimation of contact stiffness and its role in the design of a friction damper, 2005, ASME. Paper 2001-GT-0290.

[89] J.A. Greenwood, J.P. Williamson, Contact of nominally flat surfaces, Proc. R. Soc. Lond. Ser. A. 295 (1442) (1966) 300–319.

[90] S. Medina, D. Nowell, D. Dini, Analytical and numerical models for tangential stiffness of rough elastic contacts, Tribol. Lett. 49 (1) (2013) 103–115.

[91] M. Eriten, A. Polycarpou, L. Bergman, Physics-based modeling for partial slip behavior of spherical contacts, Int. J. Solids Struct. 47 (18–19) (2010) 2554–2567.

[92] D. Zhang, Y. Xia, F. Scarpa, J. Hong, Y. Ma, Interfacial contact stiffness of fractal rough surfaces, Sci. Rep. 7 (1) (2017) 1–9.

[93] J. Armand, L. Pesaresi, L. Salles, C.W. Schwingshackl, A multiscale approach for nonlinear dynamic response predictions with fretting wear, 2016, ASME. Paper GT2016-56201.

[94] J. Yuan, L. Salles, C. Schwingshackl, Effects of the geometry of friction inter-faces on the nonlinear dynamics of jointed structure, in: Nonlinear Structures & Systems, vol. 1, Springer, 2022, pp. 67–74.

[95] A.E.H. Love, A Treatise on the Mathematical Theory of Elasticity, at the University Press, 1906.

[96] I.A. Polonsky, L.M. Keer, Fast methods for solving rough contact problems: A comparative study, J. Tribol. 122 (1) (2000) 36.

[97] N.N. Balaji, W. Chen, M.R. Brake, Traction-based multi-scale nonlinear dynamic modeling of bolted joints: Formulation, application, and trends in micro-scale interface evolution, Mech. Syst. Signal Process. 139 (2020) 106615.

[98] L. Pareschi, G. Russo, Implicit–explicit Runge–Kutta schemes and applications to hyperbolic systems with relaxation, J. Sci. Comput. 25 (2005) 129–155.

[99] K. Park, Practical aspects of numerical time integration, Comput. Struct. 7 (3) (1977) 343–353.

[100] J. Dormand, P. Prince, A family of embedded Runge-Kutta formulae, J. Comput. Appl. Math. 6 (1) (1980) 19–26.

[101] N.M. Newmark, A method of computation for structural dynamics, J. Eng. Mech. Div. 85 (3) (1959) 67–94.

[102] J. Chung, G.M. Hulbert, A family of single-step houbolt time integration algorithms for structural dynamics, Comput. Methods Appl. Mech. Engrg. 118 (1) (1994) 1–11.

[103] M.A. Dokainish, K. Subbaraj, A survey of direct time-integration methods in computational structural dynamics—I. Explicit methods, Comput. Struct. 32 (6) (1989) 1371–1386.

[104] W. Press, B. Flannery, S. Teukolsky, W. Vetterling, Numerical Recipes: the Art of Scientific Computing, Cambridge University Press, 1986.

[105] C. Gastaldi, T.M. Berruti, Competitive time marching solution methods for systems with friction-induced nonlinearities, Appl. Sci. 8 (2) (2018) 291.

[106] L. Charroyer, O. Chiello, J.-J. Sinou, Self-excited vibrations of a non-smooth contact dynamical system with planar friction based on the shooting method, Int. J. Mech. Sci. 144 (2018) 90–101.

[107] B. Van de Vrande, D. Van Campen, A. De Kraker, An approximate analysis of dry-friction-induced stick-slip vibrations by a smoothing procedure, Nonlinear Dynam. 19 (1999) 159–171.

[108] T.M. Cameron, J.H. Griffin, An alternating frequency/time domain method for calculating the steady-state response of nonlinear dynamic systems, J. Appl. Mech. 56 (1) (1989) 149–154.

[109] S. Nacivet, C. Pierre, F. Thouverez, L. Jezequel, A dynamic Lagrangian frequency–time method for the vibration of dry-friction-damped systems, J. Sound Vib. 265 (1) (2003) 201–219.

[110] A. Herzog, M. Krack, L. Panning-von Scheidt, J. Wallaschek, Comparison of two widely-used frequency-time domain contact models for the vibration simulation of shrouded turbine blades, in: Turbo Expo: Power for Land, Sea, and Air, Volume 7B: Structures and Dynamics, 2014, V07BT33A018.

[111] D. Laxalde, F. Thouverez, Complex non-linear modal analysis for mechanical systems: Application to turbomachinery bladings with friction interfaces, J. Sound Vib. 322 (4) (2009) 1009–1025.

[112] D. Charleux, C. Gibert, F. Thouverez, J. Dupeux, Numerical and experimental study of friction damping blade attachments of rotating bladed disks, Int. J. Rotating Mach. 2006 (2006) 1–13.

[113] E.P. Petrov, D.J. Ewins, Analytical formulation of friction interface elements for analysis of nonlinear multi-harmonic vibrations of bladed disks, J. Turbomach. 125 (2) (2003) 364–371.

[114] E.P. Petrov, D.J. Ewins, Effects of damping and Varying Contact Area at blade-disk joints in forced response analysis of bladed disk assemblies, J. Turbomach. 128 (2) (2005) 403–410.

[115] J.-H. Wang, W. Chen, Investigation of the vibration of a blade with friction damper by HBM, J. Eng. Gas Turb. Power 115 (2) (1993) 294–299.

[116] J. Chen, C. Menq, Periodic response of blades having three-dimensional nonlinear shroud constraints, J. Eng. Gas Turb. Power 123 (4) (2001) 901–909.

[117] B. Cochelin, A path-following technique via an asymptotic-numerical method, Comput. Struct. 53 (5) (1994) 1181–1192.

[118] M. Krack, J. Gross, Harmonic Balance for Nonlinear Vibration Problems, Springer, 2019.

[119] E.J. Doedel, AUTO: A program for the automatic bifurcation analysis of autonomous systems, Congr. Numer. 30 (265–284) (1981) 25–93.

[120] A. Dhooge, W. Govaerts, Y.A. Kuznetsov, Matcont: A matlab package for numerical bifurcation analysis of odes, ACM Trans. Math. Software 29 (2) (2003) 141—164.

[121] E.L. Allgower, K. Georg, Numerical Continuation Methods: An Introduction, vol. 13, Springer Science & Business Media, 2012.

[122] G. Moore, A. Spence, The calculation of turning points of nonlinear equations, SIAM J. Numer. Anal. 17 (4) (1980) 567–576.

[123] R. Seydel, Practical bifurcation and stability analysis, in: Interdisciplinary Applied Mathematics, vol. 5, Springer-Verlag, New York, 2010.

[124] Y.A. Kuznetsov, Elements of Applied Bifurcation Theory, vol. 112, Springer, New York, 1998.

[125] S. Baguet, B. Cochelin, On the behaviour of the ANM continuation in the presence of bifurcations, Commun. Numer. Methods Eng. 19 (6) (2003) 459–471.

[126] R. Alcorta, B. Chouvion, O. Montagnier, Dynamics of a non-linear jeffcott rotor in supercritical regime, Int. J. Non-Linear Mech. 148 (2023) 104272.

[127] A. Lazarus, O. Thomas, A harmonic-based method for computing the stability of periodic solutions of dynamical systems, C. R. Méc. 338 (9) (2010) 510–517.

[128] L. Peletan, S. Baguet, M. Orkhani, G. Jacquet-Richardet, A comparison of stability computational methods for periodic solution of nonlinear problems with application to rotordynamics, Nonlinear Dynam. 72 (3) (2013) 671–682.

[129] C. Joannin, F. Thouverez, B. Chouvion, Reduced-order modelling using nonlinear modes and triple nonlinear modal synthesis, Comput. Struct. 203 (2018) 18–33.

[130] S. Quagebeur, B. Chouvion, F. Thouverez, L. Berthe, Energy transfer between nodal diameters of cyclic symmetric structures exhibiting polynomial nonlinearities: Cyclic condition and analysis, Mech. Syst. Signal Process. 139 (2020) 106604.

[131] D. Laxalde, F. Thouverez, J.-P. Lombard, Forced response analysis of integrally bladed disks with friction ring dampers, J. Vib. Acoust. 132 (1) (2010) 011013.

[132] W. Tang, B.I. Epureanu, Nonlinear dynamics of mistuned bladed disks with ring dampers, Int. J. Non-Linear Mech. 97 (2017) 30–40.

[133] A. Lupini, M. Mitra, B.I. Epureanu, Application of tuned vibration absorber concept to blisk ring dampers: A nonlinear study, J. Eng. Gas Turb. Power 141 (10) (2019) 101016.

[134] W. Tang, B.I. Epureanu, Geometric optimization of dry friction ring dampers, Int. J. Non-Linear Mech. 109 (2019) 40–49.

[135] Y. Sun, J. Yuan, E. Denimal, L. Salles, Nonlinear modal analysis of frictional ring damper for compressor blisk, J. Eng. Gas Turb. Power 143 (3) (2021) 031008.

[136] S.R. Idelsohn, A. Cardona, A reduction method for nonlinear structural dynamic analysis, Comput. Methods Appl. Mech. Engrg. 49 (3) (1985) 253–279.

[137] M.P. Mignolet, A. Przekop, S.A. Rizzi, S.M. Spottswood, A review of indirect/non-intrusive reduced order modeling of nonlinear geometric structures, J. Sound Vib. 332 (10) (2013) 2437–2460.

[138] L. Renson, G. Kerschen, B. Cochelin, Numerical computation of nonlinear normal modes in mechanical engineering, J. Sound Vib. 364 (2016) 177–206.

[139] M. Peeters, R. Viguié, G. Sérandour, G. Kerschen, J.-C. Golinval, Nonlinear normal modes, Part II: Toward a practical computation using numerical continuation techniques, Mech. Syst. Signal Process. 23 (1) (2009) 195–216.

[140] J. Chen, C. Menq, Prediction of the resonant response of frictionally constrained blade systems using constrained mode shapes, in: Turbo Expo: Power for Land, Sea, and Air, vol. 78668, American Society of Mechanical Engineers, 1998, V005T14A047.

[141] E. Ferhatoglu, E. Cigeroglu, H.N. Özgüven, A new modal superposition method for nonlinear vibration analysis of structures using hybrid mode shapes, Mech. Syst. Signal Process. 107 (2018) 317–342.

[142] D. Wang, An improved nonlinear dynamic reduction method for complex jointed structures with local hysteresis model, Mech. Syst. Signal Process. 149 (2021) 107214.

[143] W. Szemplińska-Stupnicka, The modified single mode method in the investigations of the resonant vibrations of non-linear systems, J. Sound Vib. 63 (4) (1979) 475–489.

[144] M. Krack, L. Panning-von Scheidt, J. Wallaschek, A method for nonlinear modal analysis and synthesis: Application to harmonically forced and self-excited mechanical systems, J. Sound Vib. 332 (25) (2013) 6798–6814.

[145] E. Ferhatoglu, E. Cigeroglu, H.N. Özgüven, A novel modal superposition method with response dependent nonlinear modes for periodic vibration analysis of large MDOF nonlinear systems, Mech. Syst. Signal Process. 135 (2020) 106388.

[146] J. Yuan, Y. Sun, C. Schwingshackl, L. Salles, Computation of damped nonlinear normal modes for large scale nonlinear systems in a self-adaptive modal subspace, Mech. Syst. Signal Process. 162 (2022) 108082.

[147] C. Joannin, B. Chouvion, F. Thouverez, M. Mbaye, J.-P. Ousty, Nonlinear modal analysis of mistuned periodic structures subjected to dry friction, J. Eng. Gas Turb. Power 138 (7) (2016) 072504.1–12.

[148] E. Petrov, A high-accuracy model reduction for analysis of nonlinear vibrations in structures with contact interfaces, J. Eng. Gas Turb. Power 133 (10) (2011) 102503.

[149] G. Battiato, C. Firrone, T. Berruti, B. Epureanu, Reduction and coupling of substructures via Gram–Schmidt interface modes, Comput. Methods Appl. Mech. Engrg. 336 (2018) 187–212.

[150] S. Rubin, Improved component-mode representation for structural dynamic analysis, AIAA J. 13 (8) (1975) 995–1006.

[151] R.M. Hintz, Analytical methods in component modal synthesis, AIAA J. 13 (8) (1975) 1007–1016.

[152] W.C. Hurty, Dynamic analysis of structural systems using component modes, AIAA J. 3 (4) (1965) 678–685.

[153] R.R. Craig, M.C.C. Bampton, Coupling of substructures for dynamic analyses, AIAA J. 6 (7) (1968) 1313–1319.

[154] R.H. MacNeal, A hybrid method of component mode synthesis, Comput. Struct. 1 (4) (1971) 581–601.

[155] L. Jézéquel, H. Seito, Component modal synthesis methods based on hybrid models, Part I: Theory of hybrid models and modal truncation methods, J. Appl. Mech. 61 (1) (1994) 100–108.

[156] J. Yuan, F. El-Haddad, L. Salles, C. Wong, Numerical assessment of reduced order modeling techniques for dynamic analysis of jointed structures with contact nonlinearities, J. Eng. Gas Turb. Power 141 (3) (2019) 031027.

[157] L. Jezequel, A hybrid method of modal synthesis using vibration tests, J. Sound Vib. 100 (2) (1985) 191–210.

[158] F. Bourquin, Component mode synthesis and eigenvalues of second-order operators: discretization and algorithm, Math. Model. Numer. Anal. 26 (3) (1992) 385–423.

[159] D.-M. Tran, Component mode synthesis methods using partial interface modes: Application to tuned and mistuned structures with cyclic symmetry, Comput. Struct. 87 (17–18) (2009) 1141–1153.

[160] S. Besset, L. Jézéquel, Dynamic substructuring based on a double modal analysis, J. Vib. Acoust. 130 (1) (2007) 011008.

[161] J. Becker, L. Gaul, CMS methods for efficient damping prediction for structures with friction, in: Proceedings of the IMAC-XXVI, Orlando, 2008.

[162] W. Witteveen, H. Irschik, Efficient mode based computational approach for jointed structures: joint interface modes, AIAA J. 47 (1) (2009) 252–263.

[163] J. Yuan, L. Salles, F.E. Haddad, C. Wong, An adaptive component mode synthesis method for dynamic analysis of jointed structure with contact friction interfaces, Comput. Struct. 229 (2020) 106177.

[164] S. Zucca, B.I. Epureanu, Bi-linear reduced-order models of structures with friction intermittent contacts, Nonlinear Dynam. 77 (3) (2014) 1055–1067.

[165] C. Jung, K. D'Souza, B.I. Epureanu, Nonlinear amplitude approximation for bilinear systems, J. Sound Vib. 333 (13) (2014) 2909–2919.

[166] M. Mitra, S. Zucca, B.I. Epureanu, Adaptive microslip projection for reduction of frictional and contact nonlinearities in shrouded blisks, J. Comput. Nonlinear Dynam. 11 (4) (2016).

[167] M.-H. Tien, K. D'Souza, A generalized bilinear amplitude and frequency approximation for piecewise-linear nonlinear systems with gaps or prestress, Nonlinear Dynamics 88 (2017) 2403–2416.

[168] A.A. Morsy, M. Kast, P. Tiso, A frequency-domain reduced order model for joints by hyper-reduction and model-driven sampling, Mech. Syst. Signal Process. 185 (2023) 109744.

[169] N.N. Balaji, T. Dreher, M. Krack, M.R. Brake, Reduced order modeling for the dynamics of jointed structures through hyper-reduced interface representation, Mech. Syst. Signal Process. 149 (2021) 107249.

[170] S.J. Wildheim, Excitation of rotationally periodic structures, J. Appl. Mech. 46 (4) (1979) 878–882.

[171] D.L. Thomas, Standing waves in rotationally periodic structures, J. Sound Vib. 37 (2) (1974) 288–290.

[172] R.M. Orris, M. Petyt, A finite element study of harmonic wave propagation in periodic structures, J. Sound Vib. 33 (1974) 223–236.

[173] A.F. Vakakis, Dynamics of a nonlinear periodic structure with cyclic symmetry, Acta Mech. 95 (1–4) (1992) 197–226.

[174] F. Georgiades, M. Peeters, G. Kerschen, J.C. Golinval, M. Ruzzene, Modal analysis of a nonlinear periodic structure with cyclic symmetry, AIAA J. 47 (4) (2009) 1014–1025.

[175] E.P. Petrov, A method for use of cyclic symmetry properties in analysis of nonlinear multiharmonic vibrations of bladed disks, J. Turbomach. 126 (1) (2004) 175–183.

[176] C. Siewert, L. Panning, J. Wallaschek, C. Richter, Multiharmonic forced response analysis of a turbine blading coupled by nonlinear contact forces, J. Eng. Gas Turb. Power 132 (8) (2010) 082501.

[177] S. Quaegebeur, B. Chouvion, F. Thouverez, Model reduction of nonlinear cyclic structures based on their cyclic symmetric properties, Mech. Syst. Signal Process. 145 (2020) 106970.

[178] M.T. Yang, J.H. Griffin, A reduced-order model of mistuning using a subset of nominal system modes, J. Eng. Gas Turb. Power 123 (4) (2001) 893–900.

[179] S.-H. Lim, R. Bladh, M.P. Castanier, C. Pierre, Compact, generalized component mode mistuning representation for modeling bladed disk vibration, AIAA J. 45 (9) (2007) 2285–2298.

[180] M. Mbaye, C. Soize, J.-P. Ousty, A reduced-order model of detuned cyclic dynamical systems with geometric modifications using a basis of cyclic modes, J. Eng. Gas Turb. Power 132 (11) (2010).

[181] M.P. Castanier, G. Óttarsson, C. Pierre, A reduced order modeling technique for mistuned bladed disks, J. Vib. Acoust. 119 (3) (1997) 439–447.

[182] R. Bladh, M.P. Castanier, C. Pierre, Reduced order modeling and vibration analysis of mistuned bladed disk assemblies with shrouds, J. Eng. Gas Turb. Power 121 (3) (1999) 515–522.

[183] M. Mbaye, C. Soize, J.-P. Ousty, E. Capiez-Lernout, Robust analysis of design in vibration of turbomachines, J. Turbomach. 135 (2) (2012) 021008.

[184] A. Madden, B.I. Epureanu, S. Filippi, Reduced-order modeling approach for blisks with large mass, stiffness, and geometric mistuning, AIAA J. 50 (2) (2012) 366–374.

[185] S. Mehrdad Pourkiaee, S. Zucca, A reduced order model for nonlinear dynamics of mistuned bladed disks with shroud friction contacts, J. Eng. Gas Turb. Power 141 (1) (2019).

[186] M. Mitra, B.I. Epureanu, Dynamic modeling and projection-based reduction methods for bladed disks with nonlinear frictional and intermittent contact interfaces, Appl. Mech. Rev. 71 (5) (2019).

[187] F. Mashayekhi, A. Nobari, S. Zucca, Hybrid reduction of mistuned bladed disks for nonlinear forced response analysis with dry friction, Int. J. Non-Linear Mech. 116 (2019) 73–84.

[188] S. Quaegebeur, B. Chouvion, F. Thouverez, Nonlinear cyclic reduction for the analysis of mistuned cyclic systems, J. Sound Vib. 499 (2021) 116002.

[189] S. Quaegebeur, B. Chouvion, F. Thouverez, Impact of mistuned underplatform dampers on the nonlinear vibration of bladed disks, J. Eng. Gas Turb. Power 143 (12) (2021) 121023.

[190] J. Brändlein, P. Eschmann, L. Hasbargen, K. Weigand, Ball and Roller Bearings: Theory Design, and Application, John Wiley and Sons, 1999.

[191] M. Allara, A model for the characterization of friction contacts in turbine blades, J. Sound Vib. 320 (3) (2009) 527–544.

[192] M. Eriten, A.A. Polycarpou, L.A. Bergman, Development of a lap joint fretting apparatus, Exp. Mech. 51 (8) (2011) 1405–1419.

[193] D. Li, C. Xu, D. Botto, Z. Zhang, M. Gola, A fretting test apparatus for measuring friction hysteresis of bolted joints, Tribol. Int. 151 (2020) 106431.

[194] P. Ranjan, A.K. Pandey, Experimental characterization and parameter identification of bolted joints under vibratory loading, Tribol. Int. 186 (2023) 108636.

[195] J. Woodhouse, T. Putelat, A. McKay, Are there reliable constitutive laws for dynamic friction? Phil. Trans. R. Soc. A 373 (2051) (2015) 20140401.

[196] A. Cabboi, T. Putelat, J. Woodhouse, The frequency response of dynamic friction: Enhanced rate-and-state models, J. Mech. Phys. Solids 92 (2016) 210–236.

[197] D.-W. Zhang, G.-C. Yang, S.-C. Lv, C. Tian, Z.-J. Li, Fretting behavior of static metal seal and testing apparatus for fretting friction with low/high temperature, Tribol. Int. 187 (2023) 108676.

[198] D. Mulvihill, M. Kartal, A. Olver, D. Nowell, D. Hills, Investigation of non-Coulomb friction behaviour in reciprocating sliding, Wear 271 (5–6) (2011) 802–816.

[199] E. Rigaud, J. Perret-Liaudet, M. Belin, L. Joly-Pottuz, J.-M. Martin, An original dynamic tribotest to discriminate friction and viscous damping, Tribol. Int. 43 (1–2) (2010) 320–329.

[200] D.J. Ewins, A survey of contact hysteresis measurement techniques, in: The Mechanics of Jointed Structures, Springer International Publishing, 2017, pp. 149–179.

[201] C.W. Schwingshackl, Measurement of friction contact parameters for nonlinear dynamic analysis, in: Conference Proceedings of the Society for Experimental Mechanics Series, Springer, New York, 2012, pp. 167–177.

[202] M.E. Kartal, D.M. Mulvihill, D. Nowell, D.A. Hills, Determination of the frictional properties of titanium and nickel alloys using the digital image correlation method, Exp. Mech. 51 (3) (2010) 359–371.

[203] M. Lavella, D. Botto, M. Gola, Design of a high-precision, flat-on-flat fretting test apparatus with high temperature capability, Wear 302 (1–2) (2013) 1073–1081.

[204] K. Asai, M.M. Gola, Experimental verification of friction behaviors under periodically-varied normal force by developing a two-directional friction test system, in: Volume 7B: Structures and Dynamics, in: GT2015, American Society of Mechanical Engineers, 2015.

[205] Q. Gao, Y. Fan, Y. Wu, J. Liu, J. Wang, L. Li, A novel test apparatus to study the mechanism of harmonic normal force on fretting wear, Tribol. Int. 191 (2024) 109091.

[206] A. Fantetti, C. Pennisi, D. Botto, S. Zucca, S. C., Comparison of contact parameters measured with two different friction rigs for nonlinear dynamic analysis, in: Proceedings of the International Conference on Noise and Vibration Engineering, 2020.

[207] A. Fantetti, S. Mariani, L. Pesaresi, D. Nowell, F. Cegla, C. Schwingshackl, Ultrasonic monitoring of friction contacts during shear vibration cycles, Mech. Syst. Signal Process. 161 (2021) 107966.

[208] T. Wei, A. Fantetti, F. Cegla, C. Schwingshackl, An optical method to monitor transparent contact interfaces during high frequency shear vibration cycles, Wear 524–525 (2023) 204840.

[209] A. Fantetti, D. Botto, S. Zucca, C. Schwingshackl, Guidelines to use input contact parameters for nonlinear dynamic analysis of jointed structures: Results of a round robin test, Tribol. Int. 191 (2024) 109158.

[210] C. Gastaldi, T.M. Berruti, M.M. Gola, The relevance of damper pre-optimization and its effectiveness on the forced response of blades, in: Proc. ASME Turbo Expo 2017, GT2017-64402, Charlotte, NC, USA, 2017.

[211] M. Lavella, Contact properties and wear behaviour of Nickel based superalloy René 80, Metals 6 (7) (2016) 159.

[212] M.M. Gola, T. Liu, A direct experimental-numerical method for investigations of a laboratory under-platform damper behavior, Int. J. Solids Struct. 51 (25–26) (2014) 4245–4259.

[213] N.F. Rieger, Damping properties of steam turbine blades, in: CISM International Centre for Mechanical Sciences, Springer, Vienna, 1988, pp. 515–541.

[214] M. Allara, S. Filippi, M.M. Gola, An experimental method for the measurement of blade-root damping, in: Volume 5: Marine; Microturbines and Small Turbomachinery; Oil and Gas Applications; Structures and Dynamics, Parts A and B, ASMEDC, 2006.

[215] F.J. Marquina, A. Coro, A. Gutie'rrez, R. Alonso, D.J. Ewins, G. Girini, Friction damping modeling in high Stress Contact Areas using microslip friction model, 2008, ASME. Paper GT2008-50359.

[216] P. Jean, C. Gibert, C. Dupont, J.-P. Lombard, Test-model correlation of dry-friction damping phenomena in aero-engines, in: Volume 5: Structures and Dynamics, Parts A and B, ASMEDC, 2008.

[217] H.R. Simmons, V. Iyengar, Effect of non-uniform blade root friction and sticking on disk stresses, in: Volume 6: Structures and Dynamics, Parts A and B, ASMEDC, 2011.

[218] C.M. Firrone, I. Bertino, Experimental investigation on the damping effectiveness of blade root joints, Exp. Mech. 55 (5) (2015) 981–988.

[219] M. Umer, D. Botto, Measurement of contact parameters on under-platform dampers coupled with blade dynamics, Int. J. Mech. Sci. 159 (2019) 450–458.

[220] M. Umer, C. Gastaldi, D. Botto, Friction damping and forced-response of vibrating structures: An insight into model validation, Int. J. Solids Struct. 202 (2020) 521–531.

[221] D. Botto, F. Cuccovillo, V. Iannotti, Experimental investigation of friction damping in blade root joints, J. Eng. Gas Turb. Power 145 (5) (2022).

[222] D.J. Alarcón Cabana, J. Yuan, C.W. Schwingshackl, A novel test rig for the validation of non-linear friction contact parameters of turbine blade root joints, in: M.R. Brake, L. Renson, R.J. Kuether, P. Tiso (Eds.), in: Nonlinear Structures & Systems, vol. 1, Springer International Publishing, Cham, 2023, pp. 215–226.

[223] R.J. Dominic, A. Graf Philip, B.B. Raju, Analytical and Experimental Investigation of Turbine Blade Damping, Tech. Rep., University of Dayton, Ohio - Air Force Office of Scientific Research, 1982.

[224] R.J. Dominic, Turbine blade friction damping study, Tech. Rep., University of Dayton Research Institute, 1985.

[225] W. Sextro, K. Popp, I. Wolter, Improved reliability of bladed disks due to friction dampers, in: ASME. Turbo Expo: Power for Land, Sea, and Air, in: Manufacturing Materials and Metallurgy, vol. 4, 1997.

[226] G. Csaba, M. Andersson, Optimization of friction damper weight, simulation and experiments, in: Turbo Expo: Power for Land, Sea, and Air, American Society of Mechanical Engineers, 1997.

[227] B. Yang, C. Menq, Characterization of contact kinematics and application to the design of wedge dampers in turbomachinery blading: Part 2 – prediction of forced response and experimental verification, ASME J. Eng. Gas Turb. Power 120 (2) (1998) 418–423.

[228] K.Y. Sanliturk, D.J. Ewins, A.B. Stanbridge, Underplatform dampers for turbine blades: Theoretical modeling, analysis, and comparison with experimental data, J. Eng. Gas Turb. Power 123 (4) (1998) 919–929.

[229] L. Panning, W. Sextro, K. Popp, Optimization of interblade friction damper design, 2000, ASME. Paper No.2000-GT-0541.

[230] J. Szwedowicz, C. Gibert, T.P. Sommer, R. Kellerer, Numerical and experimental damping assessment of a thin-walled friction damper in the rotating setup with high pressure turbine blades, ASME. J. Eng. Gas Turb. Power 130 (1) (2008) 012502–012502–10.

[231] I. Sever, E. Petrov, D. Ewins, Experimental and numerical investigation of rotating bladed disk forced response using underplatform friction dampers, ASME J. Eng. Gas Turb. Power 130 (4) (2008) 042503–042511.

[232] C. Firrone, Measurement of the kinematics of two underplatform dampers with different geometry and comparison with numerical simulation, J. Sound Vib. 323 (2009) 313–333.

[233] T. Berruti, A test rig for the investigation of the dynamic response of a bladed disk with underplatform dampers, Mech. Re.Commun. 37 (6) (2010) 581–583.

[234] A. Bessone, F. Toso, T. Berruti, Investigation on the dynamic response of blades with asymmetric under platform dampers, in: N.Y. ASME (Ed.), in: Turbo Expo: Power for Land, Sea, and Air, vol. 7B, 2015.

[235] M.M. Gola, M. Braga dos Santos, T. Liu, Design of a new test rig to evaluate underplatform damper performance, in: Proceedings of ESDA, Istanbul, Turkey, 2010.

[236] L. Pesaresi, L. Salles, A. Jones, J. Green, C. Scwingshackl, Numerical and experimental investigation of an underplatform damper test rig, Appl. Mech. Mater. 849 (2016) 1–12.

[237] N. Sazhenkov, I. Semenova, M. Nikhamkin, S. Semenov, A substructure-based numerical technique and experimental analysis of turbine blades damping with underplatform friction dampers, Procedia Eng. 199 (2017) 820–825.

[238] D. Botto, C. Gastadi, M.M. Gola, M. Umer, An experimental investigation of the dynamics of a blade with two under-platform dampers, J. Eng. Gas Turb. Power 140 (3) (2017).

[239] L. Pesaresi, M. Stender, V. Ruffini, C.W. Schwingshackl, DIC measurement of the kinematics of a friction damper for turbine applications, in: Dynamics of Coupled Structures, vol. 4, Springer International Publishing, 2017, pp. 93–101.

[240] A. Fantetti, C. Gastaldi, T. Berruti, Modeling and testing friction flexible dampers: Challenges and peculiarities, Exp. Tech. 42 (4) (2018) 407–419.

[241] C. Gastaldi, T. Berruti, Experimental verification of the dynamic model of turbine blades coupled by a sealing strip, Appl. Sci. 8 (11) (2018) 2174.

[242] D. Botto, M. Umer, A novel test rig to investigate under-platform damper dynamics, Mech. Syst. Signal Process. 100 (2018) 344–359.

[243] A. Fantetti, R. Setchfield, C. Schwingshackl, Nonlinear dynamics of turbine bladed disk with friction dampers: Experiment and simulation, Int. J. Mech. Sci. 257 (2023) 108510.

[244] J. Szwedowicz, T. Secall-Wimmel, P. Dünck-Kerst, Damping performance of axial turbine stages with loosely assembled friction bolts: The nonlinear dynamic assessment, J. Eng. Gas Turb. Power 130 (3) (2008).

[245] R. Drozdowski, L. Völker, M. Häfele, D.M. Vogt, Experimental and numerical investigation of the nonlinear vibrational behavior of steam turbine last stage blades with friction bolt damping elements, in: Volume 8: Microturbines, Turbochargers and Small Turbomachines; Steam Turbines, American Society of Mechanical Engineers, 2015.

[246] E. Ferhatoglu, D. Botto, S. Zucca, An experimental investigation on the dynamic response variability of a turbine blade with midspan dampers, J. Eng. Gas Turb. Power 145 (1) (2022).

[247] L. Pešek, M. Hajžman, L. Půst, V. Zeman, M. Byrtus, J. Brůha, Experimental and numerical investigation of friction element dissipative effects in blade shrouding, Nonlinear Dynam. 79 (3) (2014) 1711–1726.

[248] S. Zucca, T. Berruti, L. Cosi, Experimental and numerical investigations on the dynamic response of turbine blades with tip pin dampers, J. Phys. Conf. Ser. 744 (2016) 012131.

[249] J. Szwedowicz, Cyclic finite element modeling of shrouded turbine blades including frictional contacts, in: Turbo Expo: Power for Land, Sea, and Air, American Society of Mechanical Engineers, 1999.

[250] F. D'Ambrosio, E. Chatelet, J. Ravoux, G. Jacquet-Richardet, Forced response of shrouded bladed disc assemblies: A jointed experimental numerical approach, in: Volume 6: Turbo Expo 2004, ASMEDC, 2004.

[251] J. Szwedowicz, R. Visser, W. Sextro, P.A. Masserey, On nonlinear forced vibration of shrouded turbine blades, J. Turbomach. 130 (1) (2007).

[252] J. Hong, Y. Shi, D. Zhang, Z. Zhu, Experimental study of damping characteristic of shrouded blade, in: Volume 5: Turbo Expo 2007, ASMEDC, 2007.

[253] B.N. Ferrante E., Simulation of the dynamic behaviour of a group of blades with friction contacts, in: Proc. of 10th VIRM, Institution of Mechanical Engineers, Woodhead Publishing, London, UK, 2012.

[254] K. Savchenko, A. Zinkovskii, I.G. Tokar', Determination of contact interaction influence on forced vibrations of shrouded blades, in: 25th Int. Congr. SoundVib. 2018, ICSV 2018 Hiroshima Cal, 2018.

[255] F. Kaptan, L.P. von Scheidt, J. Wallaschek, Numerical and experimental study of shrouded blade dynamics considering variable operating points, in: Volume 7C: Structures and Dynamics, American Society of Mechanical Engineers, 2018.

[256] C. Cui, H. Ma, Y. Jin, F. Xie, T. Yang, S. Liu, Numerical and experimental investigation on the vibro-impact responses analysis of shrouded blade, J. Low Freq. Noise Vib. Act. Control 38 (3–4) (2018) 1188–1201.

[257] L.R. Tamatam, D. Botto, S. Zucca, A novel test rig to study the effect of fretting wear on the forced response dynamics with a friction contact, Nonlinear Dynam. 105 (2) (2021) 1405–1426.

[258] K. Grant, C. Gastaldi, T.M. Berruti, R. Kellerer, The numerical and experimental evaluation of a coupled blade dynamic limit response with friction contacts, J. Eng. Gas Turb. Power 145 (4) (2022).

[259] R. Ahmed, C.M. Firrone, S. Zucca, A test rig for the full characterization of the dynamics of shrouded turbine blades, Mech. Syst. Signal Process. 189 (2023) 110080.

[260] D. Laxalde, C. Gibert, F. Thouverez, Experimental and numerical investigations of friction rings damping of blisks, 2008, ASME. Paper No.GT2008 - 50862.

[261] L. de Oliveira, P. Varoto, M. Peres, Shaker structure interaction: Overview and updated results, ICSV 2011, in: 18th International Congress on Sound and Vibration 2011, vol. 3, 2011, pp. 2516–2523.

[262] B.R. Pacini, R.J. Kuether, D.R. Roettgen, Shaker-structure interaction modeling and analysis for nonlinear force appropriation testing, Mech. Syst. Signal Process. 162 (2022) 108000.

[263] K. D'Souza, E. Kurstak, K. Ruff, M.G. Dunn, A new experimental facility for characterizing bladed disk dynamics at design speed, AIAA J. 58 (6) (2020) 2682–2690.

[264] A. Mabilia, C. Gibert, F. Thouverez, E. De Jaeghere, L. Sanchez, L. Giovannoni, Modal testing of a full-scale rotating woven composite fan using piezoelectric excitation, in: K.L. Cavalca, H.I. Weber (Eds.), Proceedings of the 10th International Conference on Rotor Dynamics, IFToMM, Springer International Publishing, Cham, 2019, pp. 291–305.

[265] J.S. Rao, Bladed disks, in: History of Mechanism and Machine Science, Springer Netherlands, 2011, pp. 299–325.

[266] R.M. Lacayo, M.S. Allen, Updating structural models containing nonlinear Iwan joints using quasi-static modal analysis, Mech. Syst. Signal Process. 118 (2019) 133–157.

[267] T. Dreher, M. Brake, B. Seeger, M. Krack, In situ, real-time measurements of contact pressure internal to jointed interfaces during dynamic excitation of an assembled structure, Mech. Syst. Signal Process. 160 (2021) 107859.

[268] A.D. Nashif, D.I. Jones, J.P. Henderson, Vibration Damping, John Wiley & Sons, 1991.

[269] C. Gastaldi, J. Gross, M. Scheel, T.M. Berruti, M. Krack, Modeling complex contact conditions and their effect on blade dynamics, J. Eng. Gas Turb. Power 143 (1) (2020).

[270] C. Gastaldi, M.M. Gola, Testing, simulating and understanding underplatform damper dynamics, in: Proceedings of the VII European Congress on Computational Methods in Applied Sciences and Engineering, ECCOMAS Congress 2016, 2016.

[271] C. Gastaldi, T.M. Berruti, Direct measurement of the damping and stiffening capabilities of cylindrical underplatform dampers, Mech. Syst. Signal Process. 139 (2020) 106632.

[272] C. Gastaldi, M.M. Gola, Pre-optimization of asymmetrical underplatform dampers, J. Eng. Gas Turb. Power 139 (1) (2016) 012504.

[273] J.-H. Wang, Design of a friction damper to control vibration of turbine blades, in: Dynamics with Friction: Modeling, Analysis and Experiment: (Part I), World Scientific, 1996, pp. 169–196.

[274] L. Panning, W. Sextro, K. Popp, Optimization of the contact geometry between turbine blades and underplatform dampers with respect to friction damping, 2002, ASME. Paper No.GT-2002-30429.

[275] Y. Yuan, A. Jones, R. Setchfield, C. Schwingshackl, Robust design optimisation of underplatform dampers for turbine applications using a surrogate model, J. Sound Vib. 494 (2021) 115528.

[276] S. Zucca, D. Botto, M.M. Gola, Range of variability in the dynamics of semi-cylindrical friction dampers for turbine blades, in: Turbo Expo: Power for Land, Sea, and Air, vol. 43154, 2008, pp. 519–529.

[277] E. Denimal, C. Wong, L. Salles, L. Pesaresi, On the efficiency of a conical underplatform damper for turbines, J. Eng. Gas Turb. Power 143 (2) (2021) 021020.

[278] E. Denimal, F. El Haddad, C. Wong, L. Salles, Topological optimization of under-platform dampers with moving morphable components and global optimization algorithm for nonlinear frequency response, J. Eng. Gas Turb. Power 143 (2) (2021) 021021.

[279] E.P. Petrov, Direct parametric analysis of resonance regimes for nonlinear vibrations of bladed disks, J. Turbomach. 129 (3) (2006) 495–502.

[280] E.P. Petrov, Explicit finite element models of friction dampers in forced response analysis of bladed disks, J. Eng. Gas Turb. Power 130 (2) (2008) 022502.

[281] C. Gastaldi, T.M. Berruti, M.M. Gola, Best practices for underplatform damper designers, Proc. Inst. Mech. Eng. C 232 (7) (2018) 1221–1235.

[282] C. Gastaldi, M.M. Gola, Criteria for best performance of pre-optimized solid dampers, J. Eng. Gas Turb. Power 141 (4) (2018).

[283] M. Hüls, L. Panning-von Scheidt, J. Wallaschek, Influence of geometric design parameters onto vibratory response and high-cycle fatigue safety for turbine blades with friction damper, J. Eng. Gas Turb. Power 141 (4) (2018).

[284] Y. Sun, J. Yuan, L. Pesaresi, E. Denimal, L. Salles, Parametric study and uncertainty quantification of the nonlinear modal properties of frictional dampers, J. Vib. Acoust. 142 (5) (2020) 051102.

[285] Y. Sun, E. Denimal, J. Yuan, L.c. Salles, Geometric design of friction ring dampers in blisks using nonlinear modal analysis and kriging surrogate model, Struct. Multidiscip. Optim. 68 (2022).

[286] A. Lupini, B.I. Epureanu, A friction-enhanced tuned ring damper for bladed disks, J. Eng. Gas Turb. Power 143 (1) (2020) 011002.

[287] Y. Sun, J. Yuan, L. Pesaresi, L. Salles, Nonlinear vibrational analysis for integrally bladed disk using frictional ring damper, J. Phys. Conf. Ser. 1106 (2018) 012026.

[288] W. Tang, S. Baek, B.I. Epureanu, Reduced-order models for blisks with small and large mistuning and friction dampers, J. Eng. Gas Turb. Power 139 (1) (2017).

[289] C. Gastaldi, T.M. Berruti, M.M. Gola, The effect of surface finish on the proper functioning of underplatform dampers, J. Vib. Acoust. 142 (5) (2020) 051103.

[290] M.E. Kartal, D.M. Mulvihill, D. Nowell, D.A. Hills, Measurements of pressure and area dependent tangential contact stiffness between rough surfaces using digital image correlation, Tribol. Int. 44 (10) (2011) 1188–1198.

[291] N. Hoffmann, M. Fischer, R. Allgaier, L. Gaul, A minimal model for studying properties of the mode-coupling type instability in friction induced oscillations, Mech. Res. Commun. 29 (4) (2002) 197–205.

[292] X. Delaune, E. de Langre, C. Phalippou, A probabilistic approach to the dynamics of wear tests, J. Trib. 122 (4) (2000) 815–821.

[293] Q. Gao, Y. Fan, Y. Wu, L. Li, D. Zhang, Insight into the influence of frictional heat on the modal characteristics and interface temperature of frictionally damped turbine blades, J. Sound Vib. (2024) 118410.

[294] L. Gallego, B. Fulleringer, S. Deyber, D. Nelias, Multiscale computation of fretting wear at the blade/disk interface, Tribol. Int. 43 (4) (2010) 708–718.

[295] J. Gross, P. Buhl, U. Weber, X. Schuler, M. Krack, Effect of creep on the nonlinear vibration characteristics of blades with interlocked shrouds, Int. J. Non-Linear Mech. 99 (2018) 240–246.

[296] E. Petrov, Analysis of sensitivity and robustness of forced response for nonlinear dynamic structures, Mech. Syst. Signal Process. 23 (1) (2009) 68–86.

[297] M. Krack, L. Panning, J. Wallaschek, C. Siewert, A. Hartung, Robust design of friction interfaces of bladed disks with respect to parameter uncertainties, 2012, ASME. Paper No.GT2012-68578.

[298] E. Ferhatoglu, S. Zucca, On the non-uniqueness of friction forces and the systematic computation of dynamic response boundaries for turbine bladed disks with contacts, Mech. Syst. Signal Process. 160 (2021) 107917.

[299] E. Ferhatoglu, C. Gastaldi, D. Botto, S. Zucca, An experimental and computational comparison of the dynamic response variability in a turbine blade with under-platform dampers, Mech. Syst. Signal Process. 172 (2022) 108987.

[300] E. Ferhatoglu, D. Botto, S. Zucca, Parametric study for model calibration of a friction-damped turbine blade with multiple test data, Nonlinear Dynam. (2024) 1–27.

[301] E. Ferhatoglu, J. Groß, M. Krack, Frequency response variability in friction-damped structures due to non-unique residual tractions: Obtaining conservative bounds using a nonlinear-mode-based approach, Mech. Syst. Signal Process. 201 (2023) 110651.

[302] B.D. Yang, C.H. Menq, Characterization of contact kinematics and application to the design of wedge dampers in turbomachinery blading: Part 1—Stick-slip contact kinematics, J. Eng. Gas Turb. Power 120 (2) (1998) 410–417.

[303] E. Ferhatoglu, S. Zucca, Determination of periodic response limits among multiple solutions for mechanical systems with wedge dampers, J. Sound Vib. 494 (2021) 115900.

[304] T. Butlin, G. Spelman, P. Ghaderi, W. Midgley, R. Umehara, Predicting response bounds for friction-damped gas turbine blades with uncertain friction coupling, J. Sound Vib. 440 (2019) 399–411.

[305] T. Butlin, P. Ghaderi, G. Spelman, W. Midgley, R. Umehara, A novel method for predicting the response variability of friction-damped gas turbine blades, J. Sound Vib. 440 (2019) 372–398.

[306] J. Liu, L. Li, Y. Fan, A comparison between the friction and piezoelectric synchronized switch dampers for blisks, J. Intell. Mater. Syst. Struct. 29 (12) (2018) 2693–2705.

[307] Y. Wu, L. Li, Y. Fan, S. Zucca, C. Gastaldi, H. Ma, Design of dry friction and piezoelectric hybrid ring dampers for integrally bladed disks based on complex nonlinear modes, Comput. Struct. 233 (2020) 106237.

[308] Y. Zhong, Z. Zhang, X. Ma, Vibration suppression of blisk using piezoelectric shunt damping with negative capacitance, in: 2022 Global Reliability and Prognostics and Health Management, PHM-Yantai, IEEE, 2022, pp. 1–5.

[309] Y. Wu, L. Li, Y. Fan, J. Liu, Q. Gao, A linearised analysis for structures with synchronized switch damping, IEEE Access 7 (2019) 133668–133685.

[310] C. Sugino, M. Ruzzene, A. Erturk, Design and analysis of piezoelectric meta-material beams with synthetic impedance shunt circuits, IEEE/ASME Trans. Mechatronics 23 (5) (2018) 2144–2155.

[311] H. Ji, Y. Guo, J. Qiu, Y. Wu, C. Zhang, C. Tao, A new design of unsymmetrical shunt circuit with negative capacitance for enhanced vibration control, Mech. Syst. Signal Process. 155 (2021) 107576.

[312] H. Yu, K.W. Wang, Vibration suppression of mistuned coupled-blade-disk systems using piezoelectric circuitry network, J. Vib. Acoust. 131 (2) (2009) 021008.

[313] M. Lasen, D. Dini, C. Schwingshackl, Experimental control of frictional contact behaviour via piezoelectric actuation, Mech. Syst. Signal Process. 211 (2024) 111198.

[314] Y. Wu, L. Li, Y. Fan, H. Ma, W. Wang, J.-L. Christen, M. Ichchou, Design of semi-active dry friction dampers for steady-state vibration: sensitivity analysis and experimental studies, J. Sound Vib. 459 (2019) 114850.

[315] Y. Wu, J. Chen, Y. Fan, L. Li, Z. Jiang, An MFC-based friction damper with adjustable normal force: conception, modelling, and experiment, Mech. Syst. Signal Process. 215 (2024) 111450.

[316] M. Lasen, D. Dini, C. Schwingshackl, Experimental control of frictional contact behaviour via piezoelectric actuation, Mech. Syst. Signal Process. 211 (2024) 111198.

[317] J. Ma, S. Dong, G. Chen, P. Peng, L. Qian, A data-driven normal contact force model based on artificial neural network for complex contacting surfaces, Mech. Syst. Signal Process. 156 (2021) 107612.

[318] A. Dong, Z. Du, Z. Yan, Friction modeling and compensation for haptic master manipulator based on deep Gaussian process, Mech. Mach. Theory 166 (2021) 104480.

[319] H. Peng, N. Song, F. Li, S. Tang, A mechanistic-based data-driven approach for general friction modeling in complex mechanical system, J. Appl. Mech. 89 (7) (2022) 071005.

[320] S. Kelly, Data-Driven Models of Blisk Structures (Ph.D. thesis), University of Michigan, 2023.

[321] Y. Wu, L. Li, Y. Fan, Nonlinear modal electromechanical coupling factor for piezoelectric structures containing nonlinearities, Chin. J. Aeronaut. (2022).

[322] Q. Gao, Y. Fan, Y. Wu, L. Li, A harmonic balance-based method to predict nonlinear forced response and temperature rise of dry friction systems including frictional heat transfer, Nonlinear Dynam. (2023) 1–29.

[323] C. Berthold, J. Gross, C. Frey, M. Krack, Development of a fully-coupled harmonic balance method and a refined energy method for the computation of flutter-induced limit cycle oscillations of bladed disks with nonlinear friction contacts, J. Fluids Struct. 102 (2021) 103233.

[324] S. Schwarz, L. Kohlmann, A. Hartung, J. Gross, M. Scheel, M. Krack, Validation of a turbine blade component test with frictional contacts by phase-locked-loop and force-controlled measurements, J. Eng. Gas Turb. Power 142 (5) (2020) 051006.

[325] M. Scheel, Nonlinear modal testing of damped structures: Velocity feedback vs. phase resonance, Mech. Syst. Signal Process. 165 (2022) 108305.

[326] L. Renson, D.A. Barton, S.A. Neild, Experimental tracking of limit-point bifurcations and backbone curves using control-based continuation, Int. J. Bifurcation Chaos 27 (01) (2017) 1730002.

[327] G. Abeloos, L. Renson, C. Collette, G. Kerschen, Stepped and swept control-based continuation using adaptive filtering, Nonlinear Dynam. 104 (4) (2021) 3793–3808.

[328] T. Karaağaçlı, H.N. Özgüven, Experimental modal analysis of nonlinear systems by using response-controlled stepped-sine testing, Mech. Syst. Signal Process. 146 (2021) 107023.

[329] A. Koyuncu, T. Karaağaçlı, M. Şahin, H.N. Özgüven, Experimental modal analysis of nonlinear amplified piezoelectric actuators by using response-controlled stepped-sine testing, Exp. Mech. 62 (9) (2022) 1579–1594.

[330] S. Schwarz, J. Reil, J. Gross, A. Hartung, D. Rittinger, M. Krack, Friction saturated limit cycle oscillations—Test rig design and validation of numerical prediction methods, J. Eng. Gas Turb. Power 146 (5) (2024).

[331] J. Blahoš, A. Vizzaccaro, L. Salles, F. El Haddad, Parallel harmonic balance method for analysis of nonlinear dynamical systems, in: Turbo Expo: Power for Land, Sea, and Air, vol. 84232, American Society of Mechanical Engineers, 2020, V011T30A028.

[332] J. Gross, V. Gupta, C. Berthold, M. Krack, A new paradigm for multi-fidelity continuation using parallel model refinement, Comput. Methods Appl. Mech. Engrg. 423 (2024) 116860.